CRCLEME
Cooperative Research Centre for
Landscape Evolution & Mineral Exploration

CSIRO
EXPLORATION
AND MINING

AMIRA
Australian Mineral Industries Research Association Limited ACN 004 448 266

OPEN FILE
REPORT
SERIES

GEOCHEMICAL EXPLORATION FOR PLATINUM GROUP ELEMENTS IN WEATHERED TERRAIN

P252 FINAL REPORT

Volume III

C.R.M. Butt, P.A. Williams, D.J. Gray, I.D.M. Robertson, K.H. Schorin, H.M. Churchward, J. McAndrew, S.J. Barnes and M.F.J. Tenhaeff

CRC LEME OPEN FILE REPORT 85

March 2001

(CSIRO Division of Exploration Geoscience Report 332R, 1992.
Second impression 2001)

CRC LEME is an unincorporated joint venture between The Australian National University, University of Canberra, Australian Geological Survey Organisation and CSIRO Exploration and Mining, established and supported under the Australian Government's Cooperative Research Centres Program.

CRC

AMIRA
Australian Mineral Industries Research Association Limited ACN 004 448 266

CRCLEME
Cooperative Research Centre for
Landscape Evolution & Mineral Exploration

CSIRO
EXPLORATION
AND MINING

GEOCHEMICAL EXPLORATION FOR PLATINUM GROUP ELEMENTS IN WEATHERED TERRAIN

P252 FINAL REPORT

Volume III

C.R.M. Butt, P.A. Williams, D.J. Gray, I.D.M. Robertson,
K.H. Schorin, H.M. Churchward, J. McAndrew,
S.J. Barnes and M.F.J. Tenhaeff

CRC LEME OPEN FILE REPORT 85

March 2001

(CSIRO Division of Exploration Geoscience Report 332R, 1992.
Second impression 2001)

CRC LEME is an unincorporated joint venture between The Australian National University,
University of Canberra, Australian Geological Survey Organisation and CSIRO Exploration and Mining
Headquarters: CRC LEME c/o CSIRO Exploration and Mining, Private Bag No 5, PO Wembley, Western Australia, 6913.

RESEARCH ARISING FROM CSIRO/AMIRA YILGARN REGOLITH GEOCHEMISTRY PROJECTS 1987-1996

In 1987, CSIRO commenced a series of multi-client research projects in regolith geology and geochemistry which were sponsored by companies in the Australian mining industry, through the Australian Mineral Industries Research Association Limited (AMIRA). The initial research program, "Exploration for concealed gold deposits, Yilgarn Block, Western Australia" had the aim of developing improved geological, geochemical and geophysical methods for mineral exploration that would facilitate the location of blind, buried or deeply weathered gold deposits. The program commenced with the following projects:

P240: Laterite geochemistry for detecting concealed mineral deposits (1987-1991). Leader: Dr R.E. Smith.
Its scope was development of methods for sampling and interpretation of multi-element laterite geochemistry data and application of multi-element techniques to gold and polymetallic mineral exploration in weathered terrain. The project emphasised viewing laterite geochemical dispersion patterns in their regolith-landform context at local and district scales. It was supported by 30 companies.

P241: Gold and associated elements in the regolith - dispersion processes and implications for exploration (1987-1991). Leader: Dr C.R.M. Butt.
The project investigated the distribution of ore and indicator elements in the regolith. It included studies of the mineralogical and geochemical characteristics of weathered ore deposits and wall rocks, and the chemical controls on element dispersion and concentration during regolith evolution. This was to increase the effectiveness of geochemical exploration in weathered terrain through improved understanding of weathering processes. It was supported by 26 companies.

These projects represented 'an opportunity for the mineral industry to participate in a multi-disciplinary program of geoscience research aimed at developing new geological, geochemical and geophysical methods for exploration in deeply weathered Archaean terrains'. This initiative recognised the unique opportunities, created by exploration and open-cut mining, to conduct detailed studies of the weathered zone, with particular emphasis on the near-surface expression of gold mineralisation. The skills of existing and specially recruited research staff from the Floreat Park and North Ryde laboratories (of the then Divisions of Minerals and Geochemistry, and Mineral Physics and Mineralogy, subsequently Exploration Geoscience and later Exploration and Mining) were integrated to form a task force with expertise in geology, mineralogy, geochemistry and geophysics. Several staff participated in more than one project. Following completion of the original projects, two continuation projects were developed.

P240A: Geochemical exploration in complex lateritic environments of the Yilgarn Craton, Western Australia (1991-1993). Leaders: Drs R.E. Smith and R.R. Anand.
The approach of viewing geochemical dispersion within a well-controlled and well-understood regolith-landform and bedrock framework at detailed and district scales continued. In this extension, focus was particularly on areas of transported cover and on more complex lateritic environments typified by the Kalgoorlie regional study. This was supported by 17 companies.

P241A: Gold and associated elements in the regolith - dispersion processes and implications for exploration (1991-1993). Leader: Dr. C.R.M. Butt.
The significance of gold mobilisation under present-day conditions, particularly the important relationship with pedogenic carbonate, was investigated further. In addition, attention was focussed on the recognition of primary lithologies from their weathered equivalents. This project was supported by 14 companies.

Most reports related to the above research projects were published as CRC LEME Open File Reports Series (Nos 1-74), with an index (Report 75), by June 1999. Publication now continues with release of reports from further projects.

P252: Geochemical exploration for platinum group elements in weathered terrain. Leader: Dr C.R.M. Butt.
This project was designed to gather information on the geochemical behaviour of the platinum group elements under weathering conditions using both laboratory and field studies, to determine their dispersion in the regolith and to apply this to concepts for use in exploration. The research was commenced in 1988 by CSIRO Exploration Geoscience and the University of Wales (Cardiff). The Final Report was completed in December 1992. It was supported by 9 companies.

P409: Geochemical exploration in areas of transported overburden, Yilgarn Craton and environs, WA.
Leaders: Drs C.R.M. Butt and R.E. Smith.
About 50% or more of prospective terrain in the Yilgarn is obscured by substantial thicknesses of transported overburden that varies in age from Permian to Recent. Some of this cover has undergone substantial weathering. Exploration problems in these covered areas were the focus of Project 409. The research was commenced in June 1993 by CSIRO Exploration and Mining but was subsequently incorporated into the activities of CRC LEME in July 1995 and was concluded in July 1996. It was supported by 22 companies.

Although the confidentiality periods of Projects P252 and P409 expired in 1994 and 1998, respectively, the reports have not been released previously. CRC LEME acknowledges the Australian Mineral Industries Research Association and CSIRO Division of Exploration and Mining for authority to publish these reports. It is intended that publication of the reports will be a substantial additional factor in transferring technology to aid the Australian mineral industry.

This report (CRC LEME Open File Report 85) is a second impression (second printing) of CSIRO, Division of Exploration Geoscience Restricted Report EG 332R, first issued in 1992, which formed part of the CSIRO/AMIRA Project P252.

Copies of this publication can be obtained from:
The Publication Officer, c/- CRC LEME, CSIRO Exploration and Mining, Private Bag 5, Wembley, WA 6913, Australia. Information on other publications in this series may be obtained from the above or from http://leme.anu.edu.au/
Cataloguing-in-Publication:

Geochemical exploration for platinum group elements in weathered terrain - Final Report.
ISBN vI: 0 64 3 06693 4 vIIA: 0 643 06694 2 vIIB: 0 643 06695 0 vIII: 0 643 06696 9 set: 0 643 06697 7
1. Geochemical prospecting 2. Weathering 3. Platinum ores
1. Butt, C.R.M. II. Title
CRC LEME Open File Report 85.
ISSN 1329-4768

TABLE OF CONTENTS

VOLUME I

VOLUME IIA

VOLUME IIB

VOLUME III

Addresses and affiliations of authors

C.R.M Butt
Division of Exploration Geoscience
CSIRO
Private Bag
Wembley 6014
Western Australia

D.J.Gray
Division of Exploration Geoscience
CSIRO
Private Bag
Wembley 6014
Western Australia

K.H.Schorin
Centro de Quimica
IVIC
Aptdo. 21827
Caracas 1020-A
Venezuela

J. McAndrew
Division of Exploration Geoscience
CSIRO
P.O. Box 136
North Ryde
NSW 2113
Australia

M.F.J. Tenhaeff
Institut fur Mineralogie und Lagerstattenlehre
Technische Hochschule
5100 Achen
Germany

P.A. Williams
Department of Chemistry
University of Western Sydney
P.O. Box 10, Kingswood
NSW 2747
Australia

I.D.M. Robertson
Division of Exploration Geoscience
CSIRO
Private Bag
Wembley 6014
Western Australia

H.M. Churchward
Division of Exploration Geoscience
CSIRO
Private Bag
Wembley 6014
Western Australia

S.J. Barnes
Division of Exploration Geoscience
CSIRO
Private Bag
Wembley 6014
Western Australia

CHAPTER 6: THE SELECTIVE EXTRACTION OF PLATINUM AND PALLADIUM FROM SOILS AND REGOLITH MATERIALS FROM MT. CARNAGE AND ORA BANDA

D.J. Gray

ABSTRACT

Selective extraction techniques have been utilized to investigate the occurence of Pt and Pd in the lateritic regolith at Mt. Carnage. The results show that:

(i) Pt and Pd are not iodide soluble, in comparison with Au, which is moderately soluble in this reagent. This could be due to a greater affinity of Pt and Pd for Fe oxides, with these metals being inaccessible to extraction without dissolution of the Fe oxides;

(ii) Pt and Pd are only poorly dissolved from Mt Carnage soil and regolith by thiosulphate, indicating the metals to be incorporated into minerals;

(iii) Pt and Pd are not soluble in reagents that dissolve exchangeable metals, carbonates, Mn oxides and poorly crystalline Fe oxides, indicating they are not present in these phases;

(iv) Almost all of the Pt and 25 to 50 % of the Pd are dissolved in citrate-dithionite reagent, which is primarily designed to dissolve Fe oxides, such as goethite and hematite;

(v) In addition to most of the Pd occurring in non-acid extractable phases, Pd associated with Fe oxides is found with Al-rich goethitic Fe oxides, in comparison with Pt which occurs with coarse, probably Al-poor, hematitic, Fe oxides. This may reflect differences in the behaviour during weathering, with Pt released deep in the profile and incorporated in Fe oxides at depth, and Pd released more gradually from the primary phase in which it occurs, and therefore being dominantly incorporated in Fe oxides found nearer the surface;

(vi) The differences in the associations of Pt and Pd with Fe oxides may explain the contrasting geochemistry of the two elements in lag (Volume IIA, Chapter 5, Section 6.2);

(vii) Most of the first row transition elements [namely Ti (partially), Mn and Co (in the lateritic zone), V, Cr, Ni and Cu], with the exception of Zn, are primarily associated with Fe oxides;

(viii) The chemical extractability of the Cr is markedly different in the laterite zone (where it is primarily associated with Fe oxides), compared with the saprolite (where it is resistant to extraction), supporting observations of chromite grains in the saprolite and absence of any separate phase Cr mineral in the laterite. This may reflect a lithological boundary between the saprolite and the laterite.

1 INTRODUCTION

Selective extraction is a technique whereby particular soil phases are dissolved in a controlled manner, and the resulting solutions analysed for trace elements of interest. These techniques can be used to investigate how trace elements such as the PGEs are distributed between the phases. Understanding such elemental distributions may be of value in further developing sampling or interpretational methods.

Various phases that could be of significance in the distribution of PGEs include phyllo-silicates (*e.g.*, kaolinite), Fe oxides (*e.g.*, goethite and hematite), Mn oxides, carbonates or resistate minerals such as chromite, zircon or monazite. A number of extractions schemes were developed for this project to investigate these potential phases. These experiments indicated notable associations of both Pt and Pd with some mineral phases. Distinct differences were observed in the associations of these two elements, and in turn they differed dramatically with results from previous work on the chemistry of Au in soils and regolith.

In addition to these chemical means of testing the distribution of Pt and Pd, a magnetic concentration method, High Gradient Magnetic Separation (HGMS) was also used. This enabled an independent test of the PGE-Fe oxide association, and introduced additional information on the nature of the association

2 IODIDE EXTRACTIONS

Iodide has been used for extraction of Au (Gray *et al.*, 1990), and was particularly effective in dissolving Au from carbonate-rich materials. Similar experiments were conducted to determine whether similar effects could be also observed for Pt and Pd, particularly in the upper carbonate-rich zone.

Iodide extractions of samples from three different drill holes, namely OB 19 and OB 23 at Ora Banda (Volume IIa, Chapter 5) and MC 24 from Mt. Carnage (Volume IIa, Chapter 5, Section 7) were carried out to establish some general hypotheses on the chemistry of extraction of Pt and Pd by this reagent. The extractant was a solution of 0.1 moles/litre (M) potassium iodide (KI) and 1 M sodium hydrogen carbonate ($NaHCO_3$), saturated with CO_2 via bubbling, which was taken to pH 7.4 with hydrochloric acid (HCl). This reagent was shaken with 25 g of sample (pulverized to < 75 μm) for one day, at a soil:solution ratio of 1:2. Following this, the suspension was centrifuged [3000 revolutions per minute (rpm) for 15 minutes (min)] and the solution decanted off and analysed for Pt and Pd by ICP-MS. An additional experiment was conducted on the same sample sets, using the same reagent conditions, except that samples were merely crushed to < 10 mm. This was done in order to test for any effect of inclusion of PGEs in impermeable aggregations.

Results from the extractions are tabulated in Appendix I and shown in Figures 1 - 3, which also indicate the horizons having significant carbonate concentrations. Platinum and Pd solubility (with the exception of some minor extraction of Pt from samples between 3 and 7 m depth at OB 19) is generally at or below the detection limit, even in the carbonate-rich zone close to the surface.

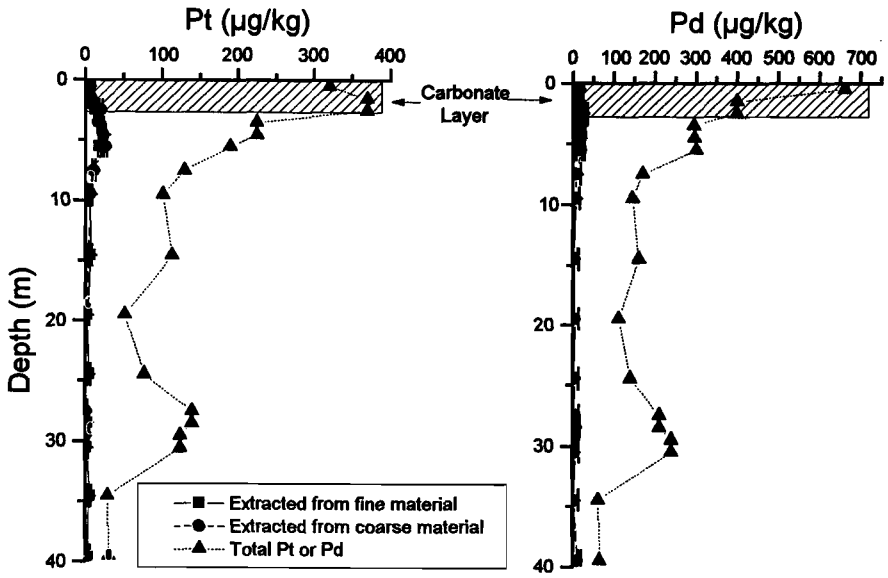

Figure 1: Extraction of Pt and Pd from OB 19 samples.

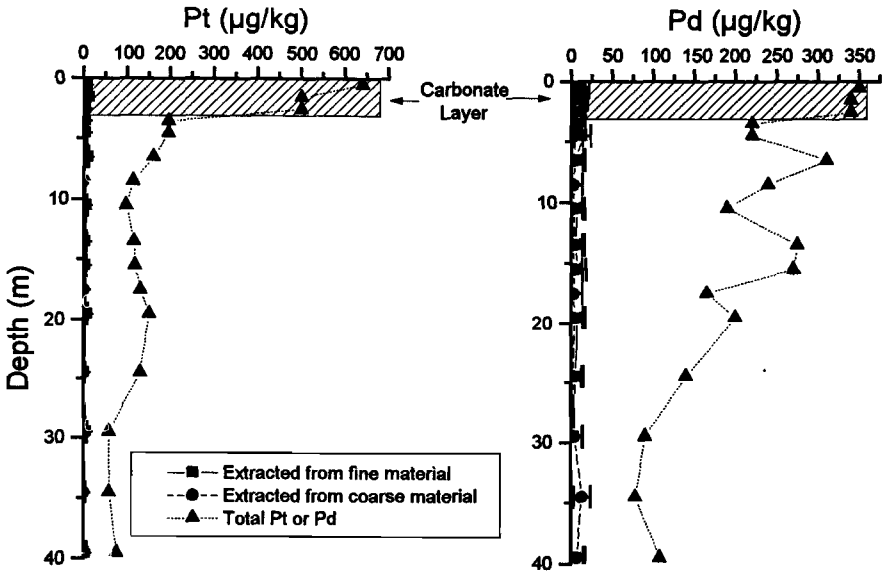

Figure 2: Extraction of Pt and Pd from OB 23 samples.

In comparison, previous investigations on the extraction of Au (Gray *et al.*, 1990) indicated that iodide could dissolve up to 30% of the Au from carbonate-rich soils. This observed difference in the behaviour of Pt and Pd with that of Au is surprising, given that equilibration studies (Volume I, Chapter 4) indicate that Pt and Pd are influenced by organic ligands in a similar manner to Au. Further work (Sections 3 - 5) has indicated that Pt and Pd are involved in different mineralogical associations at the Ora Banda and Mt. Carnage sites than observed for Au elsewhere. In particular, these metals appear to occur in resistant primary minerals or strongly associated with Fe oxides, and therefore may only be dissolved by reagents capable of dissolving such phases.

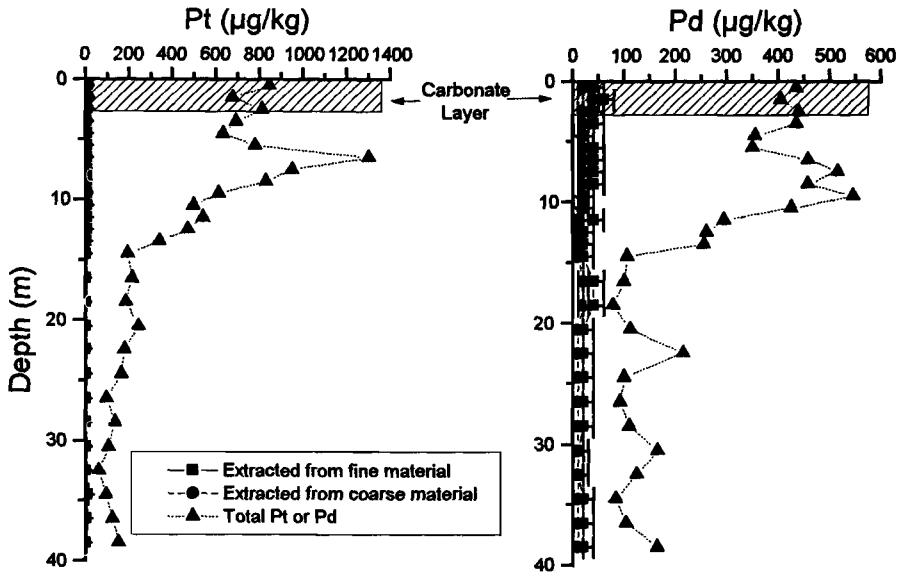

Figure 3: Extraction of Pt and Pd from MC 24 samples.

3 SELECTIVE EXTRACTION EXPERIMENT A - EASILY EXTRACTABLE PHASES

3.1 Experimental

This experiment was conducted on six different samples, namely:

(i) MC 24 0-1m (soil);
(ii) MC 24 1-2m (in duplicate) MC 24 3-4m and MC 24 6-7m (lateritic zone);
(iii) MC 24 14-15m (in duplicate) and MC 24 28-29m (saprolite);

which were chosen to exemplify a range of regolith horizons. All extractions were conducted in polypropylene centrifuge tubes into which 1.25 g solid was added. Extractions were then conducted sequentially, as described below. For all of the extractions, following acid digestion, solutions were made up to 20 mL with 1M HCl / 0.3M HNO3 and analysed for Na, K, Ca and Mg by AAS, for Pt and Pd by ICP-MS and for Al, Ba, Co, Cr, Cu, Fe, Mn, Ni, Ti, V, Y, Zn and Zr by ICP-AES. Interference problems were encountered in ICP-MS analysis for Pd in the solutions, and therefore only the fire assay data for the total Pd and for the Pd in the residue were used. Using this data, a 'total extractable' Pd (equal to the total of all the extractions measured for the other elements) was calculated by difference.

3.1.1 Exchangeable Cation Phase (neutral ammonium acetate)

Forty mL 1 M ammonium acetate (NH_4Ac) pH 7 was added to 1.25g sample and the tube agitated for 1 hour (hr). The tube was centrifuged (2000 rpm for 5 min) and the solution decanted. An additional 10 mL of NH_4Ac was added and the suspension dispersed. The suspension was then re-centrifuged as above and the solution decanted. The combined solution was filtered (0.45 µm membrane filter), evaporated and digested with aqua-regia.

3.1.2 Carbonate Phase (acid ammonium acetate)

To the sample remaining from the previous extraction was added 10 mL 1M NH_4Ac pH 5.0, and the tube agitated for 5 hr. The tube was centrifuged and the solution decanted. An additional 10 mL of

deionized water was added and the suspension dispersed, re-centrifuged and decanted. The combined solution was filtered, evaporated and digested with aqua-regia.

3.1.3 Manganese Oxide Phase (dilute hydroxylamine)

To the sample remaining from the previous extraction was added 35 mL 0.1M hydroxylamine hydrochloride ($NH_2OH.HCl$) / 0.01M HNO_3, and the tube agitated for 30 min. Following this, the tube was centrifuged and then the solution decanted. An additional 10 mL of 0.1M ammonium chloride (NH_4Cl) was added and the suspension dispersed, re-centrifuged and decanted. The combined solution was filtered, evaporated and digested with aqua-regia.

3.1.4 'Amorphous' Iron Oxide Phase (hydroxylamine)

To the sample remaining from the previous extraction was added 35 mL 0.25M $NH_2OH.HCl$ / 0.25M HCl, and the tube agitated at 50°C for 30 min. Following this, the tube was centrifuged and then the solution decanted. An additional 10 mL of 0.1M NH_4Cl was added and the suspension dispersed, re-centrifuged and decanted. The combined solution was filtered, evaporated and digested with aqua-regia.

3.1.5 Crystalline Iron Oxide Phase (partial extraction; hydroxylamine then citrate/dithionite)

To the sample remaining from the previous extraction was added 35 mL 1M $NH_2OH.HCl$ / 25% glacial acetic acid, and the tube agitated at 80°C for 16 hr. Following this, the tube was centrifuged and then the solution decanted. An additional 10 mL of 0.1M NH_4Cl was added and the suspension dispersed, re-centrifuged and decanted. To the tube was then added 35 mL 0.3M ammonium citrate (NH_4Cit) pH 7, and the suspension dispersed. Following this, 0.25 g sodium dithionite ($Na_2S_2O_4$) was added and the tube agitated for 16 hr. The tube was then re-centrifuged and decanted. Another 35 mL 0.3M NH_4Cit pH 7 and 0.15 g $Na_2S_2O_4$ was added as above and the tube agitated for 16 hr, then re-centrifuged and decanted as above. An additional 10 mL of 0.1M NH_4Cl was added and the suspension dispersed, centrifuged and decanted. The combined solution was filtered, evaporated down and digested with aqua-regia.

At this stage, the solids were still strongly coloured, indicating that substantial proportions of the Fe oxides were still present. This was also confirmed by XRD of the solids.

3.1.6 Residue dissolution

Most of the extraction residue was sent for fire assay ICP-MS analysis for Pt and Pd. The remaining 0.25g was mixed with 1.000g lithium metaborate in a Pt crucible and heated to 1000°C for at least 1 hr. This fusion was then dissolved in 1M HNO_3, 0.02% Triton X100 and 0.2% tartaric acid, made up to 100 mL and analysed for Al, Ba, Co, Cr, Cu, Fe, Mn, Ni, Ti, V, Y, Zn and Zr by ICP-AES.

Results for the extractions are compiled in Appendix II and illustrated in Figures 4 - 22.

3.2 Major Element Results

As expected, Al (Figure 4) was found predominantly in the residue, though minor amounts were also dissolved with the Mn oxide and amorphous hydrous Fe oxides (possibly due to poorly crystalline Al phases such as allophane) and in the crystalline Fe oxides (possibly due to Al incorporated in Fe oxides). Iron dissolved by citrate dithionite (Figure 5) presumably represents minerals such as hematite or goethite (with only partial Fe oxide dissolution in this experiment), with smaller amounts of Fe observed in the amorphous Fe phase. Separate Mn oxide phases were observed (Figure 6) at depth, possibly from release of Mn during weathering of primary minerals, and in the 0-1m sample, possibly due to specific surface breakdown of minerals by organic ligands (Huang and Keller, 1970, 1971) or to physical transport of weathered saprolite from elsewhere. Manganese does not occur in a separate phase in the laterite and mottled zones between 1 - 10 m, but is instead associated with Fe oxides.

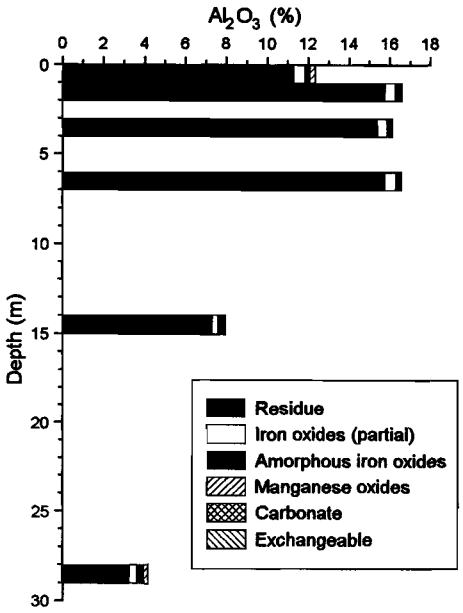

Figure 4: Al extraction from MC24 samples - Experiment A.

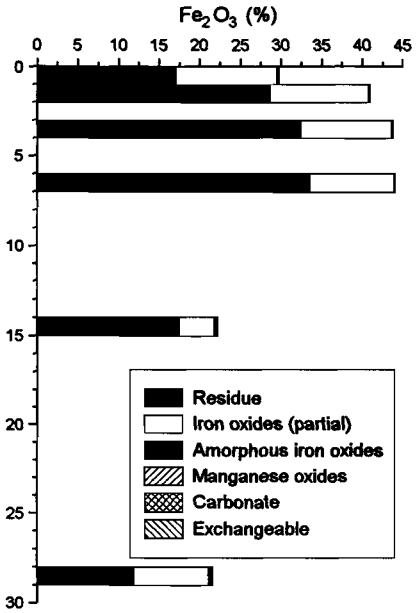

Figure 5: Fe extraction from MC24 samples - Experiment A.

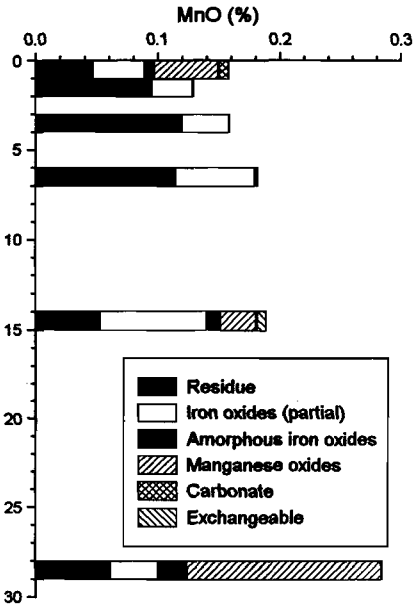

Figure 6: Mn extraction from MC24 samples - Experiment A.

High Ca concentrations (Figure 7) were observed at the surface, where it is found in the exchangeable phase (possibly as gypsum) and in carbonates (as calcite and dolomite), and at depth in an insoluble phase (possibly in tremolite or saponite). The distribution of Mg (Figure 8) is similar to Ca, whereas Na (Figure 9) is found primarily in the exchangeable phase. (The Na observed in the residue is probably an artefact of the high Na content of the previous extractant.)

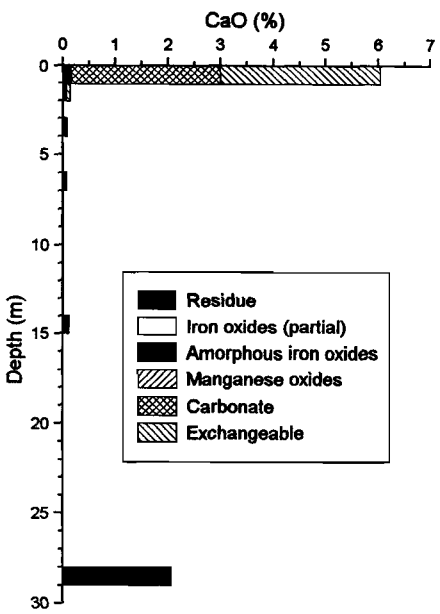

Figure 7: Ca extraction from MC24 samples - Experiment A.

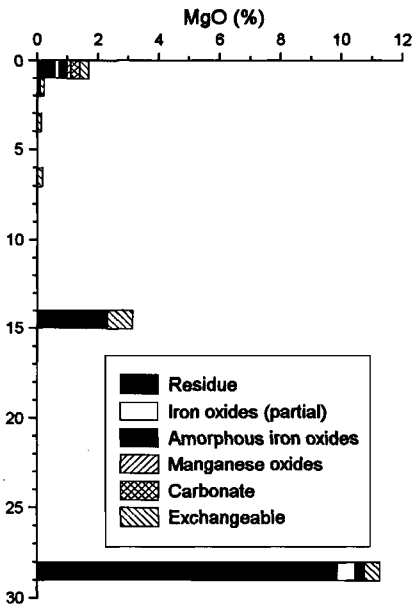

Figure 8: Mg extraction from MC24 samples - Experiment A.

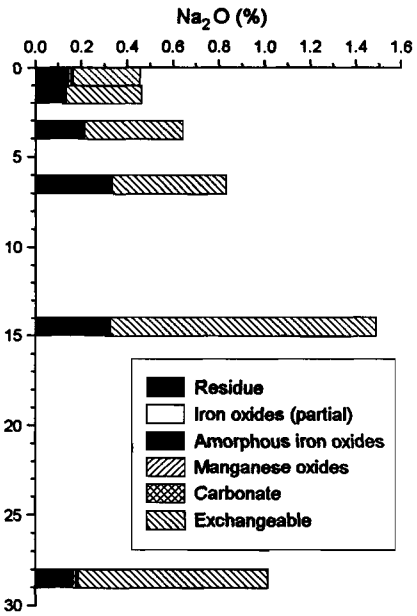

Figure 9: Na extraction from MC24 samples - Experiment A.

3.3 Minor Element Results

Titanium is generally resistant to dissolution (Figure 10), though some Ti is dissolved with the crystalline Fe oxide phase. This is consistent with observations of various extractable Ti-Fe oxides in weathering profiles (Bailey *et al.*, 1956; Anand and Gilkes, 1984), such as psuedorutile ($Fe_2Ti_3O_9$; Grey and Reid, 1975; Fitzpatrick *et al.*, 1978), and the observed substitution of Ti for Fe in crystalline Fe oxides (Hutton, 1977). Both Zr and Zn were totally resistant to the reagents used in this experiment (Figures 11 and 12), with Zr presumably located in resistant minerals such as zircon, and Zn possibly located in spinels.

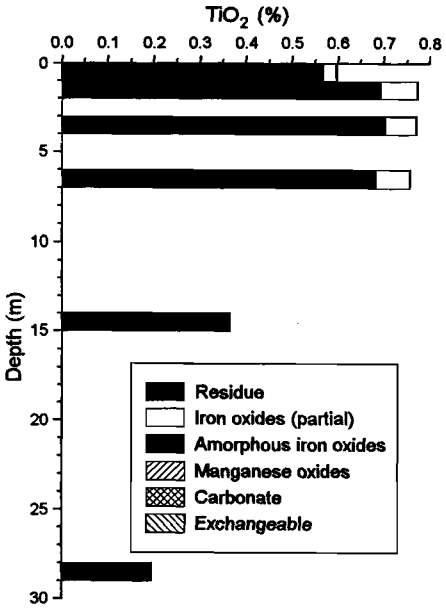

Figure 10: Ti extraction from MC24 samples - Experiment A.

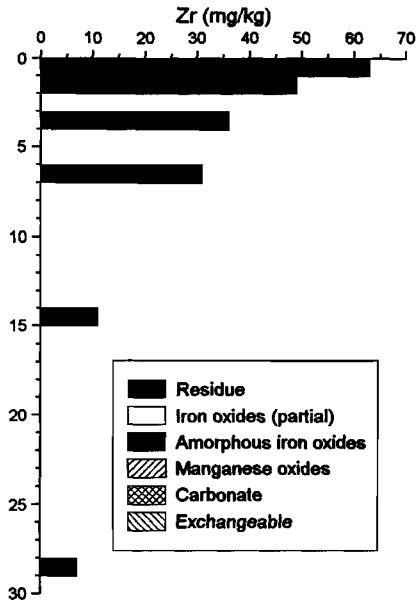

Figure 11: Zr extraction from MC24 samples - Experiment A.

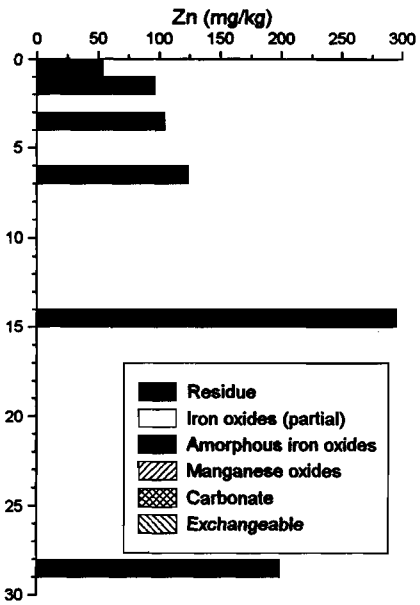

Figure 12: Zn extraction from MC24 samples - Experiment A.

Barium, most abundant at the surface and at 14-15m, appears to be associated with a number of different phases (Figure 13). The relatively low amounts of Ba in the residue suggest little tendency to form barite in this system, possibly due to high alkalinities causing Ba carbonates to form. Yttrium (Figure 14) also shows mixed associations, whereas Co (Figure 15) has a strong tendency to be associated with Mn when separate Mn oxide phases are present (*i.e.*, 0-1m and at depth; Figure 6).

Copper, V, Cr and Ni (Figures 16 - 19) are at least partially associated with crystalline Fe oxides, although significant concentrations may occur in the residue fractions. Copper, V and Ni are also present in the amorphous Fe and Mn oxide phases, particularly in the 0-1m sample..

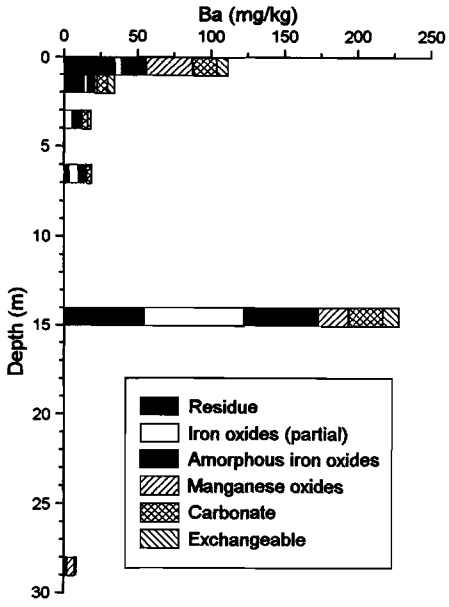

Figure 13: Ba extraction from MC24 samples - Experiment A.

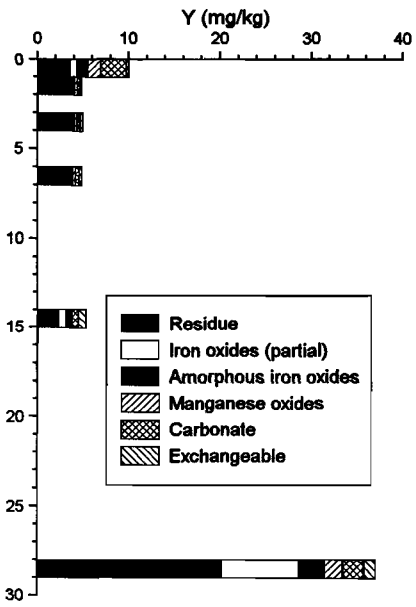

Figure 14: Y extraction from MC24 samples - Experiment A.

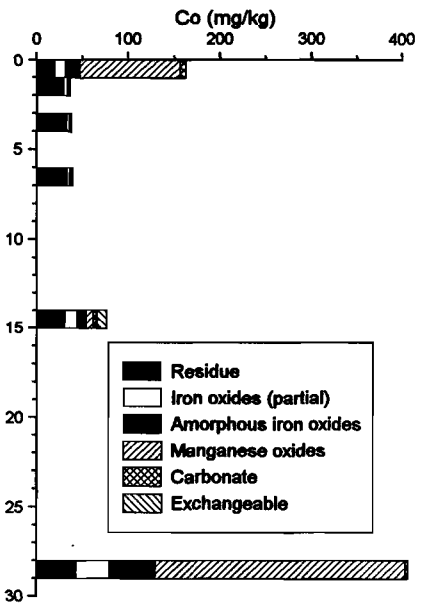

Figure 15: Co extraction from MC24 samples - Experiment A.

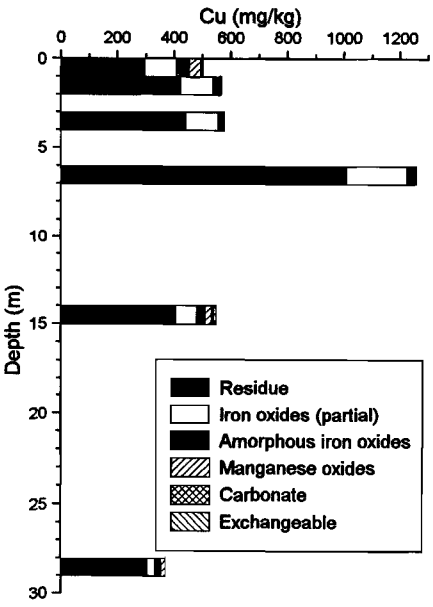

Figure 16: Cu extraction from MC24 samples - Experiment A.

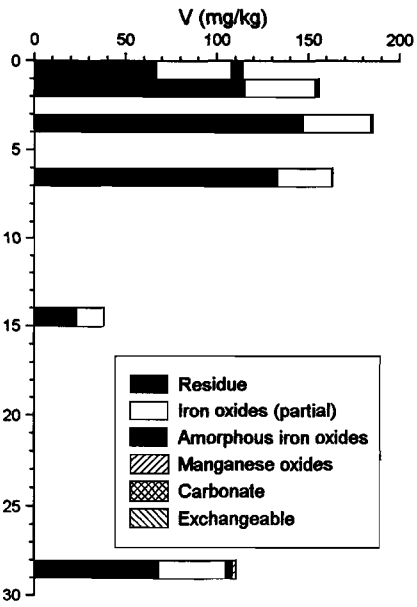

Figure 17: V extraction from MC24 samples - Experiment A.

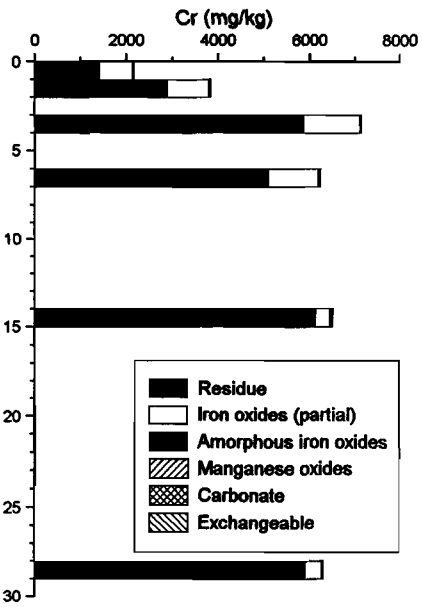

Figure 18: Cr extraction from MC24 samples - Experiment A.

3.4 Platinum and Palladium Results

Particularly significant concentrations of Pt (Figure 20) and, to a lesser extent, Pd (Figure 21) were extracted, and seem to be particularly associated with the Fe oxide phase. Similarly to the other minor elements, increased concentrations of Pt were dissolved from the more amorphous phases at 0-1m and 28 - 29 m.

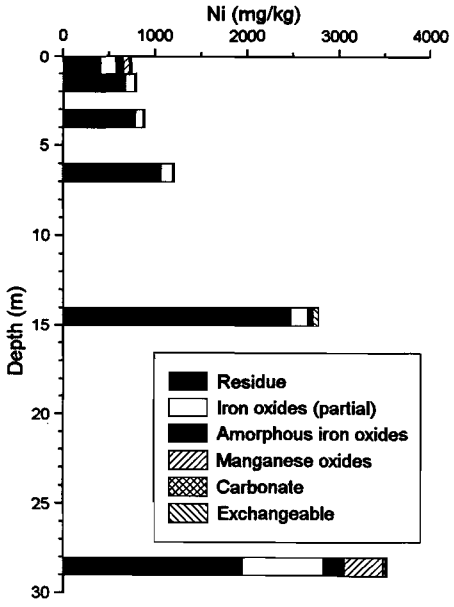

Figure 19: Ni extraction from MC24 samples - Experiment A.

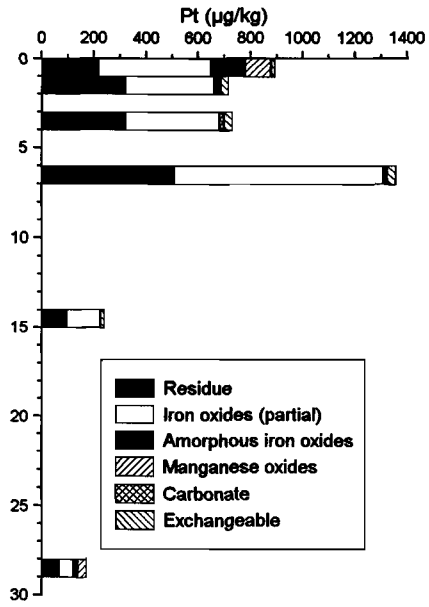

Figure 20: Pt extraction from MC24 samples - Experiment A.

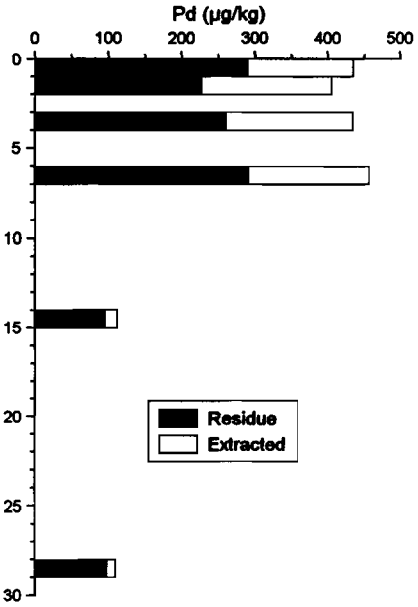

Figure 21: Pd extraction from MC24 samples - Experiment A.

These data suggest that the Fe oxide fraction is of major importance in controlling the distribution of Pt and Pd, in addition to the incorporation of the first row transition elements. Subsequent experiments concentrated on the Fe oxide fraction, both in terms of obtaining more information on the form of the association, and demonstrating it to be genuine and not an experimental artefact.

4 SELECTIVE EXTRACTION EXPERIMENT B - IRON OXIDE PHASES

4.1 Introduction

The citrate-dithionite (CD) solution is highly selective for free Fe oxides, such as goethite and hematite, in the upper lateritic horizons, but it is less selective in deeper saprolite samples (*e.g.* MC 24 28-29m), because it may attack other Fe-rich phases such as saponite. In this experiment, a citrate-thiosulphate (CT) reagent was used as a blank to ensure that dissolved Pt and Pd were genuinely associated with Fe oxides and not just extracted from some other phase as a side-reaction. This reagent should have as great (or greater) extractive strength for Pt and Pd (Volume I, Chapter 3), but little ability to dissolve Fe oxides. Thus, comparison of the results from the CD and CT extractions should indicate how much of the Pt and Pd dissolved by CD is associated with Fe oxides.

4.2 Citrate Dithionite Scheme

Three samples were tested: namely MC 24 0-1m, MC 24 3-4m and MC 24 28-29m. In order to avoid problems with Pd analysis of solutions observed for Experiment A, solutions for Pt and Pd analysis were dried on pure silica powder in plastic duranols, which were then used directly for Pb collection fire assay. This method gave good reproducibility (< 5 % error) and recovery. The extractions were done twice: the first (in which two MC 24 0-1m samples were used) yielded solutions for Al, Co, Cr, Fe, Mn and Ni analysis by AAS and for Ti analysis using the spectrophotometric Tiron method (Pruden and King, 1969); the second (using a reagent blank) yielded solutions for Pt and Pd analysis, as described above. All extractions were conducted sequentially, as described below.

4.2.1 Crystalline iron oxide phase (citrate dithionite)

Thirty five mL 0.3M NH_4Cit pH 7 was added to 1.2g sample, and the suspension dispersed. Following this, 0.25 g $Na_2S_2O_4$ was added and the tube agitated for 30 min at 80°C. The tube was then centrifuged (4000 rpm, 15 min) and decanted. An additional 10 mL of 0.1M NH_4Cl was added and the suspension dispersed, centrifuged and decanted. Where PGE analysis was required, the combined solution was then dried over silica, and then sent for fire assay. Where analyses of the other elements (Al, Co, Cr, Fe, Mn, Ni and Ti) were required, the combined solution was dried and digested with aqua-regia and the solution was made up to 25 mL with 1M HCl / 0.3M HNO_3 for analysis. This encompassed one CD treatment.

This process was repeated four times (*i.e.*, a total of five CD treatments, with analyses for each individual treatment). At this stage the solids were no longer strongly coloured, indicating that virtually all of the Fe oxides had been dissolved.

4.2.2 Aqua-regia extraction

To the sample remaining from the previous extraction was added 16 mL concentrated (conc) HCl, the suspension dispersed, 9 mL conc HNO_3 added and the tube heated for 60 min at 80°C. The tube was then centrifuged and decanted. An additional 10 mL of 0.2M HCl was added and the suspension dispersed, centrifuged and decanted. Where PGE analysis was required, the combined solution was then dried over silica, and then sent for fire assay. Where analyses of the other elements (Al, Co, Cr, Fe, Mn, Ni and Ti) were required, the combined solution was taken to near-dryness and then made up to 25 mL with 1M HCl / 0.3M HNO_3 for analysis. This encompassed one aqua-regia treatment.

This process was repeated two times (*i.e.*, a total of three aqua-regia treatments, with analyses for each individual treatment).

4.2.3 Residue Analysis

The sample remaining in the centrifuge tubes from the previous extraction was carefully removed and dried over silica, and then analysed for Pt and Pd by fire assay.

4.3 Citrate Thiosulphate Scheme

The same samples were tested as for the CD extraction (Section 4.2), with the same analytical scheme. 35 mL 0.3M NH_4Cit pH 7 was added to 1.2g sample, and the suspension dispersed. Following this, 0.25 g sodium thiosulphate ($Na_2S_2O_3$) was added and the tube agitated for 60 min at 80°C. The tube was then centrifuged (4000 rpm, 15 min) and decanted. The analyses were performed as for the CD extraction. This encompassed one CT treatment.

This process was repeated four times (*i.e.*, a total of five CT treatments, with analyses for each individual treatment). At this stage the solids were still strongly coloured, indicating that substantial proportions of the Fe oxides were still present.

4.4 General Results

Tabulated results for the two extraction schemes are listed in Appendix III, and illustrated in Figures 23 - 31. Where duplicate MC24 0-1m samples were extracted, data for both samples is shown, so as to indicate the sampling and analytical errors. Thus, for example, Figure 22a shows the cumulative Fe dissolved with ongoing CD treatments. For ease of comprehension, this has been plotted as % of the total Fe. MC24 3-4 (from the laterite zone) shows a linear Fe dissolution for the first 3 CD treatments, with the remainder of the Fe dissolved in the fourth treatment. This is consistent with all of the Fe being present in this sample as free Fe oxides, such as goethite and hematite. MC24 0-1m shows a similar dissolution, while MC24 28-29m did not show complete Fe dissolution, even after 5 CD

treatments, with about half of the remaining Fe dissolved by aqua-regia. Thus, the saprolitic sample MC24 28-29m, unlike the laterite material, may contain Fe in a number of phases, including free Fe oxides, other, less CD extractable phases (possibly saponite), and a resistate phase (possibly ilmenite).

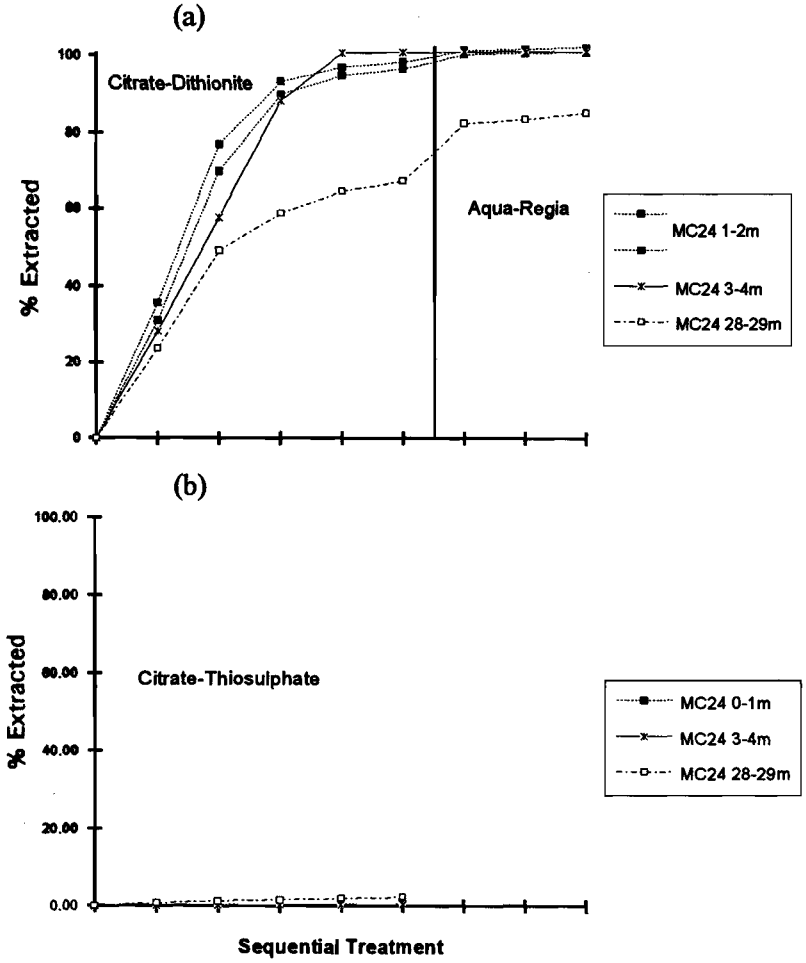

Figure 22: Sequential Extraction of Fe from MC24, using (a) citrate-dithionite, and (b) citrate-thiosulphate.

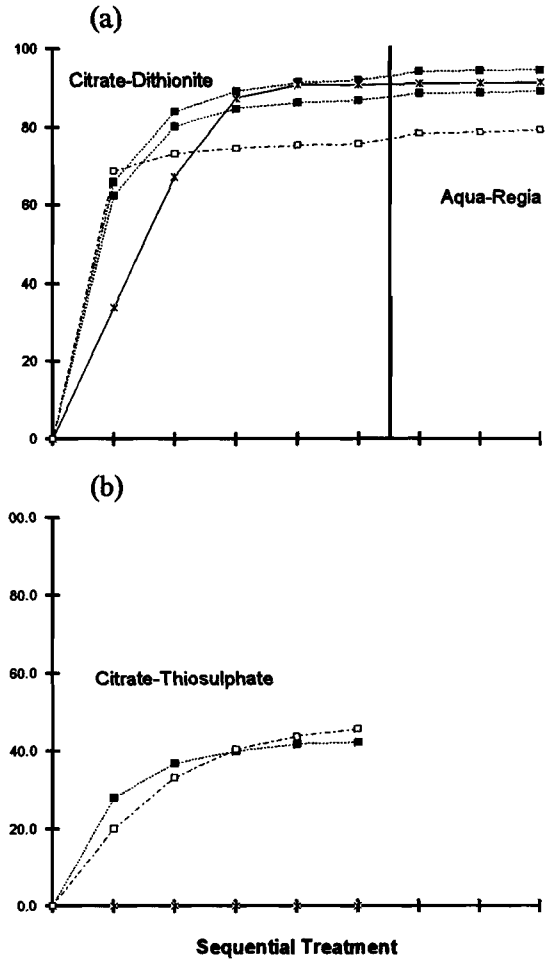

Figure 23: Sequential Extraction of Mn from MC24, using (a) citrate-dithionite, and (b) citrate-thiosulphate.

Dissolution of Fe oxides with the CD solution is initaited by reduction of Fe by dithionite, with the citrate providing the ligating capacity to maintain metals in solution. The CT treatment was very poor at dissolving Fe (Figure 22b), due to the absence of a reducing agent.

The dissolution of Mn from MC24 3-4m (Figure 23a,b) showed virtually the same trend as Fe, consistent with earlier observations (Section 3.2; Figure 6) that Mn is primarily located in Fe oxides at this depth. The 0-1m and 28-29m samples showed faster dissolution of Mn with CD, and appreciable dissolution with CT, due to the high solubility of the separate phase Mn oxides in these samples (Section 3.2).

Extraction results for Cr from MC24 3-4m (Figure 24) indicated that Cr was primarily contained in Fe oxides at this depth. The 0-1m sample showed some unextractable Cr, whereas at 28-29m 80% of the Cr could not even be extracted after 3 aqua-regia treatments, indicating the predominance of Cr in a resistate phase, presumably chromite ($FeCr_2O_4$).

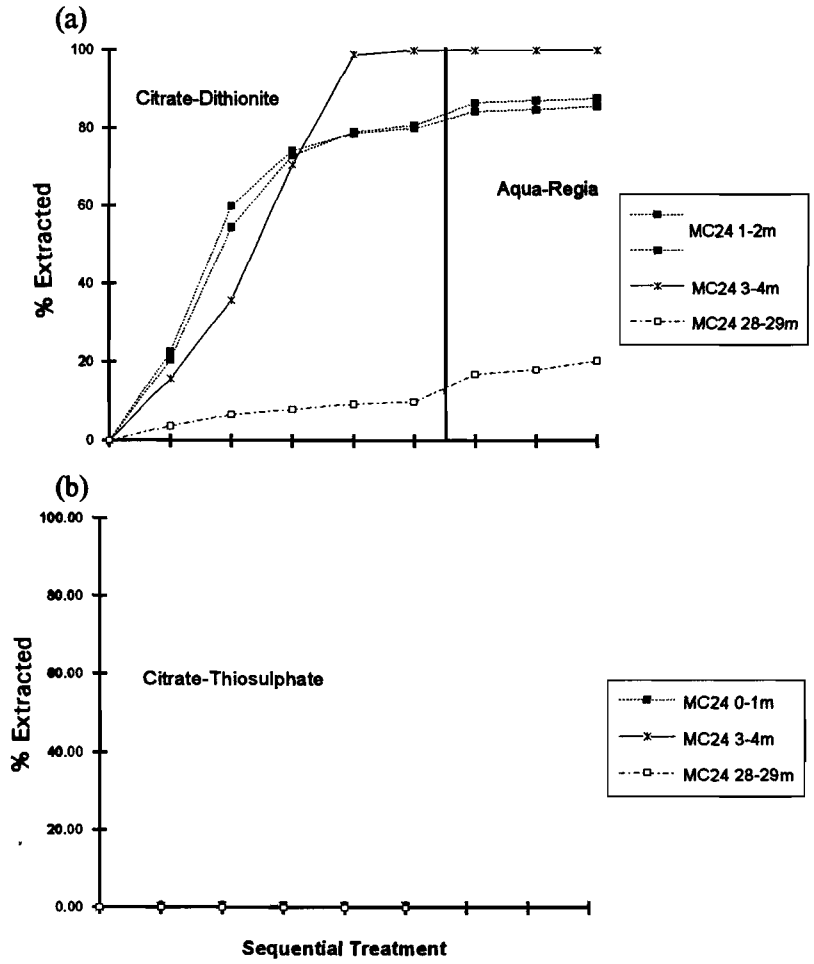

Figure 24: Sequential extraction of Cr from MC24, using (a) citrate-dithionite, and (b) citrate-thiosulphate.

The 10 - 15% of the Al dissolved by CD (Figure 25) possibly represents poorly crystalline Al minerals and Al substituted in Fe oxides. The remainder of the Al was highly insoluble, except at 0-1m, where an additional 40% of the Al was dissolved by aqua-regia. The behaviour of Ti (Figure 26) was similar, with some dissolved with the Fe oxides and most of the remainder being highly intractable.

Dissolution of Co (Figure 27) closely matched that of Mn (Figure 23), supporting previous observations (Section 3.2). The Ni extraction data (Figure 28) suggests that most of the Ni is associated with Fe oxides in the two shallow samples, but with an additional, aqua-regia soluble, fraction.

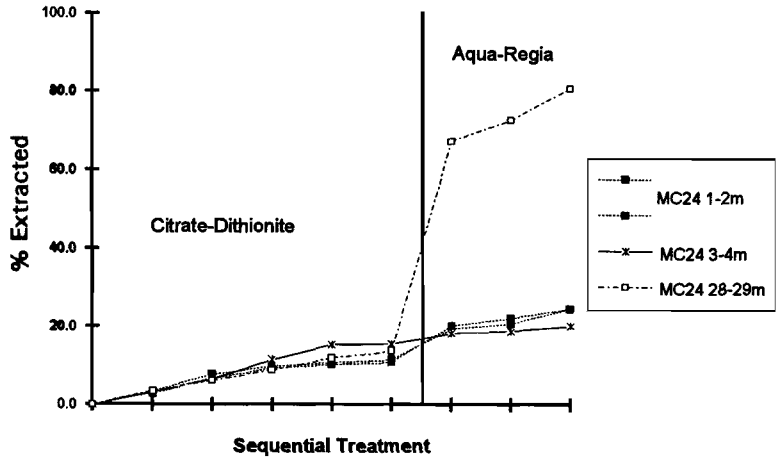

Figure 25: Sequential extraction of Al from MC24 using citrate-dithionite.

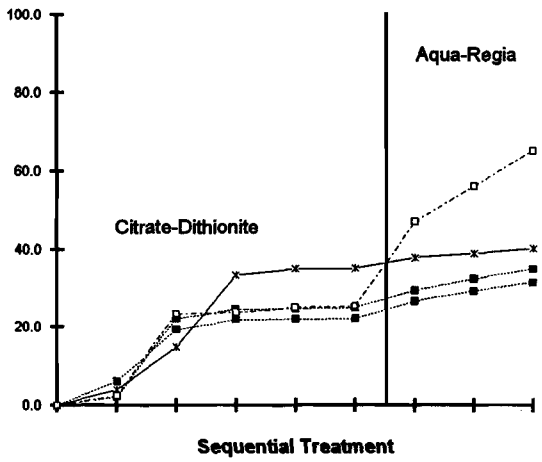

Figure 26: Sequential extraction of Ti from MC24 using citrate-dithionite.

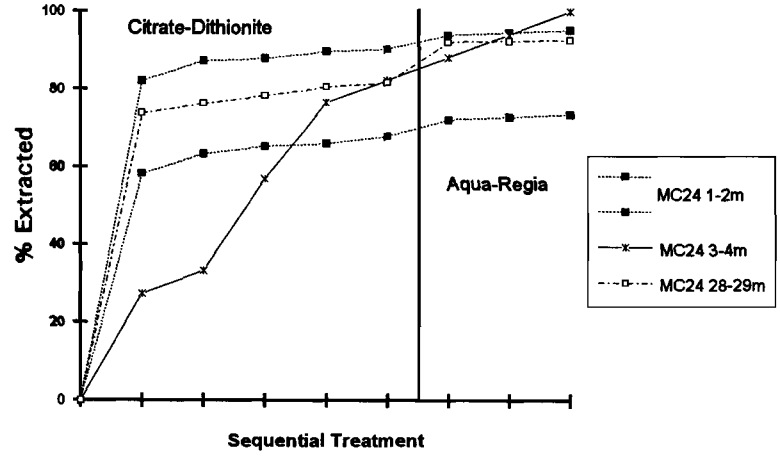

Figure 27: Sequential extraction of Co from MC24 using citrate-dithionite.

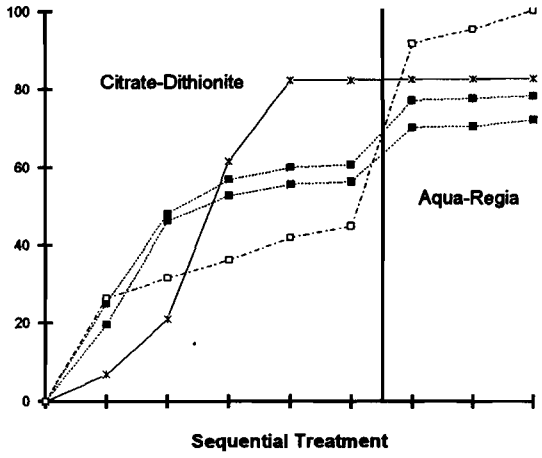

Figure 28: Sequential extraction of Ni from MC24 using citrate-dithionite.

4.5 Platinum and Palladium Results

Between 30 and 60 % of the Pt is dissolved by CD (Figure 29a), while less than 20% is dissolved by CT (Figure 29b). Given that thiosulphate should have a strong capacity to dissolve Pt and Pd if the solution has access to the element (Volume I, Chapter 3), this indicates that in the upper lateritic horizons a major proportion of the Pt is integrally associated with the Fe oxides. Note that CT does dissolve Mn oxides present as separate phases (Figure 23b), so that the low solubility of Pt in CT also indicates that only a small (< 20%) proportion of the Pt can be associated with Mn oxides, consistent with earlier observations (Figure 20).

Palladium (Figure 30) is less strongly associated with Fe oxides than Pt. In the Fe-rich MC24 3-4m sample, a maximum of about 25% of the Pd is associated with Fe oxides, with even lower contents in the other samples. Most of the Pd is extracted with aqua-regia, indicating that the Pd is NOT primarily associated with chromite (note the low solubility of Cr in aqua-regia; Figure 24a). Thus, it is not clear from this experiment what phase is holding Pd in these samples.

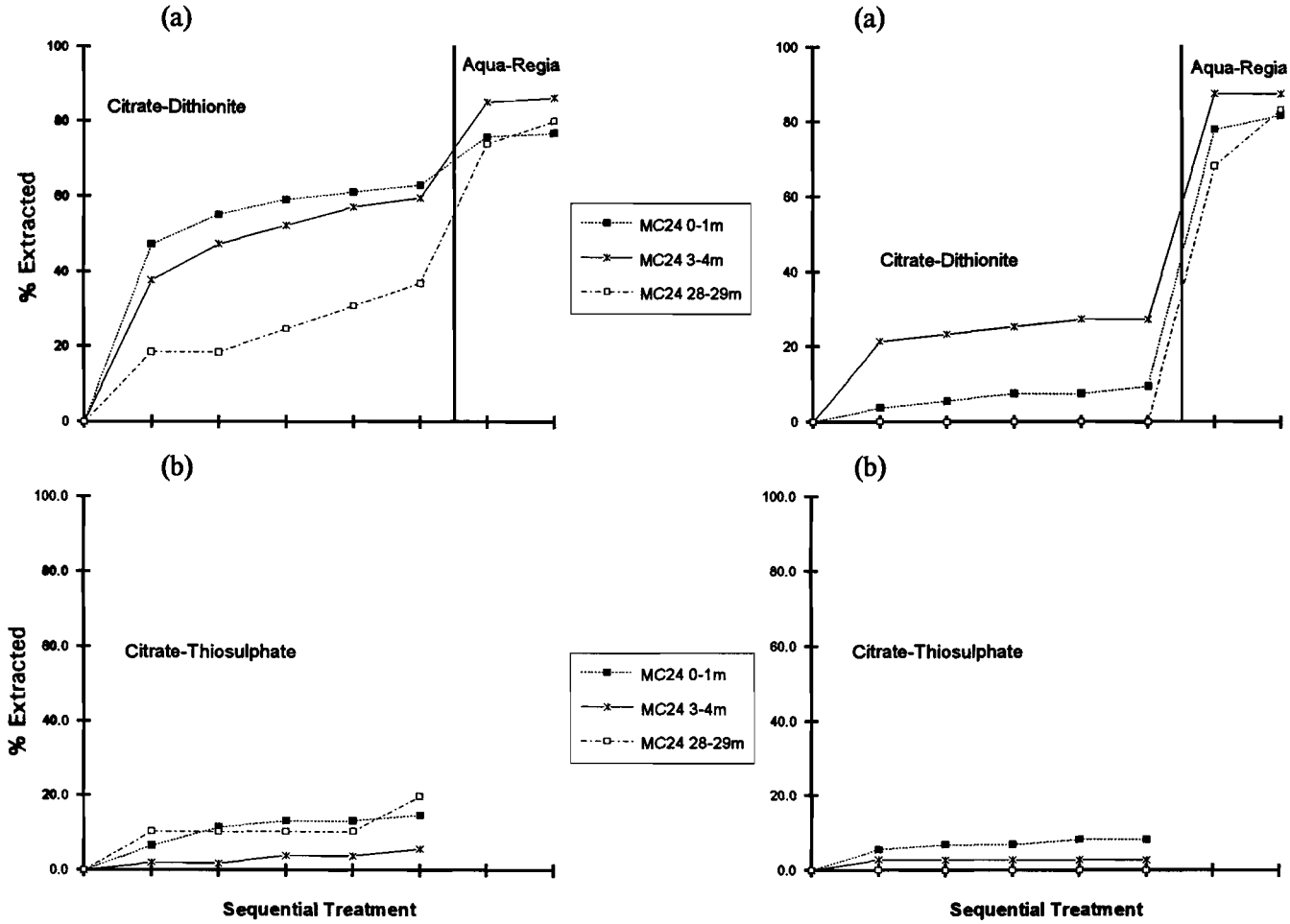

Figure 29: Sequential extraction of Pt from MC24, using (a) citrate-dithionite, and (b) citrate-thiosulphate.

Figure 30: Sequential extraction of Pd from MC24, using (a) citrate-dithionite, and (b) citrate-thiosulphate.

5 EXPERIMENT C - HIGH GRADIENT MAGNETIC SEPARATION AND SELECTIVE EXTRACTION

5.1 Introduction

Results from the previous experiments indicated that a large proportion of the Pt and a minor proportion of the Pd is associated with Fe oxides in MC24 samples, which is clearly of significance in understanding the geochemistry of these elements. However, there are potential complications in selective extraction interpretations. Citrate-dithionite may not just extract crystalline Fe oxides, but may also solubilize sub-crystalline alumina and/or silica (and possibly other sub-crystalline phases) that have been "occluded" within crystalline Fe oxides (Gray, 1986). In addition to resolving whether this effect is important, it is also of interest to determine whether Pt and Pd are hosted by goethite or hematite, since these minerals have different origins in soils (Dixon and Weed, 1989). The experiment described here was formulated to further investigate some of these items, and to provide further information on these elements.

The extraction regime involved Tamm's acid oxalate (TAO) extraction, followed by CD extraction. Various workers (Fey and le Roux, 1977; Fitzpatrick *et al.*, 1978; Schwertmann *et al.*, 1982; Childs *et al.*, 1983; Farmer *et al.*, 1983; 1984) have demonstrated that TAO effectively dissolve various weakly crystalline Fe, Al, Si and Ti minerals, without dissolving crystalline Al, Fe, Si or layer silicate

minerals (McKeague and Day, 1966; Yershova *et al.*, 1981), whereas, as discussed earlier (Section 4.1), CD is highly selective for Fe oxides in oxidized weathered profiles. Many workers have utilized TAO and CD extractants together, in differentiation of profiles (McKeague and Day, 1966; Blume and Schwertmann, 1969; McKeague *et al.*, 1971); in analysing pedological processes (Ball and Beaumont, 1972; Alexander, 1974; Herbauts, 1982); and in determining Al substitution in Fe oxides (Bigham *et al.*, 1978; Torrent *et al.*, 1980). Thus, this scheme represents use of a common pedological tool.

In this investigation, two additional techniques, High Gradient Magnetic Separation (HGMS) and Differential X-ray Diffraction (D-XRD), were used in order to provide additional information on the associations of Pt and Pd with mineral phases. The descriptions and rationale of these techniques are given in Sections 5.2 and 5.3. By a combination of all these methods, important phases for Pt and Pd accumulation in soil and regolith were able to be recognized.

5.2 High Gradient Magnetic Separation

Clearly, the investigation of the role of Fe oxides would be greatly facilitated by utilising a method causing concentration of Fe oxides. High Gradient Magnetic Separation (HGMS) is a procedure for the separation of material into a magnetic fraction in which all of the common Fe oxides in the regolith may be concentrated, not just magnetic and maghemite, as in most other magnetic concentration methods. Comprehensive description of the theory and practises of HGMS is given in Schulze (1988) and only a brief description of relevant factors will be given here.

In effect, any material with a high magnetic susceptibility will be concentrated by this procedure, whereas any diamagnetic material will not be concentrated. The magnetic susceptibilities of some representative compounds are shown in Table 1. Magnetic susceptibility is a function of unpaired electrons, and therefore is high in mid-row transition metals (*e.g.*, Fe and Mn), and lower in metals at the beginning (*e.g.*, Ti) or end (*e.g.*, Pt and Pd) of the transition row, and will be negative in totally electron paired compounds, such as minerals of Al, Si or Ca. Thus, Fe and Mn oxide minerals and Fe-rich clay minerals such as nontronite will have a high magnetic susceptibility and are likely to be concentrated by HGMS, whereas quartz and clay minerals such as kaolinite will not be.

Using HGMS, previous workers (Schulze and Dixon, 1979; Hughes, 1982) have achieved Fe oxide concentrations from 1.3 up to ten times, with work on lateritic soils in the Northern Territory (Gray, 1986) concentrating Fe oxides up to 3 times. Poor Fe oxide concentration is sometimes observed, which could be due to clay-Fe oxide binding preventing separation of these two phases. Various authors (Follett, 1965; Jefferson *et al.*, 1975; Gendler *et al.*, 1981; Yershova *et al.*, 1981) have observed, in laboratory syntheses and nature, strong binding of Fe oxides with the clay minerals kaolinite and smectite. Golden and Dixon (1985) describe how, in a kaolin-Fe oxide system, the presence of three pedological phases - free Fe oxides, free kaolin, and kaolin bound to Fe oxides - will explain the presence of high levels of kaolin in their magnetic concentrates.

Therefore, it is expected that this method, although not achieving total separation between the Fe oxide and 'clay' phases, should enable production of Fe oxide enriched materials (called magnetic concentrates), and Fe oxide depleted materials (called non-magnetic residues). Comparison of the elemental concentrations, and the selective extraction results, for these different sub-samples should enhance our understanding of the Pt and Pd association with various soil phases.

Table 1: Magnetic Susceptibility of Important Elements and Compounds.

Element/Compound	Magnetic Susceptibility (10^{-6} cgs) *
NaCl	-30
$CaCO_3$	-38
$CaSO_4.2H_2O$	-74
Al_2O_3	-37
SiO_2	-30
TiO_2	+6
Cr_2O_3	+1960
Mn_2O_3	+14100
Fe_2O_3	+3586
Co_2O_3	+4560
NiO	+660
CuO	+239
ZnO	-46
Au	-28
Pd	+567
Pt	+202
Pt_2O_3	-38

* Collated from Weast (1984)

5.3 Differential X-ray Diffraction

D-XRD involves computer acquisition of the XRD pattern of a sample before and after selective dissolution of specific phases, such as Fe oxides. The two patterns are subtracted from each other, following normalization, giving by difference the XRD pattern due to the dissolved phases alone. This has been shown to allow determination of Fe oxides at lower concentrations than by conventional XRD: Schulze (1981) stated that Fe oxides could be detected by D-XRD down to 1.8 % Fe and Brown and Wood (1985), using a more sophisticated technique of computer simulation of the differential pattern, could determine hematite and goethite contents down to 1 %.

Additionally, the ability to produce D-XRD patterns of the soil Fe oxides without interferences from reflections from other minerals enables calculation of mineral parameters that generally would not be possible using normal XRD patterns. In this study, D-XRD was used to calculate the relative levels of goethite and hematite, based on the integrated intensities of representative reflections (Torrent *et al.*, 1980; Kämpf and Schwertmann, 1982; Brown and Wood, 1985). As described below, these concentrations may be related to the degree or nature of the association between PGEs and Fe oxides in the regolith.

5.4. Methods

5.4.1 Particle Size Analysis and Separation

Particle size separation was required to prepare < 2 μm slurries for HGMS. The six samples utilized were MC 24 3-4m, MC 24 6-7m, MC 24 8-9m, MC 24 14-15m, MC 24 22-23m and MC 24 28-29m, which were ground to < 75 μm. The samples (50 g) were dispersed in 1000 mL water, using Calgon (sodium polyphosphate) at pH 8.5 as required. The < 2 μm fraction, as defined by Stokes' Law (McIntyre, 1974), was collected by siphoning off the upper 10 or 20 cm of the suspension, 8 or 16 h

respectively after agitation, at 20°C. This process was repeated up to eight times, until the suspension collected was virtually clear. The collected suspensions were combined.

The 2 - 20 μm fraction was separated by washing all the sediment left from the clay separation into a 250 mL beaker and adjusting the suspension up to 10 cm height. The mixture was agitated at 20°C and the suspension decanted off 4 min 48 sec later. This process was repeated until the decanted suspension was virtually clear. The suspensions were combined and dried at 60 - 70°C.

The remaining solid residue from the separation (the > 20 μm fraction) was dried at 60 - 70°C.

5.4.2 High Gradient Magnetic Separation

The < 2 μm fractions of the six samples were treated by HGMS to concentrate the Fe-rich fraction. The method is described in Appendix IV. The three different fractions produced were:

(i) the untreated sample (*i.e.*, the < 2 μm fraction);
(ii) the magnetic concentrate (MC);
(iii) the non-magnetic residue (NMR).

The > 20 μm, 2 - 20 μm, < 2 μm, MC and NMR fractions were analysed by NAA, XRF and fire assay ICP-MS for SiO_2, Al_2O_3, Fe_2O_3, MnO, MgO, CaO, Na_2O, K_2O, TiO_2, P_2O_5, Ba, Ce, Cl, Cr, Co, Cu, Ga, Ni, S, Sr, V, Y, Zn, Zr, Pt and Pd, and mineralogically analysed by XRD. The Na_2O and P_2O_5 values are meaningless due to contamination from Na and P in the Calgon used to disperse the suspension. The elements La, Nb, Pb, Rb, were analysed for, but were below the detection limits [about 10 mg/kg (ppm) for these samples]. The < 2 μm, MC and NMR fractions of the six samples were then used for sequential extractions, as described below.

5.4.3 Tamm's Acid Oxalate Extraction

Twenty mL TAO reagent (0.175M ammonium oxalate / 0.100M oxalic acid) was added to 1.2g sample, and the mixture shaken for 4 hr in the dark. The tube was then centrifuged (4000 rpm, 15 min) and the solution decanted. An additional 10 mL of 0.1M NH_4Cl was added and the suspension dispersed, re-centrifuged and decanted. The combined solution was then split: 90% was dried over silica, and then sent for fire assay ICP-MS analysis for Pt and Pd; the remaining 10% of the solution was digested with aqua-regia and made up to 50 mL with 0.2M HCl for analysis for Fe, Mn, Cr, Al, Na, Cu and Ni by AAS, for Ti by the Tiron method and for PO_4 by the Fogg and Wilkinson (1958) method.

5.4.4 Citrate Dithionite Extraction

To the sample remaining from the previous extraction was added 35 mL 0.3M NH_4Cit pH 7, and the suspension dispersed. Following this, 0.5 g $Na_2S_2O_4$ was added and the tube agitated for 30 min at 80°C. The tube was then centrifuged (4000 rpm, 15 min) and decanted. Additional CD treatments were made until the Fe oxide colour was bleached from the solid. An additional 10 mL of 0.1M ammonium chloride (NH_4Cl) was added and the suspension dispersed, re-centrifuged and decanted. The combined solution was then split: 90% was dried over silica, and then sent fire assay ICP-MS analysis for Pt and Pd; the remaining 10% of the solution was digested with aqua-regia and made up to 50 mL with 0.2M HCl for analysis for Fe, Mn, Cr, Al, Na, Cu, Ni, Ti and PO_4 as above.

5.5 Particle Size Separation Results

Results for all of the fractions (*i.e.*, > 20 μm, 2 - 20 μm, < 2 μm, MC and NMR) are tabulated in Appendix V. The particle size distributions vary down the profile (Figure 30): the three samples within the laterite zone (3-4m, 6-7m, 8-9m) were similar, whereas the saprolite (14-15m) has the highest proportion of the < 2 μm fraction. The proportion of coarser material increased with depth below 20 m.

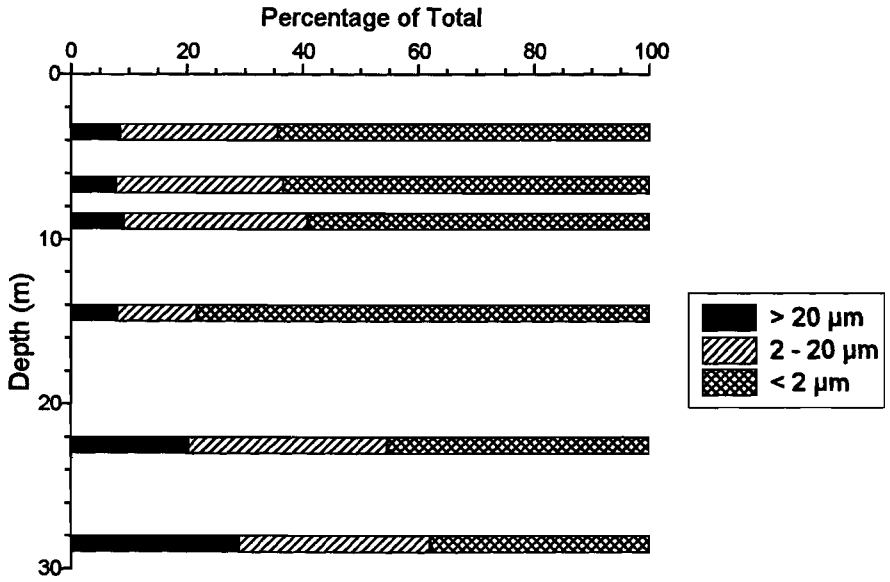

Figure 30: Particle size distribution of MC24 samples.

As can be seen from Figure 30, if an element had a similar concentration in each size fractions for one of the shallow samples, then 60% of the total concentration would be accounted for by the < 2 µm fraction, because 60% of the material is in this fraction. On the basis of this effect, the particle size separations of some of the elements of interest are shown in Figures 31 - 35. Thus, for MC24 0-1m, of the 16.7% Al_2O_3 in the entire sample, only 0.48% (= 3% of all of the Al_2O_3) is accounted in the > 20 µm fraction, whereas 14.1% (= 85% of all of the Al_2O_3 in the sample) is in the < 2 µm fraction (Figure 32), presumably as clay minerals such as kaolinite. This preponderance of Al in the < 2 µm fraction is repeated down the profile, indicating that Al is primarily located in fine-grained dispersed minerals (*e.g.*, kaolinite, smectite, saponite) throughout this profile.

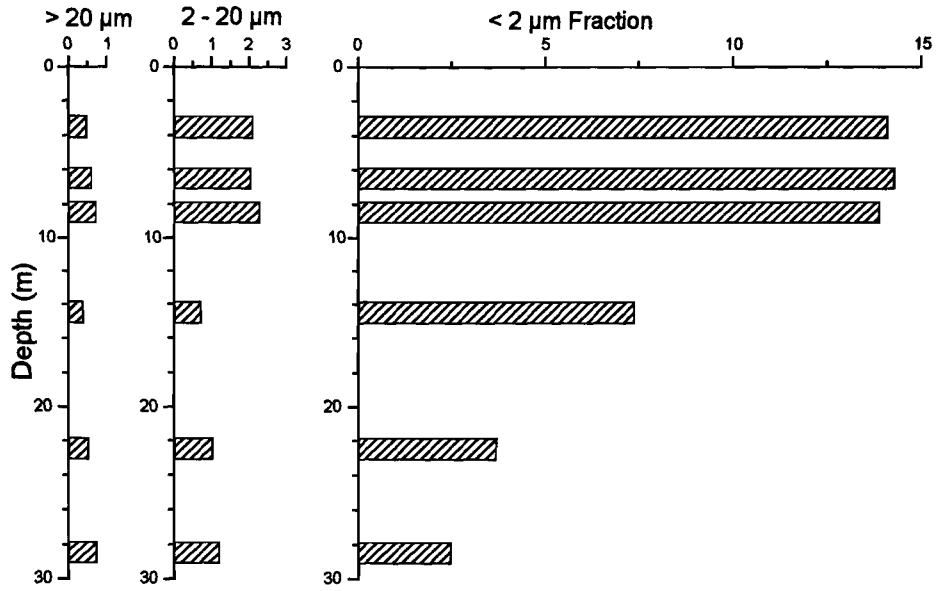

Figure 31: Absolute quantities (in %) of Al_2O_3 in the > 20 µm, 2 - 20 µm and < 2 µm fractions.

Data for Fe (Figure 32) indicate that it is primarily located in the 2 - 20 µm and < 2 µm fractions above 15m depth, and in the coarser fractions at depth. This does not mean that Fe in the coarser fractions

has a crystal size greater than 2 μm: XRD of the coarser fractions showed that the Fe oxides present in these fractions had virtually the same line broadening, and therefore similar crystal size, as in the < 2 μm fraction. Therefore, the high Fe in the 2 - 20 μm fraction appears to be caused by Fe oxide mineral aggregations that were not dispersed by the separation method.

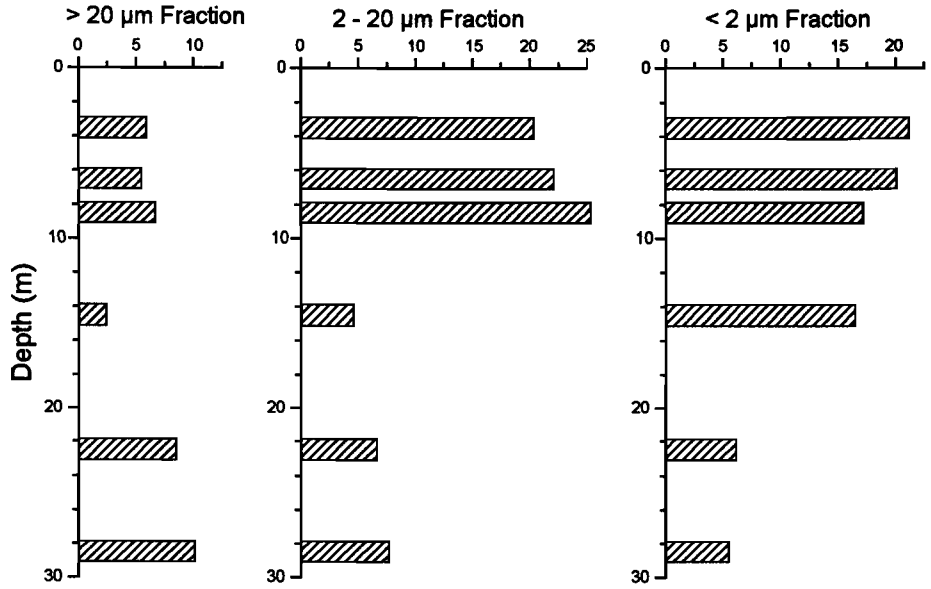

Figure 32: Absolute quantities of Fe_2O_3 (in %) in the > 20 μm, 2 - 20 μm and < 2 μm fractions.

Above 10 m depth, corresponding to the zone where Mn is incorporated into Fe oxides (Section 3.2, Figure 6), Mn is contained primarily in the 2 - 20 μm fraction, with moderate contents accounted for in the < 2 μm fraction (Figure 33). At depth, where Mn is present dominantly as easily extractable oxides, it is concentrated in the > 20 μm fraction. As with Fe, this does not represent large crystal size, but instead some consolidation into large aggregates that are not broken up during dispersion.

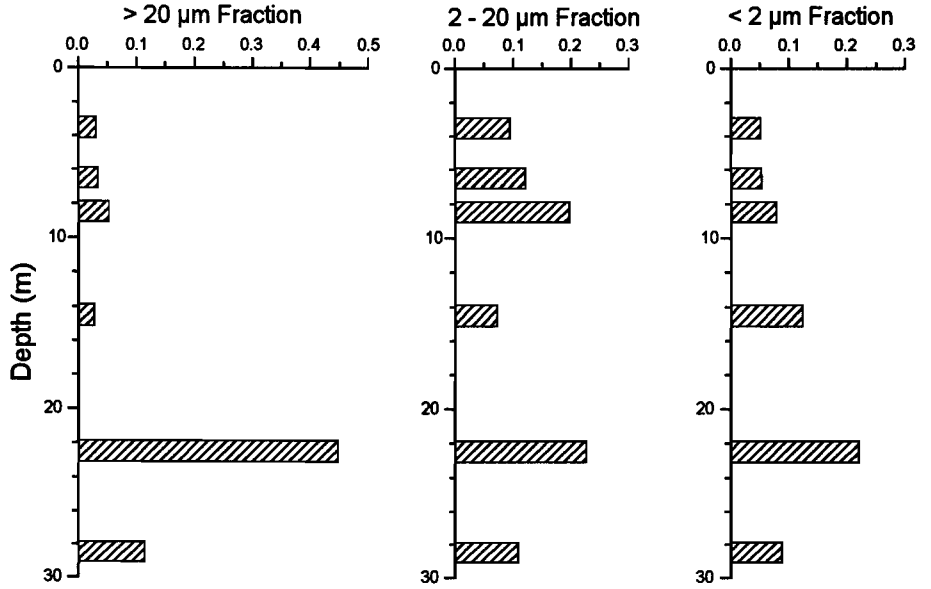

Figure 33: Absolute quantities of MnO (in %) in the > 20 μm, 2 - 20 μm and < 2 μm fractions.

The distribution of Pt (Figure 34) is similar to that of Fe (Figure 32) above 15m depth, in that both elements are primarily located in the 2 - 20 μm and < 2 μm fractions.

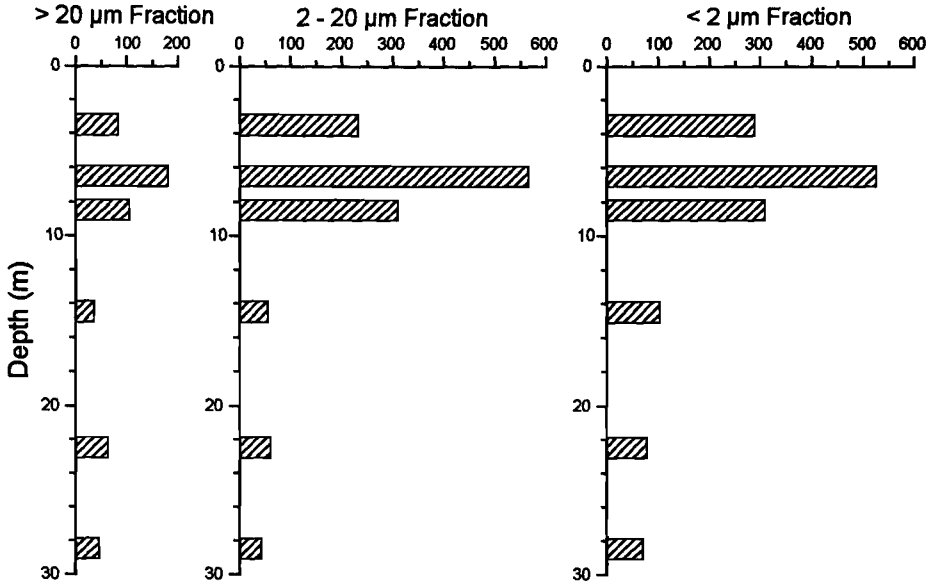

Figure 34: Absolute quantities of Pt (in μg/kg) from the > 20 μm, 2 - 20 μm and < 2 μm fractions.

The Pd distribution (Figure 35) differs from that for the other elements and is dominantly in the < 2 μm fractions of the samples. These data for Pt and, particularly Pd, demonstrate why attempts to investigate the mineralogy of PGEs by scanning electron microscopy have been unproductive.

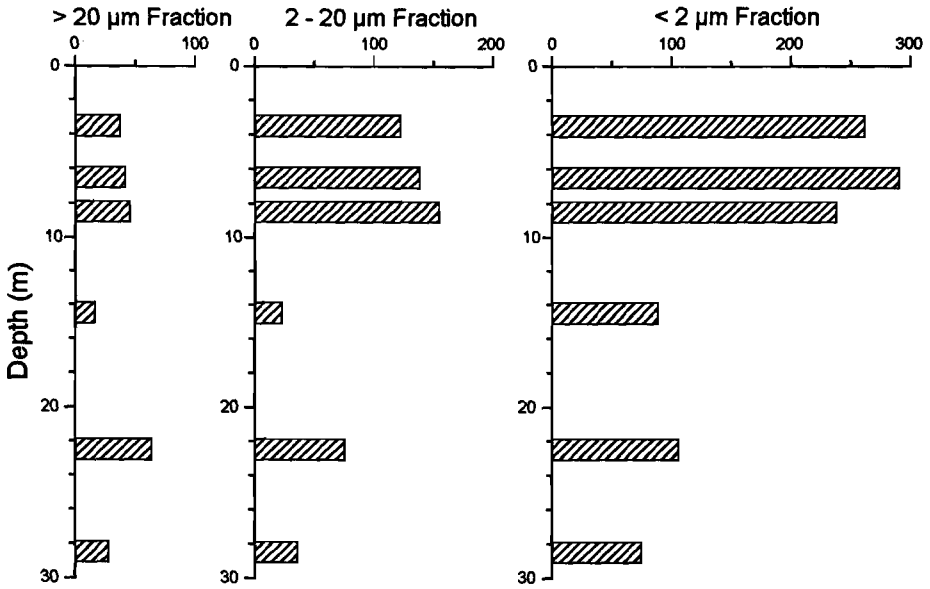

Figure 35: Absolute quantities of Pd (in μg/kg) from the > 20 μm, 2 - 20 μm and < 2 μm fractions.

5.6 High Gradient Magnetic Separation / Selective Extraction

The results for the HGMS of the MC24 samples are tabulated in Appendix V, with extraction results given in Appendix VI, and critical data shown in Figures 36 - 42. In the top 10 m of profile MC 24, Fe (Figure 36) was predominantly in the CD extractable phase[1] (crystalline Fe oxides), which was strongly concentrated by HGMS. D-XRD (Section 5.8) confirmed that the HGMS concentrate consists of goethite and hematite. A much smaller amount of Fe was found in the TAO extractable phase[1], indicating only minor amounts of 'amorphous' Fe oxides are present. The absolute and proportional amounts of resistate Fe was significantly greater in the deeper samples, and was poorly concentrated by HGMS, suggesting it represents Fe contained in minerals with only small magnetic susceptibilities (*e.g.*, saponite), rather than undissolved Fe oxides. Therefore, in these deeper samples. the total Fe was only weakly concentrated by HGMS, whereas CD extractable Fe was strongly concentrated by HGMS in all samples

The effect whereby different phases are concentrated by HGMS to different degrees can be seen even more graphically for Al (Figure 37). The resistate phase represents Al in various non-Fe dominated minerals (kaolinite, saponite, etc.), and is reduced in the magnetic concentrate, due to dilution by the raised level of Fe. On the other hand, CD extractable Al, which presumably represents Al substituted in Fe oxides, is, as expected, concentrated by HGMS. The small levels of TAO extractable Al possibly represent amorphous and/or cryptocrystalline Al minerals.

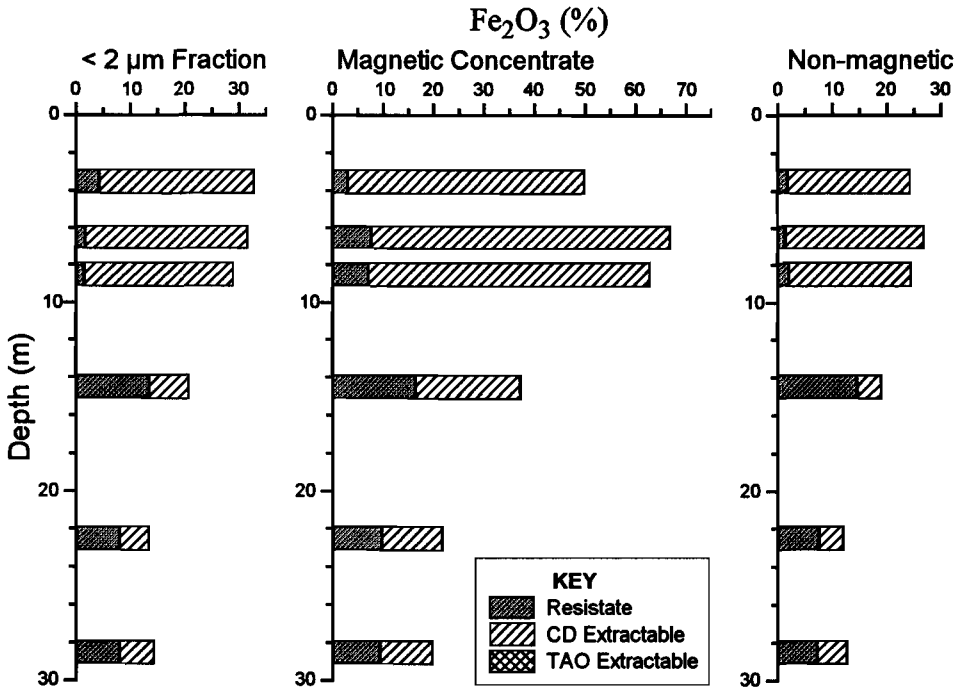

Figure 36: Selective extraction results for Fe, from HGMS fractions of MC 24 samples.

As discussed previously (Section 3.2; Figure 6), Mn is associated with Fe in the laterite zone (*i.e.*, above 10 m), and therefore will only be extracted with CD (Figure 38). Below this depth, Mn is found in separate oxide phases, which extract with TAO. These Mn oxides are even more strongly concentrated by HGMS than the Fe oxides (Figure 36).

[1] For brevity these phases are denoted as the CD phase and the TAO phase.

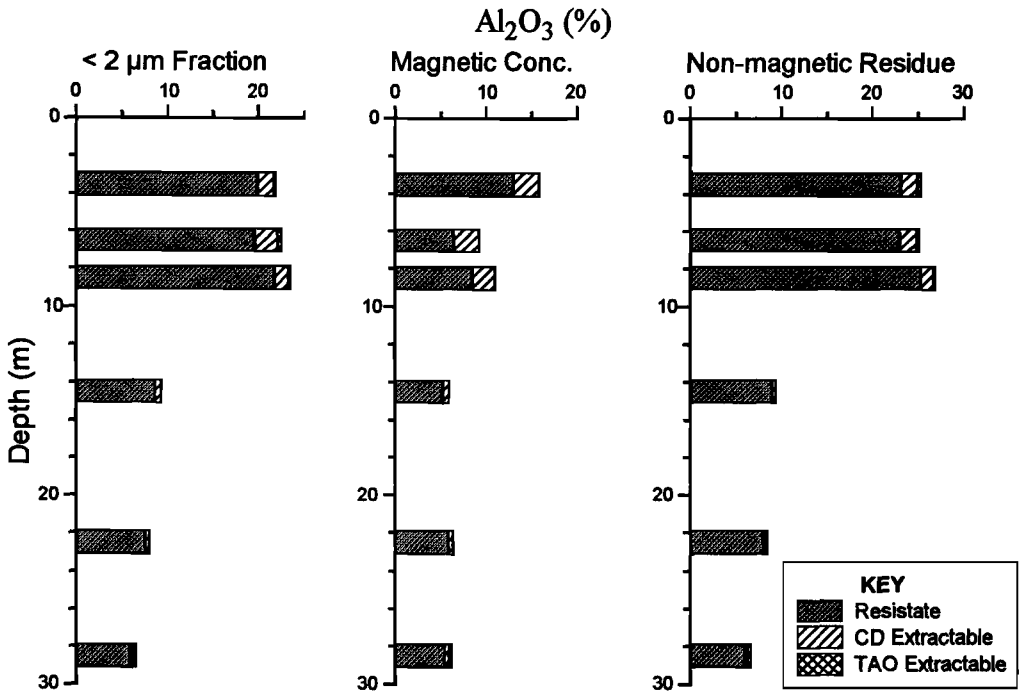

Figure 37: Selective extraction results for Al, from HGMS fractions of MC 24 samples.

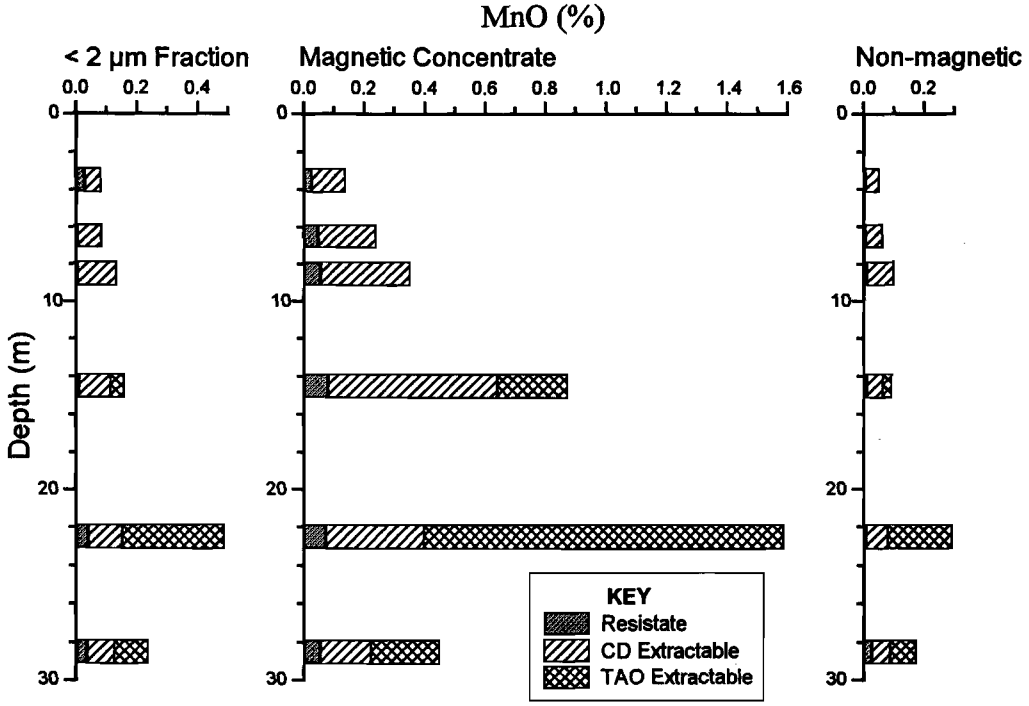

Figure 38: Selective Extraction Results for Mn, from HGMS fractions of MC 24 Samples

Chromium shows distinct changes with depth (Figure 39): above 10 m it is primarily associated with Fe oxides; whereas below 10 m only a small proportion of the Cr is CD extractable. This difference may reflect a lithological boundary (Volume IIA, Chapter 5, Section 7.4), or be a function of more intense weathering in the upper horizons. Titanium (Figure 41) shows similar effects, though in some samples the effects are less clear cut, possibly due to the presence in some samples of mixed Fe-Ti oxides with varying magnetic susceptibilities, and therefore different degrees of HGMS concentration.

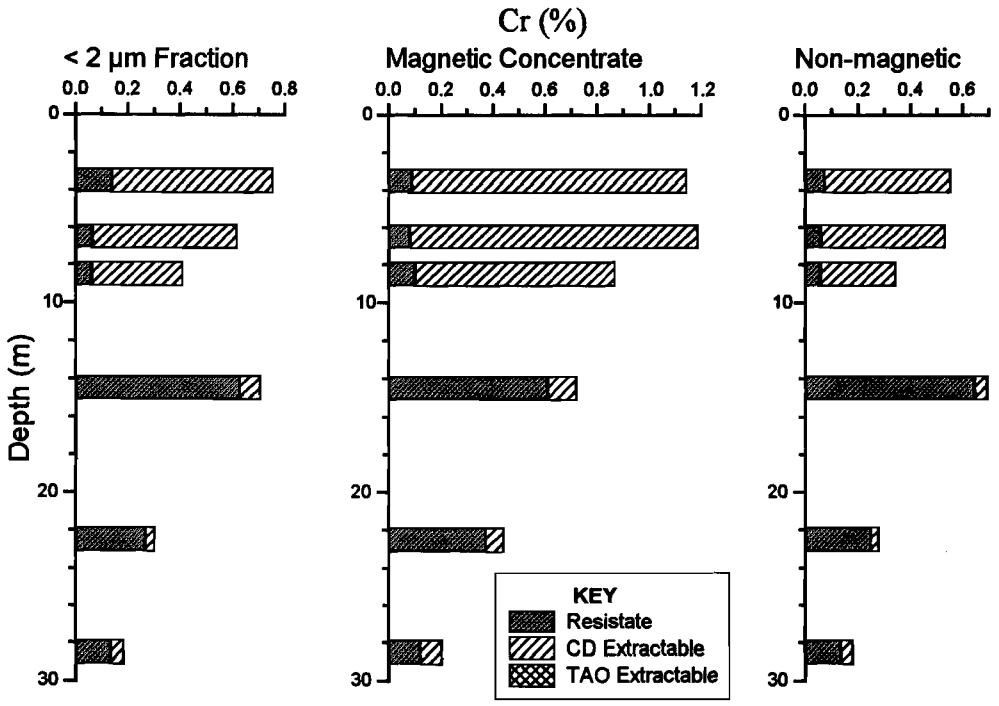

Figure 39: Selective extraction results for Cr, from HGMS fractions of MC 24 samples.

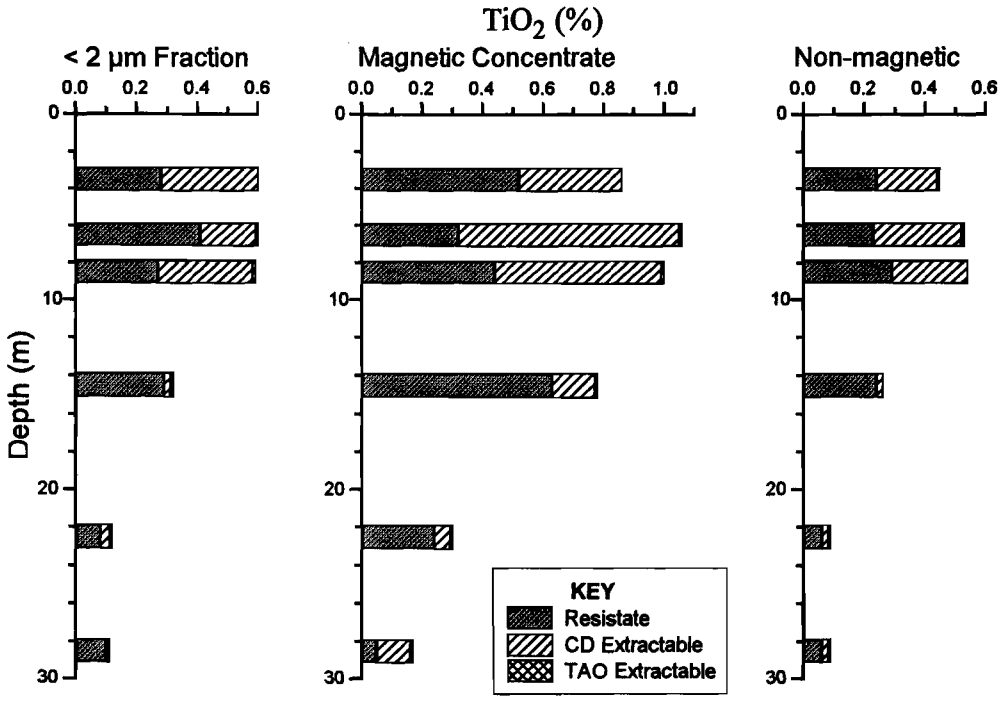

Figure 40: Selective extraction results for Ti, from HGMS fractions of MC 24 samples.

Results for Pt (Figure 41) indicate that, in the < 2 µm fraction, it is almost exclusively associated with Fe oxides. This is demonstrated both in terms of the virtually exclusive dissolution with CD, and in the high level of concentration with HGMS. Note that the non-CD extractable Pt fraction observed in the whole sample (Section 4.4; Figure 29), was not observed here, indicating that the minor component of Pt not associated with Fe oxides is greater than 2 µm in size.

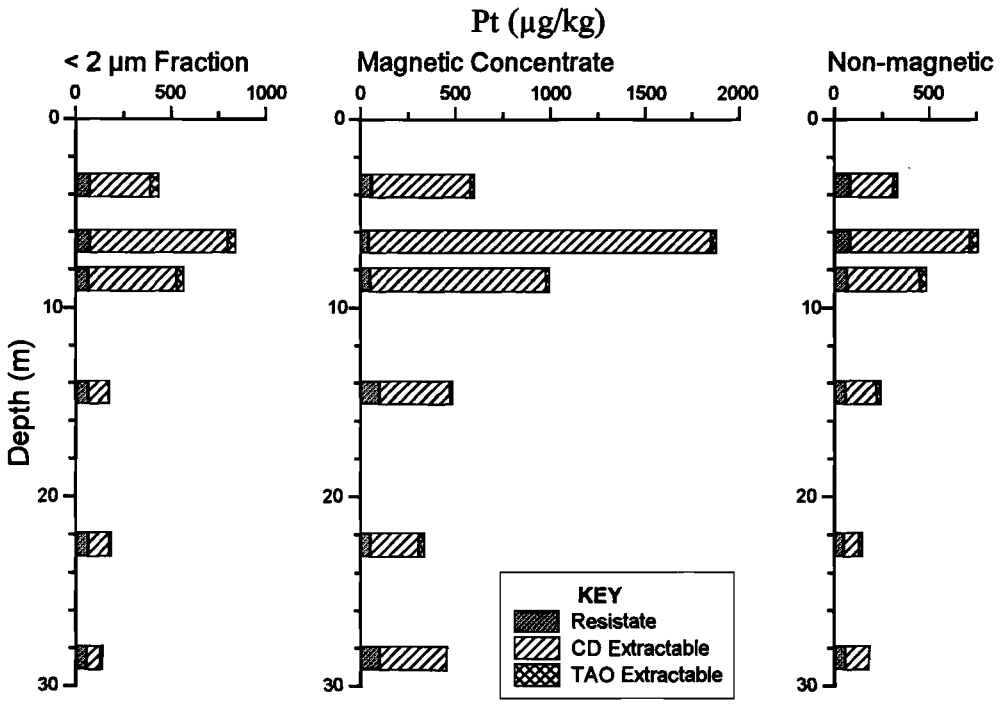

Figure 41: Selective extraction results for Pt, from HGMS fractions of MC 24 samples.

As discussed previously (Section 4.4; Figures 29 and 30), Pd (Figure 42) shows different mineralogical associations than Pt. Much less Pd is extracted by the TAO or CD reagents, with the form of the resistate Pd not known. The CD-extractable Pd shows only a small concentration by the HGMS procedure, in contrast to CD-extractable Pt, Fe, Mn, Cr (Figures 41, 36, 38, 39), Ni and Cu (Appendix VI), which are highly concentrated by HGMS. Thus, Pd differs from Pt in that only half of the Pd is associated with Fe oxides, and that association is with different Fe oxides than for Pt.

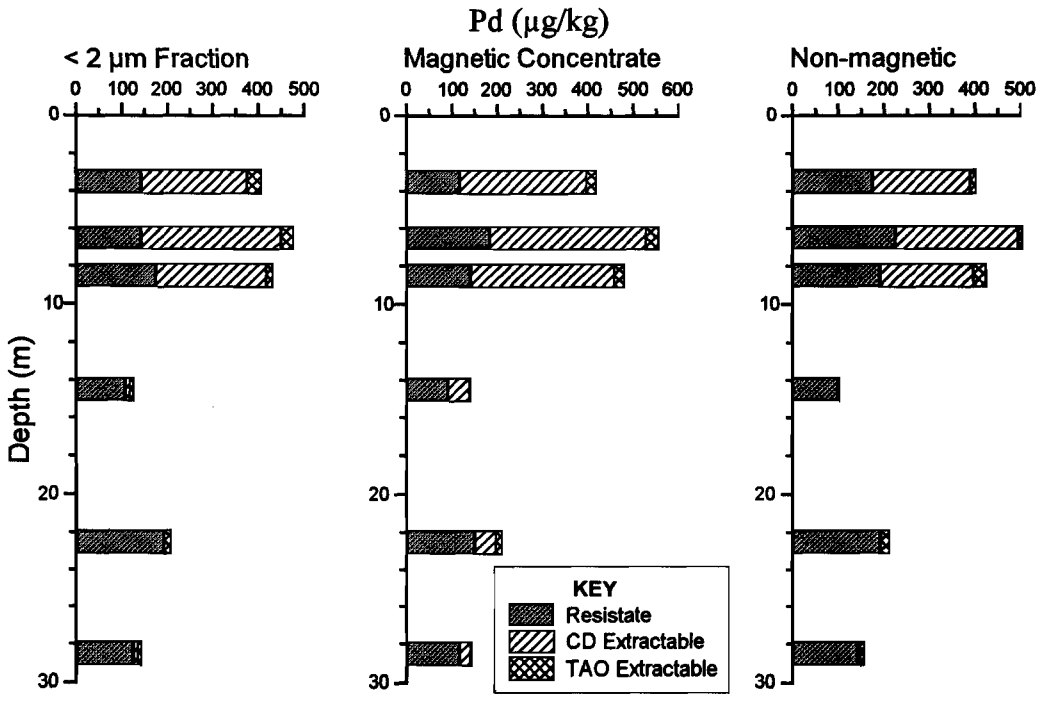

Figure 42: Selective extraction results for Pd, from HGMS fractions of MC 24 samples.

5.7 D-XRD Investigation

Use of D-XRD enabled clear resolution of the hematite and goethite reflections (Figure 43). The patterns have been corrected for mass absorption (Brindley, 1980), so that the peak sizes are directly proportional to the concentration of each mineral. Thus, as previously indicated by the extraction data (Section 5.6; Figure 37), goethite and hematite are clearly concentrated by HGMS. In addition, comparisons of relative intensities indicate that hematite is generally much more highly concentrated than goethite. This is demonstrated in Figures 44 and 45, which show the hematite and goethite contents (in arbitrary units, based on heights of several reflections) in all of the fractions. Hematite is most strongly concentrated by HGMS in the 6-7 and 8-9 m samples, whereas the greatest enrichment of goethite was observed at 14-15 m. The total extractable Fe pattern (Figure 46) is a combination of these minerals. The smaller levels of extractable Fe below 20 m depth, where hematite and goethite contents are very low, may reflect some contribution from Fe extracted from saponite. Extractable Al (Figure 47) is concentrated by HGMS, though only weakly. This is probably because higher substitutions of Al are expected in the smaller, more disordered goethites, which are only poorly concentrated by HGMS.

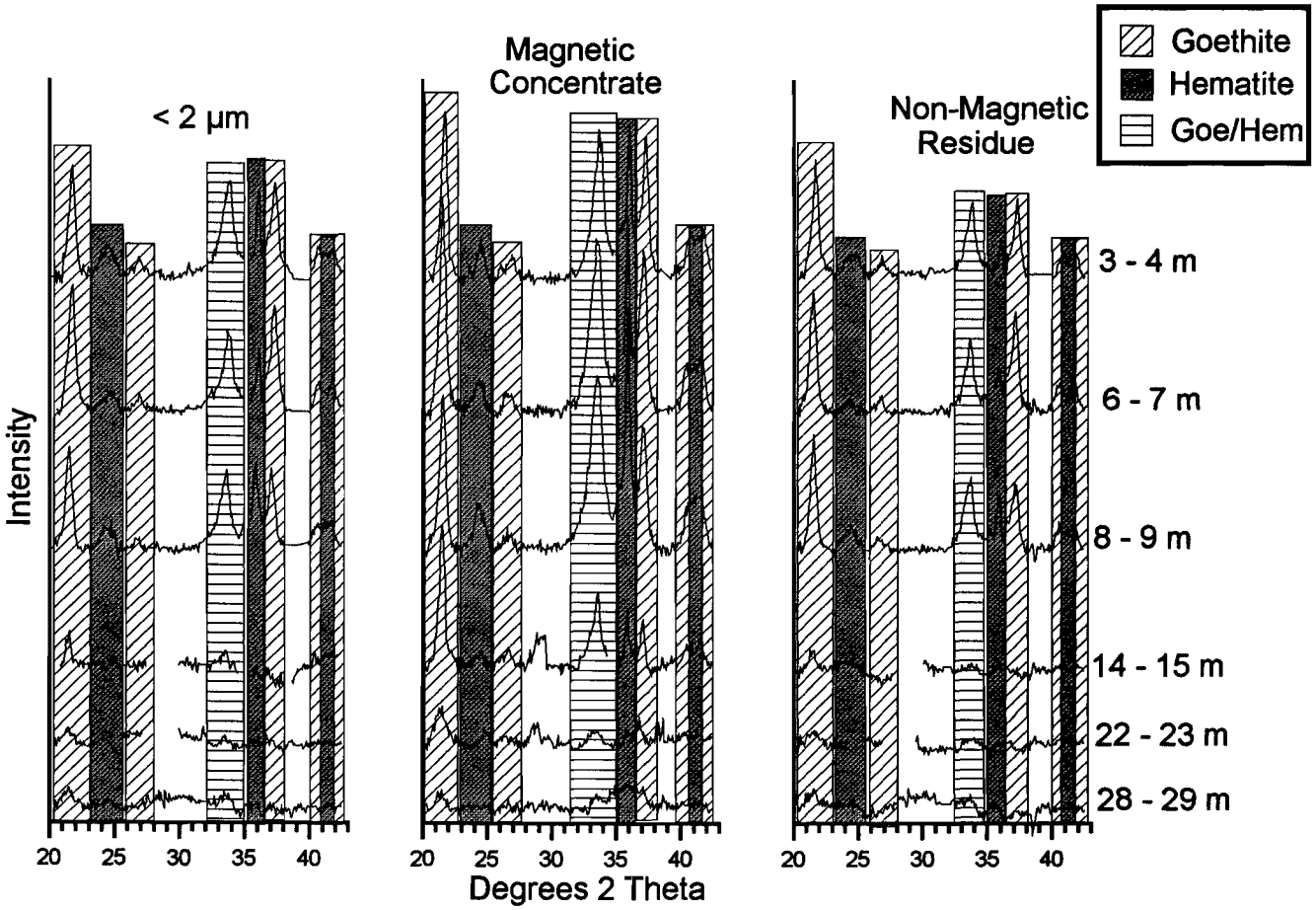

Figure 43: D-XRD Patterns for all MC24 samples investigated, with shading representing source of each reflection.

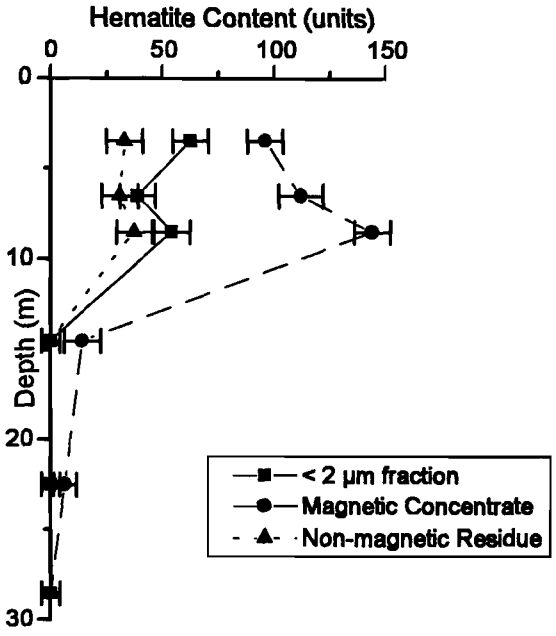

Figure 44: Hematite content (arbitrary units) of < 2 µm, MC and NMR fractions from MC24.

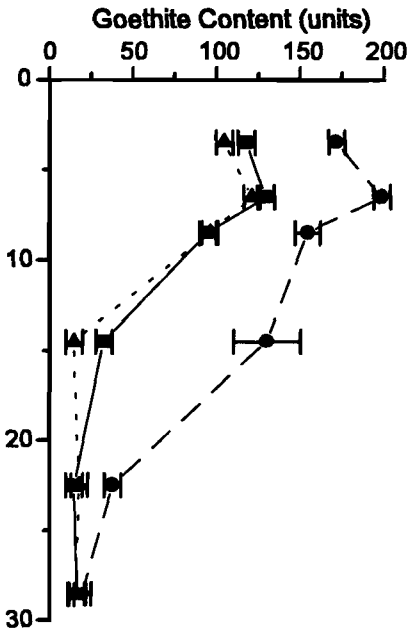

Figure 45: Goethite content (arbitrary units) of < 2 µm, MC and NMR fractions from MC24.

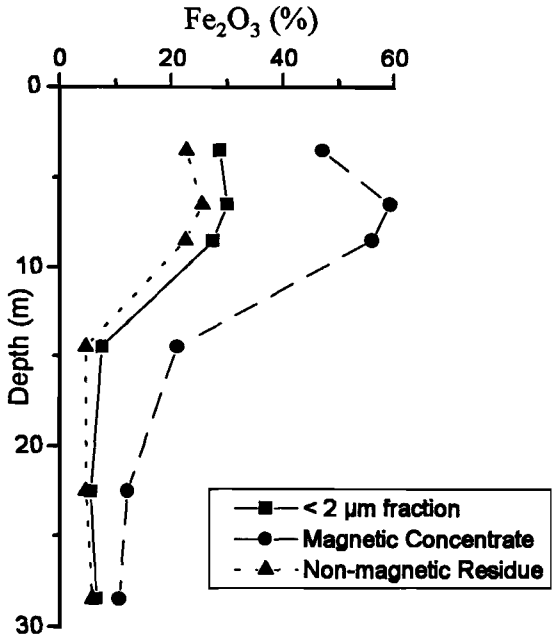

Figure 46: Total extractable Fe from < 2 µm, MC and NMR fractions from MC24.

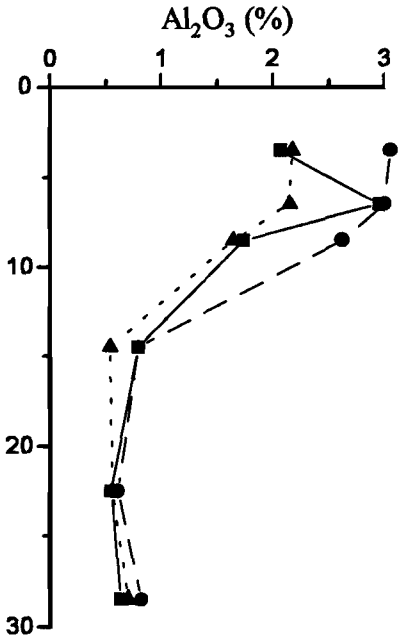

Figure 47: Total extractable Al from < 2 µm, MC and NMR fractions from MC24.

In the 6-7 and 8-9 m samples, extractable Pt (Figure 48) is more strongly concentrated by HGMS than is extractable Fe (Figure 46), but does appear to match the degree of concentration of hematite (Figure 44). This suggests (but does not prove) that Pt is associated with hematite. Conversely, extractable Pd (Figure 49) is only weakly enhanced by the HGMS procedure, and appears to match most closely with the pattern observed for Al (Figure 48). This suggests that Pd may be associated with smaller, Al-rich, goethitic Fe oxides.

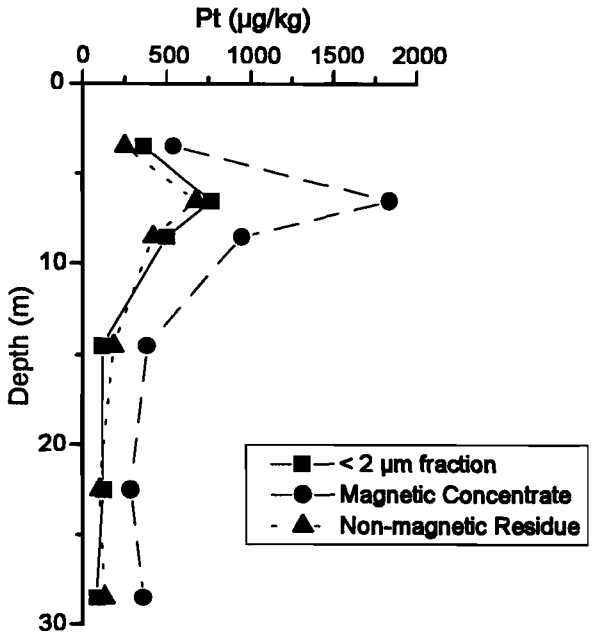

Figure 48: Total extractable Pt from < 2 µm, MC and NMR fractions from MC24.

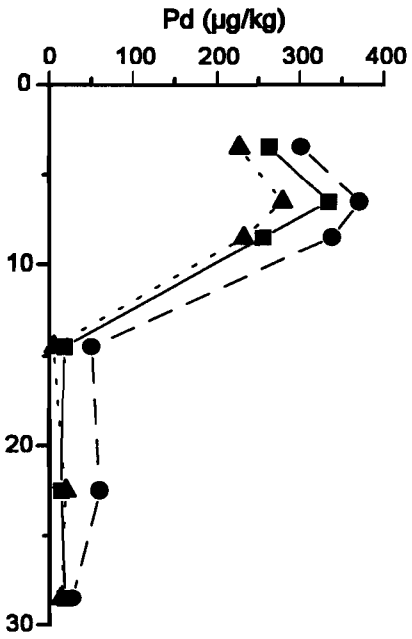

Figure 49: Total extractable Pd from < 2 µm, MC and NMR fractions from MC24.

The major difference in the mineralogy of Pt and Pd, despite the similar chemistry of these two elements, probably reflects different weathering histories. Hematite is commonly formed via aggregation and dehydration of poorly crystalline Fe oxides (Fischer and Schwertmann, 1975; Schwertmann and Murad, 1983). Thus, if Pt was released during early weathering, when Fe is initially precipitating in poorly crystalline forms, it will be incorporated in and/or on these Fe oxides, and then ultimately into hematite.

Goethite forms via slow crystallization of Fe oxides (Schwertmann, 1971; Schwertmann and Murad, 1983). Given the initially low Al in these rocks, the more aluminous oxides are presumably late-stage. Therefore, it is possible that the data for Pd represent release from a very slowly weathering phase. About half of the Pd thus remains non-extractable, with some having been released slowly and incorporated into the more recent Al-rich goethite.

6 SUMMARY

Platinum and Pd are not iodide soluble, in comparison with Au (Gray *et al.*, 1990) which is highly soluble in carbonate horizons. This is despite similarities in the behaviour of all three metals in biologically active environments (Section 4). This difference, as described below, may be due to much stronger binding of Pt and Pd with Fe oxides: Pt and Pd occur as the 2+ ion, which may have some affinity for Fe, whereas Au most commonly occurs as the 1+ ion (Gray, 1988) which has a much poorer affinity for Fe, due to its low charge and large size (ionic radius of Au^{+} is 1.37 Å, compared with 0.80 Å for Pt^{2+} and Pd^{2+}, and 0.64 Å for Fe^{3+}; Weast, 1984).

Most of the transition metals are strongly associated with Fe, notably Mn and Co (within the laterite zone), Cr (above 10m), V, Ni and Cu, and Ti (partially). Platinum is also primarily associated with Fe oxides. The inability of thiosulphate alone to dissolve Pt indicates that the Pt has been incorporated into the Fe oxides, rather than merely sorbed onto the exterior. In addition, HGMS results suggest that this association tends to be with the larger hematitic Fe. This would be consistent with Pt at depth being in readily weathered phases. As the Pt is weathered out it is then incorporated in the newly

forming Fe oxides, resulting in a low mobility. Once incorporated in these oxides, Pt remains immobile as long as Fe oxides are stable. The increase in the Pt in the amorphous Fe and Mn phases at 0-1m (Figure 21) may represent partial breakdown of the Fe oxides, and therefore release of the Pt, in this shallow sample. Similar effects in the 0-1m sample are also observed for Mn and Co (Figures 6 and 15), with separate Mn oxides observed, and for Cu, V and Ni (Figures 16, 17 and 20), which, like Pt, show higher concentrations in the Mn oxide and amorphous Fe oxide phases.

There is a non-extractable Pt phase, which includes up to 40% of the Pt (Figure 30), not seen in the < 2 μm fractions (Figure 42), suggesting this phase is a greater than 2 μm in size. This could represent primary Pt in resistant phases. The resistance to weathering could be due to the larger particle size.

Palladium shows a very different distribution from Pt. It mostly occurs in the < 2 μm fraction (Figure 36), *i.e.*, in very small minerals, but generally less than half is associated with Fe oxides. In addition, this Pd is associated with different Fe oxides than Pt: specifically with the Fe oxides poorly concentrated by HGMS, *i.e.*, fine Al-rich goethite. It is possible that this represents a very late release of Pd from its primary form, followed by accumulation into large-stage goethites. As the Pd may be weathering at the present day (albeit slowly) this could represent a possible mechanism for the mobilization of Pd. Extractions of the whole sample (Figure 31) suggest that Pd in the > 2 μm fraction is primarily non CD-extractable.

In conclusion, the distributions of Pt and Pd appear to be fundamentally controlled by their initial mineralogy, which in the case of Pd, may still be partially controlling the chemistry close to the regolith surface, and the affinity of these metals for Fe oxides. Once incorporated in Fe oxides, the mobility of Pt and Pd will be strongly controlled by the Fe oxide stability. The tendency for Pt to be incorporated into larger hematitic Fe oxides, and for Pd to be incorporated into smaller Al-rich Fe oxides, may also be consistent with observations of the differing distributions of these two metals in ferruginous lag.

References

Alexander, E.B, 1974. Extractable iron in relation to soil age on terraces along the Truckee River, Nevada. Soil Science Society of America Proceedings, 38: 121-124.

Anand, R.R. and Gilkes, R.J., 1984. Weathering of ilmenite in a lateritic pallid zone. Clays and Clay Minerals, 32:363-374.

Bailey, S.W., Cameron, E.M., Spedden, H.R. and Wegge, R.J. (1956). The alteration of ilmenite in beach sands. Economic Geology, 51: 263-279.

Ball, D.F. and Beaumont, P., 1972 . Vertical distribution of extractable Fe and Al in soil profiles from a brown earth - peaty podzol association. Journal of Soil Science, 23: 298-308.

Bigham, J.M., Golden, D.C., Bowen, L.H., Buol, S.W. and Weed, S.B., 1978. Iron oxide mineralogy of well-drained ultisols and oxisols: I. Characterization of iron oxides in soil clays by Mossbauer spectroscopy, X-ray diffractometry, and selected chemical techniques. Soil Science Society of America Journal, 42: 816-825.

Blume, H.P. and Schwertmann, U., 1969. Genetic evaluation of profile distribution of aluminum, iron, and manganese oxides. Soil Science Society of America Proceedings, 33: 438-444.

Brindley, G.W., 1980. Quantitative X-ray mineral analysis of clays. In "Crystal Structures of Clay Minerals and their X-Ray Identification." (Eds G.W. Brindley and G. Brown) pp 411-438. (Mineralogical Society: London.)

Brown, G. and Wood, I.G., 1985 . Estimation of iron oxides in soil clays by profile refinement combined with differential X-ray diffraction. Clay Minerals, 20: 15-27.

Childs, C.W., Parfitt, R.L. and Lee, R., 1983. Movement of aluminium as an inorganic complex in some podzolized soils, New Zealand. Geoderma, 29: 139-155.

Dixon, J.B. and Weed, S.B., (Eds.), 1989. Minerals in Soil Environments (2nd Ed.). (Madison, Wisconsin: Soil Science Society of America, 1989.)

Farmer, V.C., Russell, J.D. and Smith, B.F.L., 1983. Extraction of inorganic forms of translocated Al, Fe and Si from a podzol B horizon. Journal of Soil Science, 34: 571-576.

Farmer, V.C., Fraser, A.R., Robertson, L. and Sleeman, J.R., 1984. Proto-imogolite allophane in podzol concretions in Australia: possible relationship to aluminous ferrallitic (lateritic) cementation. Journal of Soil Science, 35: 333-340.

Fey, M.V. and le Roux, J., 1977. Properties and quantitative estimation of poorly crystalline components in sesquioxidic soil clays. Clays and Clay Minerals, 25: 285-294.

Fischer, W.R. and Schwertmann, U., 1975. The formation of hematite from amorphous iron(III) hydroxide. Clays and Clay Minerals, 23: 33-37

Fitzpatrick, R.W., le Roux, J. and Schwertmann, U., 1978. Amorphous and crystalline titanium and iron-titanium oxides in synthetic preparations, at near ambient conditions, and in soil clays. Clays and Clay Minerals, 26: 189-201.

Fogg, D.N. and Wilkinson, N.T., 1958. The colorimetric determination of phosphorus. Analyst, 83: 406-414.

Follet, E.A.C., 1965. The retention of amorphous, colloidal 'ferric hydroxide' by kaolinites. Journal of Soil Science, 16: 334-341.

Gendler, T.S., Yershova, L.S., Karpachevskiy, L.O and Kuz'min, R.N., 1981. Nuclear gamma resonance study of iron oxides and hydroxides on kaolinite. Soviet Soil Science, 13(6): 87-90.

Golden, D.C. and Dixon, J.B., 1985. Silicate and phosphate influence on kaolin-iron oxide interactions. Soil Science Society of America Journal, 49: 1568-1576.

Gray, D.J., 1986. The geochemistry of uranium and thorium during weathering of chloritic schists at the Alligator Rivers Uranium Province, N.T., Australia. (PhD Dissertation: University of Sydney, Sydney, NSW, Australia.)

Gray, D.J., 1988. The Aqueous Chemistry of Gold in the Weathering Environment. (AMIRA P240/P241). CSIRO Division of Exploration Geoscience Restricted Report EG 4R. 64 p.

Gray, D.J., Lintern, M.J. and Longman, G.D., 1990. Chemistry of Gold in some Western Australian Soils. (AMIRA P241: Weathering Processes). CSIRO Division of Exploration Geoscience Restricted Report 126R. 62 p.

Grey, I.E. and Reid, A.F., 1975. The structure of pseudorutile and its role in the alteration of ilmenite. American Mineralogist, 60: 898-906.

Herbauts, J., 1982. Chemical and mineralogical properties of sandy and loamy-sandy ochreous brown earths in relation to incipient podzolization in a brown earth-podzol evolutive sequence. Journal of Soil Science, 33: 743-762.

Huang, W.H. and Keller, W.D., 1970. Dissolution of rock-forming silicate minerals in organic acids: simulated first-stage weathering of fresh mineral surfaces. American Mineralogist, 55: 2076-2094.

Huang, W.H. and Keller, W.D., 1971. Dissolution of clay minerals in dilute organic acids at room temperature. American Mineralogist, 56: 1082-1095.

Hughes, J.C., 1982. High gradient magnetic separation of some soil clays from Nigeria, Brazil and Colombia. I. The interrelationships of iron and aluminium extracted by acid ammonium oxalate and carbon. Journal of Soil Science, 33, 509-519.

Hutton, J.T., 1977. Titanium and zirconium minerals. In "Minerals in Soil Environments." (Eds J.B. Dixon and S.B. Weed) pp 673-688. (Soil Science Society of America: Madison, Wisconsin)

Jefferson, D.A., Tricker, M.J. and Winterbottom, A.P., 1975. Electron-microscopic and Mossbauer spectroscopic studies of iron-stained kaolinite minerals. Clays and Clay Minerals, 23: 355-360.

Kämpf, N. and Schwertmann, U., 1982. Note: Quantitative determination of goethite and hematite in kaolinitic soils by X-ray diffraction. Clay Minerals, 17: 359-363.

McIntyre, D.S., 1974. Appendix 4. Definitions of particle size by settling velocity and standard sieves. In "Methods for Analysis of Irrigated Soils." (Ed J. Loveday) pp 188-192. (Technical Communication No. 54 of the Commonwealth Bureau of Soils, Wilkie and Co. Ltd.: Clayton, Victoria.)

McKeague, J.A. and Day, J.H., 1966. Dithionite- and oxalateextractable Fe and Al as aids in differentiating various classes of soils. Canadian Journal of Soil Science, 46: 13-22.

McKeague, J.A., Brydon, J.E. and Miles, N.M., 1971. Differentiation of forms of extractable iron and aluminum in soils. Soil Science Society of America Proceedings, 35: 33-38.

Pruden, G. and King, H.G.C., 1969. A scheme of semi-micro analysis for the major elements in clay minerals, based on modifications to conventional methods of silicate analysis. Clay Minerals, 8: 1-13.

Schulze, D.G., 1981. Identification of soil iron oxide minerals by Differential X-ray diffraction. Soil Science Society of America Journal, 45: 437-440.

Schulze, D.G. (1988). Separation and concentration of iron oxide containing phases. NATO. Advanced Study Institutes. Series C, No. 217, 1988, pp. 63-81

Schulze, D.G. and Dixon, J.B., 1979. High gradient magnetic separation of iron oxides and other magnetic minerals from soil clays. Soil Science Society of America Journal, 43: 793-799.

Schwertmann, U., 1971. Transformation of hematite to goethite in soils. Nature, 232: 624-625.

Schwertmann, U. and Murad, E., 1983. Effect of pH on the formation of goethite and hematite from ferrihydrite. Clays and Clay Minerals, 31: 277-284.

Schwertmann, U., Schulze, D.G. and Murad, E., 1982. Identification of ferrihydrite in soils by dissolution kinetics, differential X-ray diffraction and Mossbauer spectroscopy. Soil Science Society of America Journal, 46: 869-875.

Torrent, J., Schwertmann, U. and Schulze, D.G., 1980. Iron oxide mineralogy of some soils of two river terrace sequences in Spain. Geoderma, 23: 191-208.

Weast, R.C., Astle, M.J. and Beyer, W.H. (1984). "CRC Handbook of Chemistry and Physics." F-154 Elements in Sea Water. (64th Edition; CRC Press Inc., Florida, USA).

Yershova, L.S., Gendler, T.S., Karpachevskiy, L.O. and Kuz'min, R.N., 1981. Changes in iron oxides at the surface of montmorillonite and their extraction with Tamm and Mehra-Jackson reagents. Soviet Soil Science, 13(8): 89-98.

Appendix I: Iodide Extraction Data

Drill Hole	Sample Depth (m)	Extracted - Fine Samples (μg/kg) Pt	Extracted - Fine Samples (μg/kg) Pd	Extracted - Coarse Samples (μg/kg) Pt	Extracted - Coarse Samples (μg/kg) Pd	Total (μg/kg) Pt	Total (μg/kg) Pd	Fe_2O_3 (%)	CaO (%)
OB19	0-1	6	14	nd	nd	320	660	13.4	7.15
	1-2	6	15	8	13	370	400	14.5	3.42
	2-3	13	22	20	26	370	400	12	1.1
	3-4	17	16	17	20	225	295	13.4	0.22
	"	20	20	nd	nd	"	"	"	"
	4-5	nd	nd	24	17	225	295	nd	nd
	5-6	18	11	26	18	190	300	14	0.17
	7-8	nd	nd	11	9	130	170	nd	nd
	9-10	5	6	7	6	102	145	17.32	0.39
	14-15	7	3	4	2	114	160	16.17	0.49
	19-20	3	3	1	4	52	112	15.45	1.02
	24-25	5	3	1	4	78	140	14.02	0.85
	27-28	nd	nd	1	4	140	210	nd	nd
	28-29	3	5	1	7	140	210	19.75	0.46
	29-30	nd	nd	1	2	125	240	nd	nd
	30-31	2	4	1	3	125	240	16.17	0.05
	34-35	6	4	1	3	30	62	15.45	1.37
	39-40	3	2	4	10	31	66	16.17	1.2
OB23	0-1	8	11	3	6	640	350	22.61	11.13
	"	7	11	nd	nd	"	"	"	"
	1-2	12	9	1	3	500	340	26.76	6.58
	2-3	5	7	1	4	500	340	34.06	2.89
	3-4	9	6	2	2	195	220	48.37	0.21
	"	1	8	nd	nd	"	"	"	"
	4-5	5	13	1	3	195	220	52.23	0.05
	"	3	13	nd	nd	"	"	"	"
	6-7	9	6	2	4	160	310	37.06	0.14
	8-9	nd	nd	1	3	114	240		
	10-11	6	6	2	3	98	190	26.19	0.05
	13-14	4	6	1	3	116	275	22.18	0.05
	15-16	4	8	2	3	118	270	28.48	0.05
	17-18	nd	nd	1	3	130	165	nd	nd
	19-20	7	7	3	4	150	200	26.62	0.05
	24-25	1	5	1	2	130	140	19.60	0.65
	29-30	5	3	1	4	58	90	15.88	0.82
	34-35	nd	nd	1	13	58	78	nd	nd
	39-40	4	5	1	7	76	108	16.46	1.52

Uncertainty: Pt - 2 μg/kg
Pd - 5 μg/kg (OB19 and OB23)

nd: not determined

Appendix I (Cont.)

Drill Hole	Sample Depth (m)	Extracted - Fine Samples (μg/kg) Pt	Pd	Extracted - Coarse Samples (μg/kg) Pt	Pd	Total (μg/kg) Pt	Pd	Fe_2O_3 (%)	CaO (%)
MC24	0-1	2	40	12	20	845	435	30.88	6.70
	1-2	8	60	14	40	675	405	41.89	0.01
	2-3	6	40	12	20	810	440	46.04	0
	3-4	4	40	8	20	690	435	45.32	0
	4-5	6	20	8	20	630	355	45.32	0
	5-6	8	40	6	20	780	350	44.18	0
	6-7	8	40	6	20	1300	457	45.61	0
	7-8	6	40	6	20	950	515	47.04	0
	8-9	6	40	8	20	830	457	46.47	0
	9-10	6	20	6	20	610	545	47.04	0
	10-11	6	20	10	20	495	425	49.47	0
	11-12	8	40	2	10	540	295	49.18	0
	12-13	8	20	4	10	470	260	53.04	0
	13-14	4	20	1	10	340	255	27.45	0
	14-15	2	20	1	10	195	106	24.3	0.01
	16-17	2	40	2	20	215	100	24.02	0
	18-19	1	40	2	20	185	78	25.02	0
	20-21	1	20	1	10	245	112	23.59	0
	22-23	1	20	1	10	180	215	22.73	0
	24-25	1	20	1	10	165	100	14.58	2.55
	26-27	1	20	1	10	98	92	19.87	2.43
	28-29	1	20	1	10	135	110	23.16	2.07
	30-31	1	10	1	10	108	165	21.73	2.65
	32-33	1	10	1	10	63	125	23.02	1.03
	34-35	10	20	1	10	94	83	20.16	1.92
	36-37	4	20	1	10	125	104	19.02	2.14
	38-39	2	20	1	10	155	165	17.59	2.53

Uncertainty: Pt - 2 μg/kg
Pd - 10 μg/kg (MC24)

Appendix II: Selective Extraction Experiment A - Easily Extractable Phases (MC24)

Sample Depth (m)	Na_2O (%) Exchangeable	Carbonate	Manganese Oxides	Amorphous Iron Oxides	Iron Oxides (partial)	Residue	Total	Expected
0-1	0.29	0.01	0.01	0.01	0.01	0.121	0.45	0.3
1-2 (a)	0.33	0.01	0.00	0.00	0.01	0.110	0.46	0.37
1-2 (b)	0.33	0.01	0.00	0.00	0.01	0.111	0.47	0.37
3-4	0.43	0.01	0.01	0.00	0.01	0.182	0.64	0.42
6-7	0.50	0.01	0.00	0.00	0.01	0.309	0.83	0.56
15-16 (a)	1.17	0.01	0.01	0.01	0.01	0.281	1.49	1.24
15-16 (b)	1.16	0.01	0.01	0.00	0.01	0.292	1.48	1.24
28-29	0.83	0.01	0.01	0.00	0.01	0.154	1.01	0.96

Sample Depth (m)	K_2O (%) Exchangeable	Carbonate	Manganese Oxides	Amorphous Iron Oxides	Iron Oxides (partial)	Residue	Total	Expected
0-1	0.05	0.01	0.01	0.01	0.02	-	0.092	-
1-2 (a)	0.13	0.01	0.00	0.01	0.02	-	0.170	-
1-2 (b)	0.03	0.01	0.00	0.00	0.02	-	0.071	-
3-4	0.02	0.01	0.01	0.00	0.02	-	0.064	-
6-7	0.03	0.01	0.00	0.00	0.02	-	0.066	-
15-16 (a)	0.07	0.01	0.01	0.01	0.02	-	0.113	-
15-16 (b)	0.08	0.01	0.01	0.00	0.02	-	0.122	-
28-29	0.05	0.01	0.01	0.01	0.02	-	0.094	-

Sample Depth (m)	MgO (%) Exchangeable	Carbonate	Manganese Oxides	Amorphous Iron Oxides	Iron Oxides (partial)	Residue	Total	Expected
0-1	0.31	0.30	0.12	0.24	0.14	0.57	1.69	1.86
1-2 (a)	0.13	0.00	0.00	0.01	0.01	0.06	0.21	0.08
1-2 (b)	0.12	0.00	0.00	0.01	0.01	0.06	0.20	0.08
3-4	0.14	0.00	0.00	0.00	0.01	0.00	0.15	0.01
6-7	0.17	0.00	0.00	0.01	0.01	0.00	0.19	0.05
15-16 (a)	0.84	0.01	0.00	0.02	0.07	2.18	3.12	3.45
15-16 (b)	0.82	0.01	0.00	0.01	0.06	2.22	3.13	3.45
28-29	0.54	0.02	0.06	0.19	0.61	9.83	11.26	11.89

Sample Depth (m)	CaO (%) Exchangeable	Carbonate	Manganese Oxides	Amorphous Iron Oxides	Iron Oxides (partial)	Residue	Total	Expected
0-1	3.06	2.82	0.03	0.01	0.03	0.08	6.04	6.7
1-2 (a)	0.08	0.00	0.00	0.01	0.02	0.01	0.13	0.01
1-2 (b)	0.07	0.01	0.01	0.01	0.03	0.01	0.14	0.01
3-4	0.04	0.00	0.02	0.01	0.03	0.00	0.10	0
6-7	0.02	0.02	0.00	0.01	0.02	0.00	0.08	0
15-16 (a)	0.04	0.00	0.02	0.01	0.02	0.01	0.10	0.01
15-16 (b)	0.04	0.00	0.01	0.01	0.03	0.00	0.10	0.01
28-29	0.03	0.01	0.00	0.01	0.03	2.00	2.08	2.07

Appendix II (Cont.)

Pt (mg/kg)								
Sample Depth (m)	Exchange-able	Carbonate	Manganese Oxides	Amorphous Iron Oxides	Iron Oxides (partial)	Residue	Total	Expected
0-1	0.016	0.000	0.098	0.130	0.432	0.215	0.892	0.845
1-2 (a)	0.032	0.000	0.000	0.000	0.360	0.322	0.714	0.675
1-2 (b)	0.032	0.000	0.000	0.048	0.320	0.317	0.717	0.675
3-4	0.032	0.016	0.000	0.000	0.359	0.321	0.727	0.69
6-7	0.032	0.000	0.000	0.016	0.798	0.509	1.354	1.3
15-16 (a)	0.016	0.000	0.000	0.000	0.128	0.094	0.238	0.235
15-16 (b)	0.016	0.000	0.000	0.000	0.128	0.097	0.241	0.235
28-29	0.000	0.000	0.032	0.016	0.056	0.065	0.169	0.135

Pd (mg/kg) (nd - not determined)								
Sample Depth (m)	Exchange-able	Carbonate	Manganese Oxides	Amorphous Iron Oxides	Iron Oxides (partial)	Residue	Total	Expected
0-1	nd	nd	nd	nd	nd	0.289	nd	0.435
1-2 (a)	nd	nd	nd	nd	nd	0.229	nd	0.405
1-2 (b)	nd	nd	nd	nd	nd	0.223	nd	0.405
3-4	nd	nd	nd	nd	nd	0.260	nd	0.435
6-7	nd	nd	nd	nd	nd	0.291	nd	0.457
15-16 (a)	nd	nd	nd	nd	nd	0.094	nd	0.112
15-16 (b)	nd	nd	nd	nd	nd	0.097	nd	0.112
28-29	nd	nd	nd	nd	nd	0.097	nd	0.11

Al (mg/kg)								
Sample Depth (m)	Exchange-able	Carbonate	Manganese Oxides	Amorphous Iron Oxides	Iron Oxides (partial)	Residue	Total	Expected
0-1	7	123	1398	1188	3000	59593	65310	68380
1-2 (a)	12	152	378	1286	2960	83578	88364	90710
1-2 (b)	6	141	429	1030	2744	83126	87475	90710
3-4	6	109	309	877	2802	81256	85359	83570
6-7	2	126	413	795	3052	83279	87668	89230
15-16 (a)	4	17	554	1451	1687	38239	41953	43770
15-16 (b)	9	16	665	1052	1772	38785	42300	43770
28-29	5	25	1220	1345	2300	17174	22069	22120

Ba (mg/kg)								
Sample Depth (m)	Exchange-able	Carbonate	Manganese Oxides	Amorphous Iron Oxides	Iron Oxides (partial)	Residue	Total	Expected
0-1	8.4	15.7	32.4	15.6	5.4	33.6	111	155
1-2 (a)	4.2	6.9	1.4	4.5	3.0	12.8	33	78
1-2 (b)	4.8	6.7	1.6	3.7	3.2	12.3	32	78
3-4	1.6	3.7	1.4	4.5	6.0	0.0	17	57
6-7	1.4	3.4	1.3	4.1	6.6	3.4	20	52
15-16 (a)	10.8	19.5	18.5	61.2	64.9	62.5	237	288
15-16 (b)	11.5	25.9	22.8	39.6	71.1	44.5	215	288
28-29	1.4	1.0	4.6	1.2	1.4	0.0	10	22

Appendix II (Cont.)

Sample Depth (m)	Cr (mg/kg) Exchange-able	Carbonate	Manganese Oxides	Amorphous Iron Oxides	Iron Oxides (partial)	Residue	Total	Expected
0-1	0.84	4.4	7.4	18	737	1395	2163	2360
1-2 (a)	0.60	3.2	2.2	13	974	2845	3837	4143
1-2 (b)	0.69	3.0	2.2	10	865	2932	3814	4143
3-4	0.68	5.4	3.1	18	1258	5854	7139	7322
6-7	0.65	4.2	2.6	13	1121	5084	6225	6678
15-16 (a)	0.73	5.3	10.2	46	339	6091	6492	6852
15-16 (b)	0.65	5.3	12.0	40	331	6151	6540	6852
28-29	0.72	2.7	6.8	17	383	5883	6293	6526

Sample Depth (m)	Fe (mg/kg) Exchange-able	Carbonate	Manganese Oxides	Amorphous Iron Oxides	Iron Oxides (partial)	Residue	Total	Expected
0-1	16	19	438	1442	87253	119033	208201	222840
1-2 (a)	52	15	77	1272	90592	194339	286346	304600
1-2 (b)	18	26	94	924	79090	205637	285789	304600
3-4	12	20	95	1127	78279	226482	306015	315090
6-7	30	29	114	1072	73057	233970	308272	332090
15-16 (a)	8	7	550	2365	30970	121394	155293	163110
15-16 (b)	16	11	633	2031	30907	122028	155626	163110
28-29	18	17	1055	2350	64303	83242	150986	164435

Sample Depth (m)	Mn (mg/kg) Exchange-able	Carbonate	Manganese Oxides	Amorphous Iron Oxides	Iron Oxides (partial)	Residue	Total	Expected
0-1	2	68	404	62	327	361	1223	1512
1-2 (a)	3	1	3	5	284	707	1002	1073
1-2 (b)	1	1	3	4	233	763	1003	1073
3-4	1	1	2	3	300	922	1230	1266
6-7	2	3	3	10	505	885	1407	1602
15-16 (a)	60	8	201	108	673	415	1465	1689
15-16 (b)	57	8	251	57	677	402	1453	1689
28-29	4	7	1231	184	299	474	2199	2391

Sample Depth (m)	Ni (mg/kg) Exchange-able	Carbonate	Manganese Oxides	Amorphous Iron Oxides	Iron Oxides (partial)	Residue	Total	Expected
0-1	3	20	73	70	179	398	743	799
1-2 (a)	2	3	2	6	126	660	798	839
1-2 (b)	1	3	1	4	111	666	787	839
3-4	1	4	2	4	97	776	884	897
6-7	2	4	2	8	135	1059	1210	1277
15-16 (a)	63	10	7	34	192	2440	2747	2872
15-16 (b)	61	10	8	29	187	2493	2788	2872
28-29	18	30	424	220	884	1943	3519	3703

Appendix II (Cont.)

Sample Depth (m)	Sr Exchange-able	(mg/kg) Carbonate	Manganese Oxides	Amorphous Iron Oxides	Iron Oxides (partial)	Residue	Total	Expected
0-1	21	26	18	0	0	0	65	95
1-2 (a)	21	8	2	0	0	0	31	20
1-2 (b)	16	5	12	0	0	0	33	20
3-4	13	6	11	0	0	0	30	5
6-7	14	13	11	0	0	0	38	6
15-16 (a)	50	3	0	0	0	0	53	38
15-16 (b)	43	3	0	0	0	0	46	38
28-29	29	12	3	0	0	0	44	21

Sample Depth (m)	Co Exchange-able	(mg/kg) Carbonate	Manganese Oxides	Amorphous Iron Oxides	Iron Oxides (partial)	Residue	Total	Expected
0-1	0	6	110	14	13	19	162	171
1-2 (a)	0	2	0	0	5	29	36	21
1-2 (b)	0	1	0	0	4	29	35	21
3-4	0	2	0	0	4	32	38	16
6-7	0	2	0	1	4	32	39	17
15-16 (a)	11	4	7	10	14	28	74	78
15-16 (b)	10	3	8	8	14	31	75	78
28-29	1	3	274	49	37	43	407	431

Sample Depth (m)	Cu Exchange-able	(mg/kg) Carbonate	Manganese Oxides	Amorphous Iron Oxides	Iron Oxides (partial)	Residue	Total	Expected
0-1	3	6	40	44	115	293	500	453
1-2 (a)	3	2	6	18	123	416	569	548
1-2 (b)	2	4	5	14	110	425	560	548
3-4	2	3	6	12	117	440	580	534
6-7	4	5	8	17	215	1006	1256	1173
15-16 (a)	11	6	25	29	78	405	553	509
15-16 (b)	9	6	21	22	82	399	539	509
28-29	0	1	18	19	29	303	370	336

Sample Depth (m)	V Exchange-able	(mg/kg) Carbonate	Manganese Oxides	Amorphous Iron Oxides	Iron Oxides (partial)	Residue	Total	Expected
0-1	0.0	0.0	0.7	5.1	41	67	114	144
1-2 (a)	0.0	0.0	0.0	2.1	42	112	156	195
1-2 (b)	0.0	0.0	0.0	1.3	36	117	155	195
3-4	0.0	0.0	0.0	0.7	37	147	184	211
6-7	0.0	0.0	0.0	0.2	30	133	164	201
15-16 (a)	0.0	0.0	0.0	0.0	14	20	34	45
15-16 (b)	0.0	0.0	0.0	0.0	15	26	41	45
28-29	0.0	0.0	2.4	2.6	37	68	110	125

Appendix II (Cont.)

Ti (mg/kg)								
Sample Depth (m)	Exchange-able	Carbonate	Manganese Oxides	Amorphous Iron Oxides	Iron Oxides (partial)	Residue	Total	Expected
0-1	0.0	0.0	1.1	5	182	3388	3576	3780
1-2 (a)	0.3	0.2	0.5	6	532	4119	4657	5100
1-2 (b)	0.2	0.4	0.5	5	447	4161	4615	5100
3-4	0.4	0.4	0.5	3	399	4210	4614	4740
6-7	0.4	0.4	0.5	7	442	4083	4532	4860
15-16 (a)	0.1	0.1	1.4	4	33	2135	2174	2280
15-16 (b)	0.2	0.3	1.2	3	30	2156	2191	2280
28-29	0.3	0.3	0.9	3	1.8	1167	1174	1200

Y (mg/kg)								
Sample Depth (m)	Exchange-able	Carbonate	Manganese Oxides	Amorphous Iron Oxides	Iron Oxides (partial)	Residue	Total	Expected
0-1	0.3	2.8	1.4	1.1	0.8	3.5	10	11
1-2 (a)	0.2	0.3	0.3	0.1	0.0	3.9	5	8
1-2 (b)	0.2	0.3	0.3	0.1	0.0	3.8	5	8
3-4	0.3	0.3	0.3	0.1	0.0	3.9	5	5
6-7	0.3	0.4	0.3	0.2	0.0	3.6	5	5
15-16 (a)	0.9	0.7	0.3	0.2	0.8	2.2	5	2
15-16 (b)	0.9	0.7	0.3	0.2	0.9	2.4	5	2
28-29	1.3	2.3	2.0	2.8	8.4	20.2	37	44

Si (mg/kg)								
Sample Depth (m)	Exchange-able	Carbonate	Manganese Oxides	Amorphous Iron Oxides	Iron Oxides (partial)	Residue	Total	Expected
0-1	148	244	219	481	961	120857	122910	131500
1-2 (a)	57	121	84	432	1161	109957	111812	116630
1-2 (b)	72	68	107	298	912	109691	111147	116630
3-4	69	74	140	345	963	93264	94856	93490
6-7	56	159	157	330	734	87323	88760	91860
15-16 (a)	159	139	202	513	1055	179900	181968	196620
15-16 (b)	86	69	380	517	894	183310	185256	196620
28-29	75	49	232	300	976	174509	176142	186100

Zn (mg/kg)								
Sample Depth (m)	Exchange-able	Carbonate	Manganese Oxides	Amorphous Iron Oxides	Iron Oxides (partial)	Residue	Total	Expected
0-1	0.0	0.0	0.0	0.0	0.0	54	54	57
1-2 (a)	0.0	0.0	0.0	0.0	0.0	107	107	107
1-2 (b)	0.0	0.0	0.0	0.0	0.0	85	85	107
3-4	0.0	0.0	0.0	0.0	0.0	104	104	115
6-7	0.0	0.0	0.0	0.0	0.0	123	123	130
15-16 (a)	0.0	0.0	0.0	0.0	0.0	259	259	368
15-16 (b)	0.0	0.0	0.0	0.0	0.0	332	332	368
28-29	0.0	0.0	0.0	0.0	0.0	199	199	269

Appendix II (Cont.)

Sample Depth (m)	Zr (mg/kg) Exchange-able	Carbonate	Manganese Oxides	Amorphous Iron Oxides	Iron Oxides (partial)	Residue	Total	Expected
0-1	0.0	0.0	0.0	0.0	0.0	63	63	78
1-2 (a)	0.0	0.0	0.0	0.0	0.0	48	48	83
1-2 (b)	0.0	0.0	0.0	0.0	0.0	51	51	83
3-4	0.0	0.0	0.0	0.0	0.0	36	36	43
6-7	0.0	0.0	0.0	0.0	0.0	31	31	48
15-16 (a)	0.0	0.0	0.0	0.0	0.0	10	10	25
15-16 (b)	0.0	0.0	0.0	0.0	0.0	12	12	25
28-29	0.0	0.0	0.0	0.0	0.0	7	7	0

Appendix III: Selective Extraction Experiment B - Iron Oxide Phases (MC24)

Appendix IIIA: Citrate-Dithionite Extractions

(Results given as cumulative extracted)

Fe (mg/kg)									
Sample	Citrate-Dithionite					Aqua-regia			Total
Depth (m)	1	2	3	4	5	1	2	3	
0 - 1 (a)	77269	166394	201349	209567	212657	219158	220061	221096	216000
0 - 1 (b)	67164	150746	194403	204851	208552	216985	217840	218254	216000
3 - 4	89570	183121	280255	319268	320000	320669	320777	320933	317000
28 - 29	38446	79850	95110	104692	108872	133715	135662	138328	162000

Al (mg/kg)									
Sample	Citrate-Dithionite					Aqua-regia			Total
Depth (m)	1	2	3	4	5	1	2	3	
0 - 1 (a)	2357	5212	6663	7364	7734	13184	14153	16835	68380
0 - 1 (b)	1934	4520	6263	6995	7351	13726	15159	16889	68380
3 - 4	2632	5328	9561	12593	12762	15100	15605	16797	83570
28 - 29	761	1366	1934	2605	3002	14892	16104	17877	22120

Cr (mg/kg)									
Sample	Citrate-Dithionite					Aqua-regia			Total
Depth (m)	1	2	3	4	5	1	2	3	
0 - 1 (a)	531	1415	1755	1858	1890	1996	2005	2025	2360
0 - 1 (b)	485	1287	1724	1866	1910	2048	2062	2074	2360
3 - 4	1150	2623	5171	7333	7452	7657	7667	7683	7322
28 - 29	245	427	519	608	648	1101	1179	1322	6526

Ni (mg/kg)									
Sample	Citrate-Dithionite					Aqua-regia			Total
Depth (m)	1	2	3	4	5	1	2	3	
0 - 1 (a)	157	370	422	445	451	563	564	577	799
0 - 1 (b)	201	385	456	480	487	616	621	626	799
3 - 4	61	189	553	739	740	741	742	744	897
28 - 29	978	1176	1341	1557	1667	3406	3545	3720	3703

Mn (mg/kg)									
Sample	Citrate-Dithionite					Aqua-regia			Total
Depth (m)	1	2	3	4	5	1	2	3	
0 - 1 (a)	944	1216	1285	1308	1317	1345	1348	1354	1512
0 - 1 (b)	996	1274	1353	1384	1393	1427	1431	1433	1512
3 - 4	430	852	1109	1152	1153	1157	1159	1162	1266
28 - 29	1644	1753	1784	1804	1813	1881	1888	1903	2391

Appendix IIIA (Cont.)

(Results given as cumulative extracted)

Co (mg/kg)									
Sample	Citrate-Dithionite					Aqua-regia			Total
Depth (m)	1	2	3	4	5	1	2	3	
0 - 1 (a)	100	108	112	113	116	123	124	126	171
0 - 1 (b)	141	149	150	153	154	161	162	163	171
3 - 4	6	7	12	16	17	18	19	20	16
28 - 29	318	328	338	347	352	397	399	400	431

Ti (mg/kg)									
Sample	Citrate-Dithionite					Aqua-regia			Total
Depth (m)	1	2	3	4	5	1	2	3	
0 - 1 (a)	83	840	933	938	953	1120	1228	1326	3780
0 - 1 (b)	233	729	828	832	837	1012	1110	1195	3780
3 - 4	191	701	1588	1665	1670	1804	1851	1913	4740
28 - 29	28	282	286	301	306	566	675	784	1200

Pt (µg/kg) (Corrected for Blank)								
Sample	Citrate-Dithionite					Aqua-regia		Total
Depth (m)	1	2	3	4	5	1	3	
0 - 1	400	467	500	517	533	642	650	845
3 - 4	260	328	361	395	412	588	597	690
28 - 29	25	25	33	42	50	100	108	135

Pd (µg/kg) (Corrected for Blank)								
Sample	Citrate-Dithionite					Aqua-regia		Total
Depth (m)	1	2	3	4	5	1	3	
0 - 1	17	25	33	33	42	342	358	438
3 - 4	92	101	109	118	118	378	378	432
28 - 29	0	0	0	0	0	75	92	110

Appendix IIIb: Citrate-Thiosulphate Extractions

(Results given as cumulative extracted)

Fe (mg/kg) (Corrected for Blank)						
Sample	Citrate-Thiosulphate					Total
Depth (m)	1	2	3	4	5	
0 - 1	316	674	823	1009	1134	216000
3 - 4	525	864	997	1114	1289	317000
28 - 29	1381	2120	2608	3318	3675	162000

Cr (mg/kg) (Corrected for Blank)						
Sample	Citrate-Thiosulphate					Total
Depth (m)	1	2	3	4	5	
0 - 1	9	12	12	12	12	2360
3 - 4	14	21	21	21	21	7322
28 - 29	6	6	6	6	6	6526

Mn (mg/kg) (Corrected for Blank)						
Sample	Citrate-Thiosulphate					Total
Depth (m)	1	2	3	4	5	
0 - 1	424	558	605	632	640	1512
3 - 4	0.7	0.7	0.7	0.7	0.7	1266
28 - 29	482	795	969	1046	1093	2391

Pt (μg/kg) (Corrected for Blank)						
Sample	Citrate-Thiosulphate					Total
Depth (m)	1	2	3	4	5	
0 - 1	56	98	112	111	125	845
3 - 4	14	13	27	26	40	690
28 - 29	14	14	14	14	27	135

Pd (μg/kg) (Corrected for Blank)						
Sample	Citrate-Thiosulphate					Total
Depth (m)	1	2	3	4	5	
0 - 1	24	30	30	37	37	438
3 - 4	12	12	12	12	12	432
28 - 29	0	0	0	0	0	110

Appendix IV: High Gradient Magnetic Separation Method

A flow cell of dimensions 3.5 cm x 6 cm x 20 cm was manufactured from clear perspex, using brass (not Fe) screws, with a structure as shown in Figure A4.1, and filled with 15 g of fine stainless steel wool.

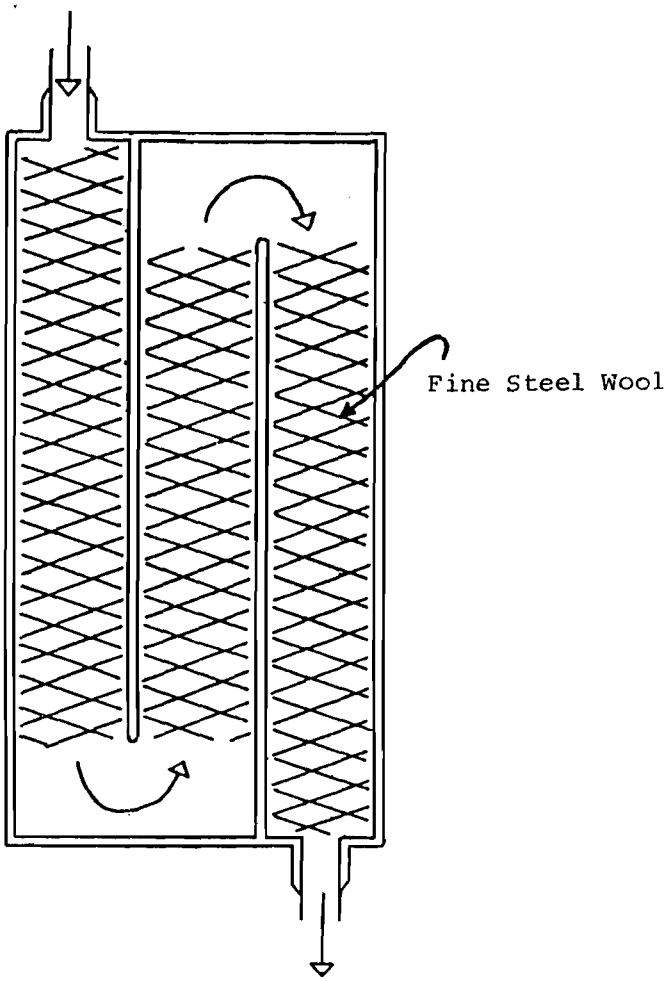

Figure A4.1: Diagrammatic structure of flow cell used for HGMS. This design is a modification of that used by Schulze and Dixon (1979).

The HGMS technique is illustrated diagrammatically in Figure A4.2 and described below. The flow cell was filled with distilled water and placed in the working gap between the two electric coils of a Rapid LHW High Gradient Magnetic Separator (owned by CSIRO, North Ryde) and the machine set at Coil Voltage = 60 Volts, Coil Current = 10 Amps. The clay suspension was then passed through the flow cell, at a rate of about 200 mL/min. Paramagnetic material was adsorbed at the surface of the steel wool. The outflow was collected and again passed through the flow cell. This process was preformed three times and then the flow cell was washed with about 300 mL distilled water. The outflow from this wash and the suspension from the magnetic collection were combined as the non-magnetic residue (NMR). The magnetic field was then turned off and the magnetic concentrate (MC) washed off the steel wool with up to 1000 mL distilled water. The resulting suspensions were dried at 60 - 70°C.

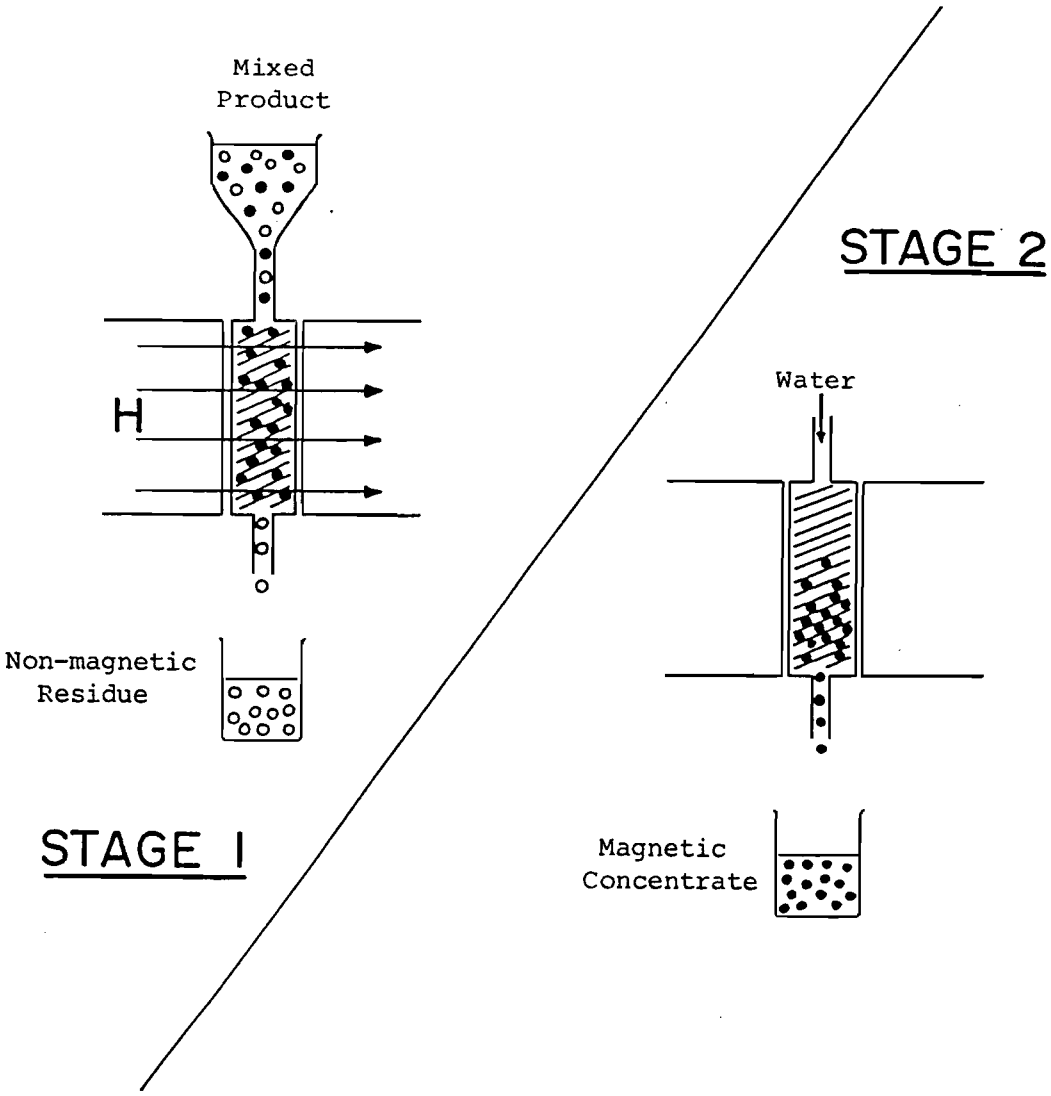

Figure A4.2: Diagrammatic illustration of the HGMS Procedure

Appendix V: Particle Size Separation and High Gradient Magnetic Separation Results

Appendix Va: Particle Size Separation - Percentage in each size fraction

MC24	< 2 μm	2-20 μm	> 20μm
3 - 4 m	64	27	8
6 - 7 m	63	29	8
8 - 9 m	59	32	9
14 - 15 m	78	14	8
22 - 23 m	45	34	20
28 - 29 m	38	33	29

Appendix Vb: High Gradient Magnetic Separation - Percentage in each size fraction

MC24	MC	NMR
3 - 4 m	34	66
6 - 7 m	15	85
8 - 9 m	16	84
14 - 15 m	8	92
22 - 23 m	15	85
28 - 29 m	23	77

Appendix Vc: Elemental Compositions of Solid samples

Sample Depth (m)	Treat-ment	SiO_2 (%)	Al_2O_3 (%)	Fe_2O_3 (%)	MnO (%)	MgO (%)	CaO (%)	Na_2O (%)	K_2O (%)	TiO_2 (%)	Ba (mg/kg)	Ce (mg/kg)	Cl (mg/kg)
3-4	Whole	20.00	15.79	45.32	0.159	0.01	0.00	0.42		1.04	6	7	
	> 20 μm	16.94	5.62	69.96	0.361	0.16	0.03	0.06	0.08	1.45	236	< 3	30
	2-20 μm	11.86	7.76	74.98	0.349	0.16	0.02	0.06	0.02	1.33	2	< 6	90
	< 2 μm	25.65	21.91	32.98	0.082	0.27	0.03	1.84	0.03	0.60	23	< 17	11920
	MC	18.43	16.06	50.06	0.138	0.22	0.02	0.24	0.02	0.86	< 2	7	2570
	NMR	29.56	25.30	24.46	0.051	0.28	0.03	2.36	0.04	0.45	7	3	13720
6-7	Whole	19.65	16.86	45.61	0.186	0.05	0.00	0.56		0.99	16	15	
	> 20 μm	12.77	7.86	71.00	0.452	0.17	0.02	0.01	0.03	1.53	209	10	70
	2-20 μm	9.13	7.08	76.85	0.423	0.19	0.01	0.07	0.02	1.16	43	< 9	140
	< 2 μm	25.50	22.54	31.79	0.085	0.29	0.01	1.99	0.03	0.60	< 10	< 9	12010
	MC	9.44	9.41	67.03	0.238	0.18	0.00	0.05	0.01	1.06	24	< 5	1550
	NMR	28.20	25.11	26.95	0.060	0.27	0.01	1.59	0.03	0.52	6	< 5	8130
8-9	Whole	20.71	16.94	46.47	0.291	0.00	0.00	0.34		0.99	8	12	
	> 20 μm	12.84	8.11	73.28	0.587	0.17	0.01	0.06	0.02	1.34	184	< 2	40
	2-20 μm	10.58	7.13	79.74	0.619	0.17	0.01	0.12	0.02	1.18	25	9	70
	< 2 μm	27.72	23.50	29.06	0.133	0.29	0.01	1.85	0.03	0.59	2	0	11730
	MC	13.01	11.17	63.19	0.351	0.17	0.00	0.03	0.01	1.01	20	7	770
	NMR	31.34	26.95	24.57	0.099	0.21	0.00	0.78	0.02	0.54	< 13	8	4450
14-15	Whole	42.06	8.27	24.30	0.241	3.45	0.01	1.24		0.48	133	11	
	> 20 μm	38.26	4.86	29.61	0.346	3.04	0.04	0.75	0.06	0.48	2405	< 26	< 10
	2-20 μm	37.83	5.32	33.72	0.538	3.22	0.04	0.8	0.07	0.84	281	0	40
	< 2 μm	45.52	9.42	21.03	0.158	3.11	0.03	1.89	0.09	0.32	37	9	7440
	MC	33.16	6.01	37.54	0.872	2.72	0.02	0.64	0.07	0.78	115	14	2740
	NMR	45.91	9.58	19.15	0.092	3.07	0.03	1.97	0.09	0.27	47	5	6930
22-23	Whole	43.79	5.03	22.73	0.848	12.17	0.00	0.81		0.31	42	104	
	> 20 μm	33.41	2.57	42.28	2.215	6.46	0.01	0.35	0.14	0.40	171	85	370
	2-20 μm	48.02	2.99	19.41	0.660	18.28	0.01	0.41	0.05	0.38	49	125	150
	< 2 μm	47.20	8.13	13.53	0.487	11.48	0.02	1.47	0.08	0.12	23	89	8070
	MC	41.50	6.51	21.91	1.586	8.98	0.02	0.57	0.11	0.31	63	238	2250
	NMR	49.02	8.57	12.18	0.290	12.17	0.02	1.72	0.07	0.09	25	65	9700
28-29	Whole	39.81	4.18	23.16	0.334	11.89	2.07	0.96		0.23	11	8	
	> 20 μm	34.96	2.59	34.89	0.396	13.63	3.94	0.34	0.02	0.31	39	< 21	10
	2-20 μm	44.22	3.67	23.30	0.329	13.86	2.49	0.59	0.04	0.26	17	3	10
	< 2 μm	45.14	6.54	14.60	0.235	10.85	0.50	2.07	0.08	0.11	5	1	15650
	MC	42.88	6.27	20.06	0.448	7.75	0.54	0.79	0.08	0.18	7	< 5	7760
	NMR	46.12	6.70	13.04	0.172	11.87	0.50	2.66	0.08	0.09	17	8	18070

Appendix Vc (Cont.)

Sample Depth (m)	Treat-ment	Cr (mg/kg)	Co (mg/kg)	Cu (mg/kg)	Ga (mg/kg)	Ni (mg/kg)	Rb (mg/kg)	S (mg/kg)	Sr (mg/kg)	V (mg/kg)
3-4 m	Whole	10071	19	741	20	907	2	2310	5	310
	> 20 µm	8002	2	530	15	605	4	290	9	358
	2-20 µm	10443	< 3	634	15	729	5	260	9	349
	< 2 µm	7553	8	689	23	1088	0	2790	10	166
	MC	11464	19	963	28	1410	7	440	3	267
	NMR	5536	< 1	573	19	969	1	3720	5	118
6-7 m	Whole	8673	19	1567	16	1215	0	2800	6	277
	> 20 µm	7559	15	953	15	784	5	300	8	283
	2-20 µm	9550	3	1425	17	1106	0	310	12	311
	< 2 µm	6179	12	1433	20	1436	0	3480	7	150
	MC	11880	16	2462	24	2030	3	260	9	323
	NMR	5311	7	1318	15	1405	< 3	2820	3	125
8-9 m	Whole	5559	37	967	16	600	1	2690	6	253
	> 20 µm	5008	5	556	15	415	0	240	12	255
	2-20 µm	5756	< 2	723	18	448	< 1	220	11	261
	< 2 µm	4100	13	971	20	754	2	3250	5	151
	MC	8691	14	1652	26	1121	8	210	4	326
	NMR	3421	12	909	18	748	< 3	1380	< 1	131
14-15 m	Whole	9060	121	772	9	3194	1	890	38	61
	> 20 µm	10289	69	626	10	2263	2	550	129	142
	2-20 µm	9001	81	589	10	2503	4	100	30	144
	< 2 µm	7105	84	612	9	3242	1	760	17	33
	MC	7235	106	1021	12	2521	7	80	18	146
	NMR	6931	81	563	7	3261	2	790	19	17
22-23 m	Whole	5384	787	1329	8	4686	1	270	16	241
	> 20 µm	12755	1136	1434	11	4933	1	20	23	523
	2-20 µm	4162	530	808	5	3474	0	0	9	179
	< 2 µm	3041	687	1067	7	4959	1	590	15	66
	MC	4446	1751	1636	9	7506	10	0	16	175
	NMR	2804	504	993	11	4595	2	740	13	51
28-29 m	Whole	6090	587	575	6	4391	1	1660	21	156
	> 20 µm	19022	547	242	6	2816	0	< 20	17	265
	2-20 µm	3386	463	414	5	3927	1	< 10	18	123
	< 2 µm	1858	499	561	5	4882	2	1080	14	53
	MC	2062	834	669	5	6052	12	10	15	81
	NMR	1816	407	544	7	4581	0	1570	15	52

Appendix Vc (Cont.)

Sample Depth (m)	Treat-ment	Y (mg/kg)	Zn (mg/kg)	Zr (mg/kg)	Pt (µg/kg)	Pd (µg/kg)
3-4 m	Whole	5	115	48	690	435
	> 20 µm	6	84	288	978	446
	2-20 µm	6	119	74	856	453
	< 2 µm	7	129	25	449	408
	MC	2	192	37	652	429
	NMR	6	109	20	388	434
6-7 m	Whole	5	130	46	1300	457
	> 20 µm	7	90	212	2314	534
	2-20 µm	6	132	75	1965	482
	< 2 µm	7	147	25	833	460
	MC	7	239	43	1983	638
	NMR	6	137	27	657	426
8-9 m	Whole	3	70	42	830	457
	> 20 µm	6	56	172	1142	502
	2-20 µm	5	69	63	975	487
	< 2 µm	1	90	22	523	402
	MC	2	154	45	1129	602
	NMR	3	88	20	448	369
14-15 m	Whole	2	368	22	195	106
	> 20 µm	4	267	78	445	208
	2-20 µm	5	298	47	411	169
	< 2 µm	3	354	16	133	114
	MC	3	285	49	820	301
	NMR	3	351	9	83	77
22-23 m	Whole	71	353	17	180	215
	> 20 µm	123	471	48	319	319
	2-20 µm	85	236	15	181	220
	< 2 µm	34	364	6	171	233
	MC	86	464	16	495	429
	NMR	22	350	6	109	191
28-29 m	Whole	44	269	13	135	110
	> 20 µm	29	406	24	164	96
	2-20 µm	43	201	17	130	110
	< 2 µm	44	265	9	186	198
	MC	57	293	18	206	137
	NMR	39	264	11	109	158

Appendix VI: HGMS Samples - Extraction Results

Sample Depth (m)		Solid Composition								
		Al_2O_3 (%)	Fe_2O_3 (%)	MnO (%)	TiO_2 (%)	Cr (mg/kg)	Cu (mg/kg)	Ni (mg/kg)	Pt (μg/kg)	Pd (μg/kg)
3-4	< 2 μm	21.91	32.98	0.082	0.60	7553	689	1088	449	408
	MC	16.06	50.06	0.138	0.86	11464	963	1410	652	429
	NMR	25.30	24.46	0.051	0.45	5536	573	969	388	434
6-7	< 2 μm	22.54	31.79	0.085	0.60	6179	1433	1436	833	460
	MC	9.41	67.03	0.238	1.06	11880	2462	2030	1983	638
	NMR	25.11	26.95	0.060	0.52	5311	1318	1405	657	426
8-9	< 2 μm	23.50	29.06	0.133	0.59	4100	971	754	523	402
	MC	11.17	63.19	0.351	1.01	8691	1652	1121	1129	602
	NMR	26.95	24.57	0.099	0.54	3421	909	748	448	369
14-15	< 2 μm	9.42	21.03	0.158	0.32	7105	612	3242	133	114
	MC	6.01	37.54	0.872	0.78	7235	1021	2521	820	301
	NMR	9.58	19.15	0.092	0.27	6931	563	3261	83	77
22-23	< 2 μm	8.13	13.53	0.487	0.12	3041	1067	4959	171	233
	MC	6.51	21.91	1.586	0.31	4446	1636	7506	495	429
	NMR	8.57	12.18	0.290	0.09	2804	993	4595	109	191
28-29	< 2 μm	6.54	14.60	0.235	0.11	1858	561	4882	186	198
	MC	6.27	20.06	0.448	0.18	2062	669	6052	206	137
	NMR	6.70	13.04	0.172	0.09	1816	544	4581	109	158

Sample Depth (m)		Tamms Acid Oxalate Extraction								
		Al_2O_3 (%)	Fe_2O_3 (%)	MnO (%)	TiO_2 (%)	Cr (mg/kg)	Cu (mg/kg)	Ni (mg/kg)	Pt (μg/kg)	Pd (μg/kg)
3-4	< 2 μm	0.321	0.206	0.001	0.00	25	nd	nd	46	32
	MC	0.271	0.225	0.001	0.00	25	nd	nd	23	23
	NMR	0.433	0.179	0.001	0.01	25	nd	nd	23	14
6-7	< 2 μm	0.492	0.205	0.001	0.01	21	nd	nd	42	28
	MC	0.224	0.288	0.001	0.01	21	nd	nd	28	28
	NMR	0.324	0.172	0.001	0.01	17	nd	nd	42	9
8-9	< 2 μm	0.297	0.184	0.001	0.01	13	nd	nd	37	14
	MC	0.213	0.316	0.001	0.01	17	nd	nd	23	23
	NMR	0.312	0.175	0.001	0.00	13	nd	nd	37	28
14-15	< 2 μm	0.187	0.312	0.046	0.01	54	nd	nd	9	9
	MC	0.126	0.389	0.233	0.01	46	nd	nd	14	5
	NMR	0.175	0.234	0.030	0.00	33	nd	nd	23	5
22-23	< 2 μm	0.163	0.272	0.335	0.01	38	400	400	14	14
	MC	0.175	0.288	1.190	0.01	42	600	1500	28	14
	NMR	0.198	0.273	0.213	0.01	33	400	400	19	19
28-29	< 2 μm	0.312	0.383	0.110	0.01	33	< 200	400	14	9
	MC	0.353	0.370	0.227	0.01	50	< 200	700	9	5
	NMR	0.383	0.392	0.086	0.01	29	< 200	400	5	9

nd: not determined

Appendix VI (Cont.)

Sample Depth (m)		Citrate - Dithionite Extraction									Residue	
		Al_2O_3 (%)	Fe_2O_3 (%)	MnO (%)	TiO_2 (%)	Cr (mg/kg)	Cu (mg/kg)	Ni (mg/kg)	Pt (μg/kg)	Pd (μg/kg)	Pt (μg/kg)	Pd (μg/kg)
3-4	< 2 μm	1.75	28.44	0.053	0.32	6125	< 200	600	315	231	75	142
	MC	2.79	46.81	0.112	0.34	10542	700	1200	519	278	58	117
	NMR	1.74	22.42	0.044	0.20	4792	< 200	500	227	213	83	175
6-7	< 2 μm	2.46	29.81	0.079	0.18	5500	800	800	722	306	75	142
	MC	2.78	59.03	0.189	0.73	11042	1600	1300	1806	343	42	183
	NMR	1.83	25.34	0.053	0.29	4708	500	800	630	269	83	225
8-9	< 2 μm	1.45	27.31	0.125	0.31	3454	400	400	463	241	67	175
	MC	2.42	55.75	0.294	0.55	7667	1100	1000	926	315	50	142
	NMR	1.34	22.36	0.088	0.25	2825	500	500	380	204	67	192
14-15	< 2 μm	0.61	7.21	0.102	0.02	775	< 200	800	106	9	67	108
	MC	0.67	20.63	0.560	0.14	1079	nd	nd	370	46	100	92
	NMR	0.37	4.33	0.051	0.02	463	nd	nd	162	0	58	100
22-23	< 2 μm	0.39	5.28	0.111	0.03	329	400	900	106	0	67	192
	MC	0.44	11.87	0.322	0.05	671	< 200	1900	255	46	50	150
	NMR	0.36	4.35	0.071	0.02	292	< 200	800	79	0	50	192
28-29	< 2 μm	0.33	6.14	0.088	0.00	479	< 200	1300	69	9	58	125
	MC	0.47	10.26	0.167	0.11	796	< 200	1800	352	23	100	117
	NMR	0.32	5.40	0.058	0.02	425	< 200	1000	125	5	58	142

nd: not determined

CHAPTER 7: GEOCHEMISTRY OF FRESH AND WEATHERED CHROMITE IN THE ORA BANDA SILL

I.D.M. Robertson, H.K. Schorin, S.J. Barnes and M.F.J. Tenhaeff

ABSTRACT

Chromite, found in abundance in the peridotites and, to a lesser extent, in the pyroxenites of the Ora Banda Sill, is relatively resistant to weathering. It consists of five major chemical components (divalent Mg, Fe^{2+}; trivalent Cr, Al and Fe^{3+}) which make it particularly sensitive to variations in the parent magma. Thus, fresh chromite from the diamond drilling at Ora Banda was investigated by microprobe and multivariate statistical analysis to determine if chromite compositions could be used to determine the rock type and/or proximity to sulphide mineralisation.

The fresh rock chromite geochemistry, particularly in terms of Cr-Al-Fe^{3+}, shows a tight group for peridotites and a much broader, scattered distribution for pyroxenites. Much of the observed scatter is due to variations in the proportion of trapped intercumulus liquid in these cumulate rocks, with a smaller scatter component due to fractional crystallisation; the peridotite is relatively poor in trapped liquid (adcumulate to mesocumulate) and the pyroxenite is rich in trapped liquid (orthocumulate). Another influence is chromite grain size (100 μm in peridotite and 40 μm in pyroxenite); smaller grains more readily re-equilibrate with the trapped liquid. There is also a significant difference between mineralised and unmineralised pyroxenite. Chromite in mineralised pyroxenite shows a trend of Al-depletion and Cr-enrichment at relatively constant Fe^{3+}, in contrast with a trend of Al-depletion and Fe^{3+}-enrichment of the chromite of unmineralised pyroxenite. It seems that the presence of sulphide impeded the build-up of Fe^{3+} in the trapped liquid. Thus the chromite compositions record the influence of the cumulus sulphide liquid component.

Microscopy of the weathered chromites (Volume IIA, Chapter 5, Section 5) shows a reticulate crack pattern (Plate 1) which is particularly prevalent near the grain margins. Microprobe analysis indicates an apparent loss of Fe^{3+} on weathering of both peridotitic and pyroxenitic chromites. This may be due to migration of Fe^{3+} into the reticulate cracks on weathering. An alternate and preferred interpretation is that the fine-grained chromites of the weathered pyroxenites tend not to survive weathering. Thus, the population tends to be biased towards larger chromites, which are more resistant to re-equilibration with the melt and are thus poorer in Fe^{3+}.

An investigation of the chromites in the intensely weathered profile at Mt. Carnage suggested that there may be a significant compositional (lithological) difference between the upper ferruginous zone and the lower, saponite-talc-tremolite zone, the upper zone being derived from pyroxenite, the lower from peridotite or from a particularly olivine-rich pyroxenite.

Insufficient background data on weathered pyroxenitic chromites was available to determine if sulphide-associated chromites could be detected in the weathered zone. The nature of the source rock could be determined but a large data set (say >40 chromite grain analyses) is necessary to make this distinction. Chromites of the Fe-rich duricrust are morphologically and geochemically related to those of the weathered peridotites, supporting the petrographic findings (Volume IIA Chapter 5, Sections 5 and 8).

WEATHERED CHROMITE

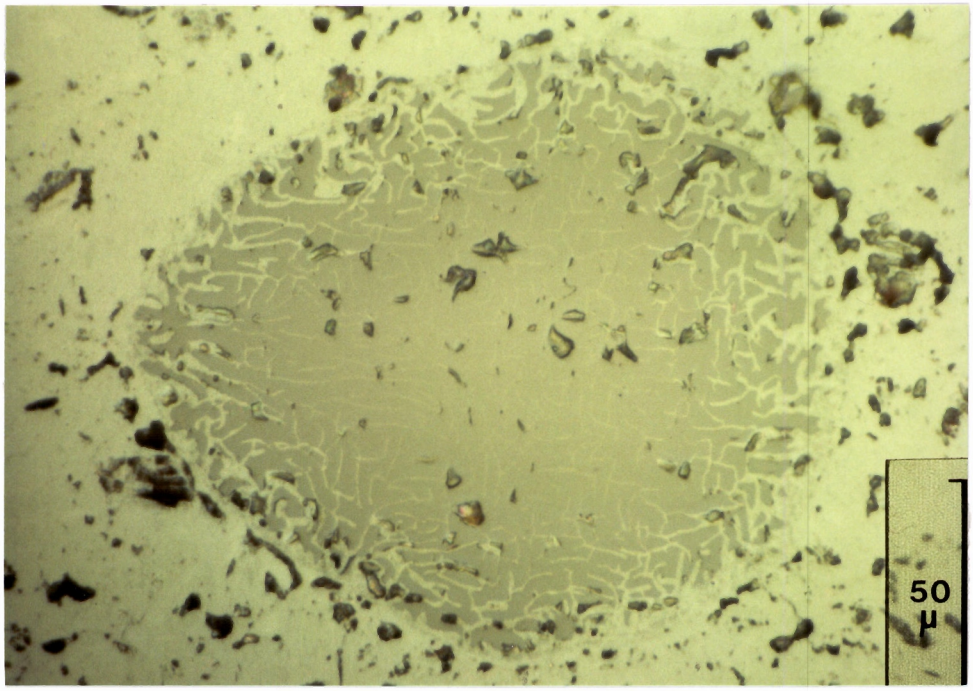

Plate 1. A crystal of weathered chromite set in goethite. Goethite has filled irregular, reticulate cracks around the rim of the chromite. Lag sample Specimen 08-1511. Co-ordinates 12606E 10997N.

1.0 INTRODUCTION

1.1 Objectives

Resistant primary chromite is preserved in the saprolites, ferruginous horizon, Fe-rich duricrust and lag overlying the Ora Banda Sill. Apart from indicating the presence of ultramafic rocks, chromite is a very useful petrogenetic indicator, as it contains 5 major chemical components and is, thus, more sensitive to variations in the parent magma than associated silicates (Thayer, 1970). The chromites of the fresh drill cores of OB DDH1 and DDH2 were examined to test if chromite geochemistry could be used as an indicator of rock type and/or mineralisation.

Although many primary silicates are transformed or destroyed by weathering, chromite is highly resistant. However reticulate cracked margins on some chromites (Volume IIA, Chapter 5; Figure 19C) indicate some alteration. By comparing fresh with weathered chromites of known horizons of the igneous stratigraphy, it was hoped to determine the nature of these changes.

The geochemistry and petrographic characteristics of the chromite of weathered rocks (saprolite, ferruginous horizon, Fe-rich duricrust and lag) could also be used to identify the underlying or source rock types. For instance, difficulties, due to intense weathering, were encountered in determining if the upper and lower PGE patterns in drill hole MC24 at Mt. Carnage are due to different parent rocks or due only to chemical weathering. The possibility of different parent rocks was investigated by comparison of their contained chromites.

1.2 Chromite Chemistry

Chromite is one of three mineral series belonging to the spinel group. The spinel group has a general structural formula of $R^{2+}R^{3+}O_4$, where R^{2+} includes the divalent ions Mg, Fe^{2+}, Ni, Mn and Zn; R^{3+} the trivalent ions Al, Fe^{3+}, Cr, Ti and V. Chromite compositions are effectively portrayed by the prism shown in Figure 1.

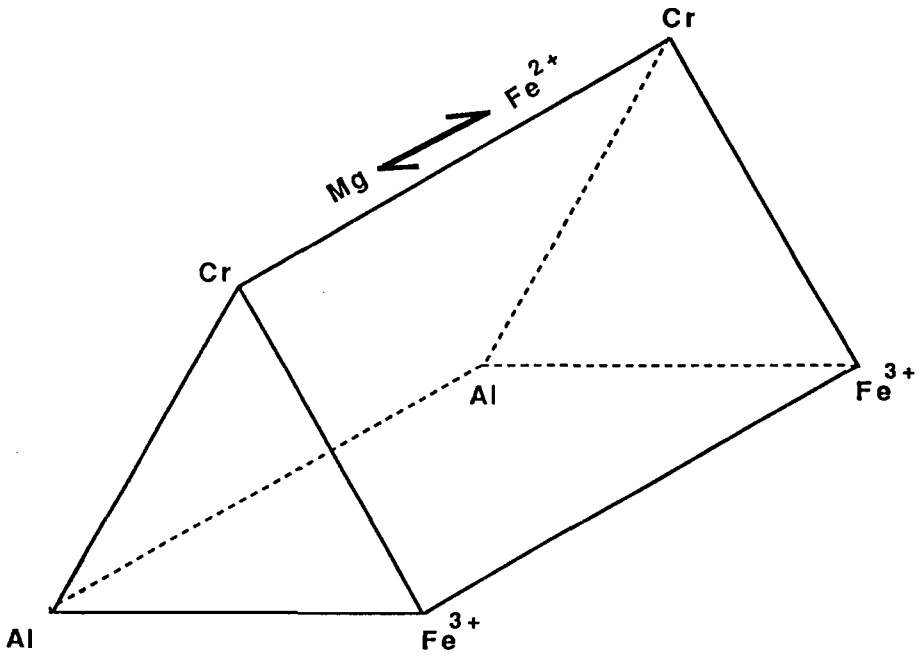

Figure 1. The compositions of chrome spinels illustrated by a prism of trivalent Cr-Al-Fe^{3+} with varying proportions of divalent Mg and Fe^{2+}.

The major trivalent ions (Al, Cr and Fe^{3+}) may be expressed by the triangular ends of the prism and the length of the prism reflects variation in the major divalent ions, largely Mg and Fe^{2+}. Thus, variations in chromite compositions may be shown in terms of the Cr-Al-Fe^{3+} ternary plot and as a plot of $Cr/(Cr+Al+Fe^{3+})$ against $Mg/(Mg+Fe^{2+})$ to reflect this prismatic relationship. Peck and Keays (1990) used plots of $100Mg/(Mg + Fe^{2+})$ against $100Cr/(Cr + Al)$ to characterize chromites from the Heazlewood River mafic-ultramafic Complex in Tasmania. However these portrayals are generalisations which do not include minor elements such as Ti, V, Mn and Zn. For more accurate distinctions, multivariate statistics must be used.

2.0 STUDY METHODS

2.1 Microprobe Analysis

The microprobe data were gathered at different times and different instruments were used due to instrument availability. The earlier work used a MAC 400S Microprobe and analyses were done in energy dispersive mode, using the methods of Ware (1981). The accelerating voltage was set to 15 kV and the beam current to 20 nA. The microprobe was standardised against a Smithsonian chromite standard. In this first pass of analysis, 173 analyses were completed on weathered Mt. Carnage chromites and 81 fresh chromites from the Ora Banda diamond drilling.

The later work used the automated Cameca SX-50 microprobe in wavelength dispersive mode, with a 30 nA beam, an accelerating voltage of 15 kV, a counting time of 40 s per element and a chromite secondary reference standard. In addition to the major elements (Al, Cr, Fe and Mg), a small suite of minor elements was determined, (Ca, Mn, Ni, Si, Ti, V and Zn). Silicon and Ca were measured to check for contamination and any analyses with appreciable contents of these elements were eliminated. In all, 222 satisfactory analyses of fresh chromites from 17 positions in the diamond drilling were obtained. Also 199 weathered chromite analyses were obtained from the lag at six sites. Where the grains were large enough, cores and rims were analysed. All chromite grains were examined in back-scattered electron mode and some were analysed incrementally from core to rim to investigate any possible zoning. Microprobe analysis was performed under the control of the WANU-SX geo-analytical package.

2.2 Statistical Analysis

A suite of SUN-resident statistical programs (Campbell 1980, 1982, 1986), provided by CSIRO's Division of Mathematics and Statistics were used for analysis of the chromite data. Prior to multivariate analysis it is necessary to ensure a normal distribution of the training data. Optimum power (λ) transformations (Box and Cox, 1964) were determined using CENSOR, as the lower limit of some of the data had been influenced by a detection limit. Robust estimates of means, standard deviations and correlations were made with WTHGRP. Robust canonical variate analysis was carried out using RBSTCV. *A posteriori* group membership and typicality indices were calculated with ALLOCN. This allocation technique is regarded as being better than canonical variate analysis as it indicates typicality of a particular reference group as well as probability of belonging. The effectiveness of each variable and combinations of variables (2, 3, 4 ...) in making the distinction was investigated with SUBSET.

3.0 Mt. CARNAGE WEATHERED PROFILE

There are distinct differences in the Pt/Pd relationships and in the gross and trace element geochemistry between the upper, ferruginous and the lower, clay-rich parts of the Mt. Carnage profile, as shown in drill section MC24 (Chapter 5; Section 7). There are two probable

interpretations; either these differences reflect differences in the weathering profile, with lithology taking no significant part, or they reflect different primary lithologies. To resolve this, 81 chromite grains from MC24 were analysed (MAC microprobe); thirty two were from the ferruginous zone (sample MC2407) and 59 from 2 samples of the saprolite (MC2431 and MC2439). No elemental zoning was observed in any of the chromites. Some of the grains of the ferruginous zone had corroded rims. Corroded spinels were not used to ascertain the characteristics of the chromites of the two zones of the profile. Plots of 100 Mg/(Mg + Fe^{2+}) (Mg#) against 100 Cr/(Cr + Al) (Cr#) for the chromites are presented in Figure 2. The circles represent the chromite compositions of the ferruginous zone, which show a broad range in Mg/Fe^{2+} ratios. The polygonal area on Figure 2 represents the chromites of the two samples of the saprolite (MC2431 and MC2439) where there is a contrasting narrow range in Mg/Fe^{2+} ratios. These results suggest that the samples MC2431 and MC2439 originate from the same parent rock, characterized by Pd > Pt (Pt/[Pt+Pd] = 40% and 48%, respectively). In contrast, the parent rock of the sample MC2407 may be different and is characterized by Pt > Pd (Pt/[Pt+Pd] = 74%).

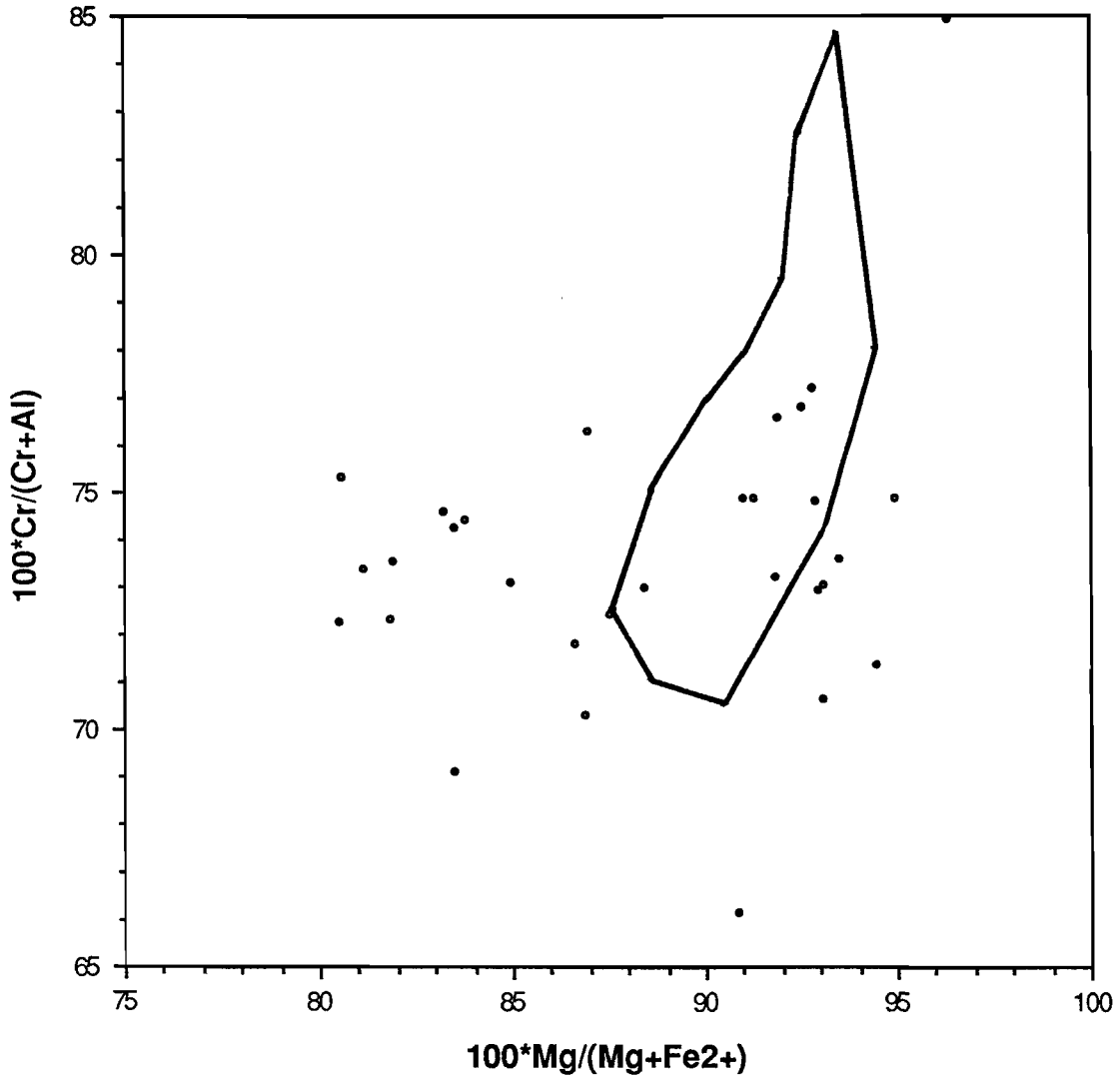

Figure 2. A plot of Cr# (100 x Cr/(Cr+Al)) against Mg# (100 x Mg/(Mg+Fe^{2+})) (after Peck and Keays, 1990) for chromite data from the weathered profile at Mt. Carnage (DH MC24). Contrasting, though overlapping, fields for chromites from the saprolite (polygon) and the ferruginous zone (circles) suggest a difference in primary rock composition.

Normative mineral compositions of 21 chromites from samples MC2407 (ferruginous zone), MC2431 and MC2439 (saprolite) were calculated. An ideal spinel formula was assumed, based on 24 cations and 32 oxygens. Ferrous iron was estimated from the stoichiometry. The main components are chromite ($Fe^{2+}Cr_2O_4$) (52% in the chromites of the saprolite; 55% in the chromites of the ferruginous zone), magnetite($Fe^{2+}Fe^{3+}{}_2O_4$) (17% in saprolite; 9% in ferruginous zone) and spinel ($MgAl_2O_4$) (15% in saprolite; 17% in ferruginous zone). The minor components are ulvospinel ($Fe^{2+}{}_2TiO_4$), gahnite ($ZnAl_2O_4$), galaxite ($MnAl_2O_4$) and coulsonite ($Fe^{2+}V_2O_4$). Hercynite ($Fe^{2+}Al_2O_4$) was found in most chromites of the samples from the saprolite but only in a few chromites of the ferruginous zone. Magnesioferrite ($MgFe^{3+}{}_2O_4$) was only estimated in chromites of sample MC2407 (ferruginous zone).

The clearest difference between the chromites of the saprolite and the ferruginous zone at Mt. Carnage are in their Fe^{3+} content and in their content of magnetite (8%). The differences in the contents of Cr and of chromite (3%) were less and in the contents of spinel of 2%, respectively. These results seem to indicate that significant differences may exist between the parent rocks from which the ferruginous material and the saprolite were formed, the former probably derived from pyroxenite and the latter from peridotite. The bulk geochemistry of *all samples* from both zones suggests that the complete profile is derived dominantly from pyroxenite, although there may be some layering in the saprolite having a more peridotitic composition. (Volume IIA, Chapter 5, Section 7.4). These conclusions are not inconsistent, since chromites from only two samples from the saprolite were examined, of which MC2431 has a low Pt/[Pt+Pd] ratio (40%).

4.0 FRESH CHROMITES

4.1 Fresh Chromite in OB DDH1 and DDH2, Ora Banda Prospect

Chromite is an important mineral in both the fresh peridotite, where it is most abundant and the grains are large (30-200; mean 100 μm), and in the pyroxenite, where it is far less abundant and the grains are smaller (10-120; mean 40 μm) (see Volume IIA, Chapter 5; Section 3.1). The fresh chromite grains were analysed by microprobe to determine if there were significant differences in composition that could be related to rock type and/or to mineralisation. The weathered chromites were later studied (Section 5) to see if similar information could be determined from surficial materials and also to investigate the changes in chromite geochemistry due to weathering.

More than 220 analyses of fresh chromites were obtained (Cameca microprobe; Section 2.1). All analyses which appeared to be of mixed phases (significant Si or Ca, excessive Ti or low totals) were eliminated. The structural formula was then calculated, assuming that Ti is present as ulvospinel. The Fe^{3+} was calculated from the chromite stoichiometry and the results are presented in Appendix 1.

The fresh chromites were grouped according to the rock type in which they occur and according to the presence or relative absence of sulphide mineralisation, as shown by their Cu content. Thus a four-fold classification was used for the fresh chromites of OB DDH1 and DDH2. BC and BCS comprise the chromites of pyroxenitic rocks, unmineralised and mineralised respectively; OB and OBS were chromites from peridotitic rocks, also unmineralised and mineralised respectively.

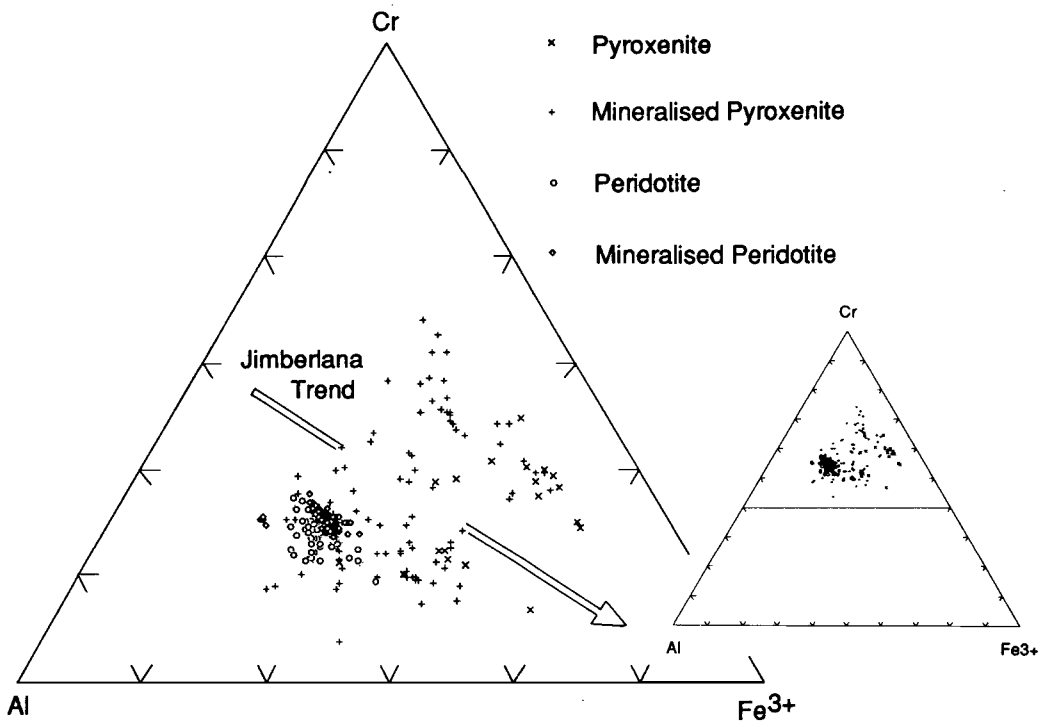

Figure 3A. Expanded ternary plot Cr-Al-Fe^{3+} of fresh chromites from the two Ora Banda diamond drillholes.

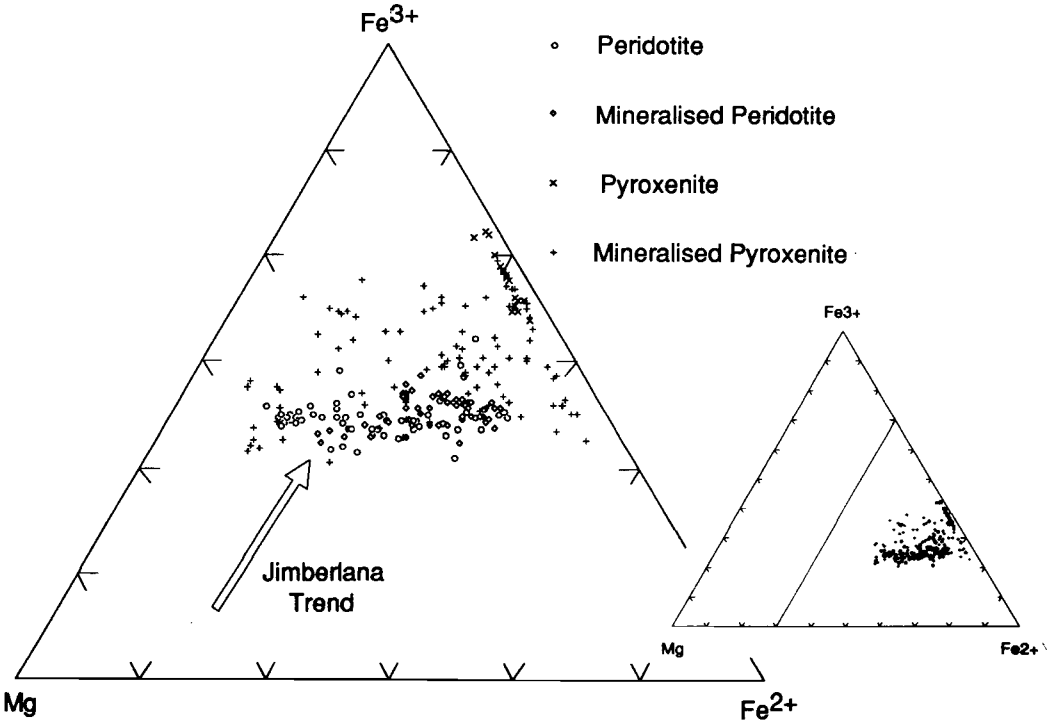

Figure 3B. Expanded ternary plot Fe^{3+}-Mg-Fe^{2+} of fresh chromites from the two Ora Banda diamond drillholes.

These fresh chromite analyses are part of the second batch of analyses (Section 2.1). On the Cr-Al-Fe^{3+} ternary plot (Figure 3A), the chromites from the peridotite (OB) and the mineralised peridotite (OBS) form closely overlapping groups. Compared to these, the chromites of the pyroxenite (BC) are enriched in Fe^{3+} relative to Al and Cr but the chromites from the mineralised pyroxenite (BCS) are different from the others and show a trend towards Al-depletion and Cr-enrichment at relatively constant Fe^{3+}. Although these latter two groups overlap slightly, they are relatively distinct and from the peridotite-related chromites (OB and OBS). Similar, relatively good separations may be made between the peridotite-, pyroxenite- and mineralised pyroxenite-related chromites on the Fe^{2+}/Fe^{3+} and the Fe/Ti plots (Figures 4A and B). There is still considerable overlap between the peridotite- and mineralised peridotite-related chromites. It remained to improve the separations of these binary and ternary plots by testing these data in multivariate space.

4.2 Multivariate Analysis of Fresh Chromite Data

Classification of chromites using the Cr-Al-Fe^{3+} ternary plot ignores the remaining six components so a multivariate technique was evaluated to see if classification could be improved. The distributions of the chromite analytical data from the pyroxenite (BC), the mineralised pyroxenite (BCS), the peridotite (OB) and the mineralised peridotite (OBS) were examined separately, using normal probability (Q-Q) plots. Outliers, which tend to distort the calculated values for the power transform (λ), were removed to a separate outlier data file. A total of 11 chromite analyses were determined as outliers in the fresh chromite data set of 241 analyses (4.5%). Nickel was deleted from the data set as it did not appear to be meaningful, due to low analytical precision.

No transformation was necessary for Fe^{2+} but log transformations were needed for Cr and Fe^{3+}; all other variables required Box-Cox power transformations. These were determined separately on each variable of each group; one variable (Zn) had been censored by its lower detection limit. A separate, compromise value for λ was selected to transform each variable of the pooled groups during all subsequent phases of data analysis.

Robust estimations of means, standard deviations and correlations were followed by robust canonical variate analysis. The results of this canonical variate analysis of four reference groups are three canonical variates (CV1, CV2, CV3; Appendix 1) of which the first two contain most of the useful information (Figure 5). The chromites of the peridotites and mineralised peridotites are not well separated but the pyroxenites and peridotites are relatively distinct, as are the mineralised pyroxenite and the pyroxenite.

Group membership probabilities and typicality indices for individual samples were calculated using 95% confidence limits for the typicality. Assessment of the results (Appendix 1; final column, "Post Type") showed (Table 4) that chromites from unmineralised peridotites could be distinguished with 64% certainty and those from mineralised peridotite with 84% certainty. However, the probability of making a correct distinction between pyroxenite- and peridotite-related chromites is much higher (70-95%). Chromites from unmineralised pyroxenite could be identified with 65% certainty and those of mineralised pyroxenites with 51% certainty on a grain-by-grain basis. Among the mineralised and unmineralised pyroxenites, some chromites could not be classified (11 and 24% respectively). From these results it is clear that a statistically significant number of chromite analyses are necessary to provide the range of data before a valid distinction may be attempted between mineralised and unmineralised groups, as the variance and degree of overlap are significant.

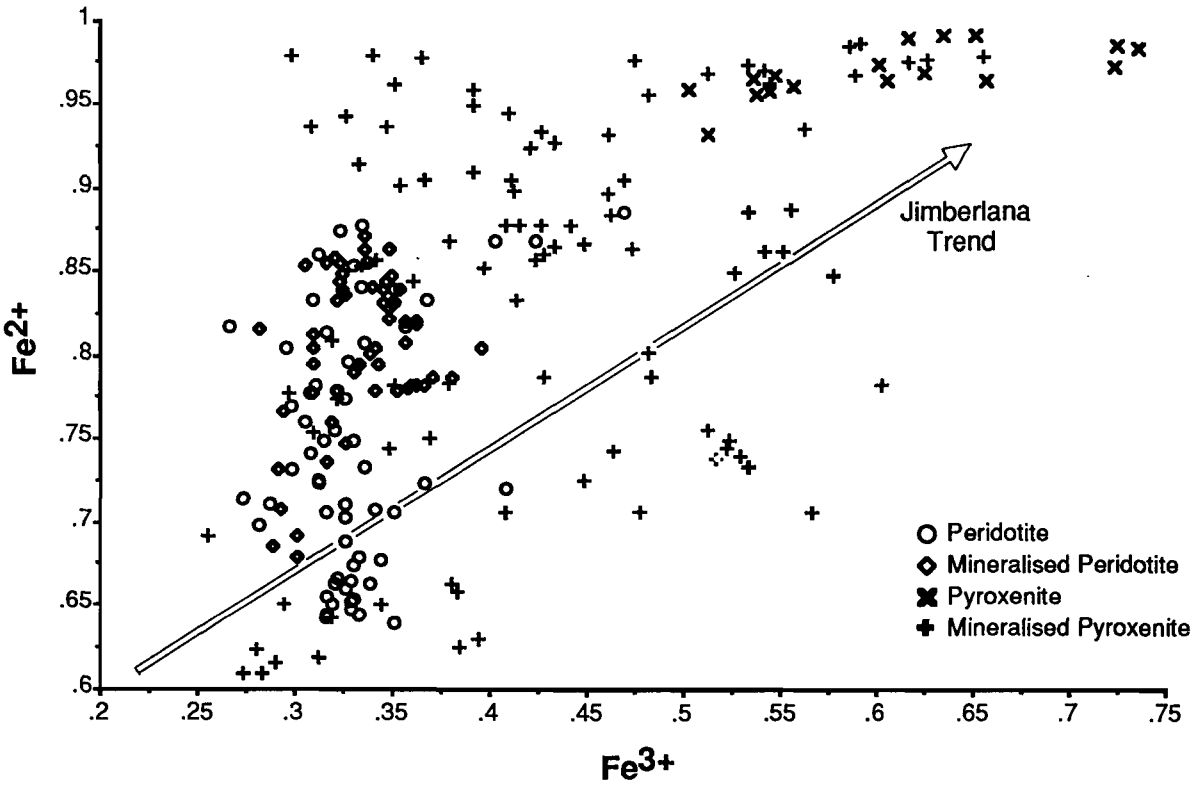

Figure 4A. Binary plot Fe^{2+}/Fe^{3+} of fresh chromites from the two Ora Banda diamond drillholes.

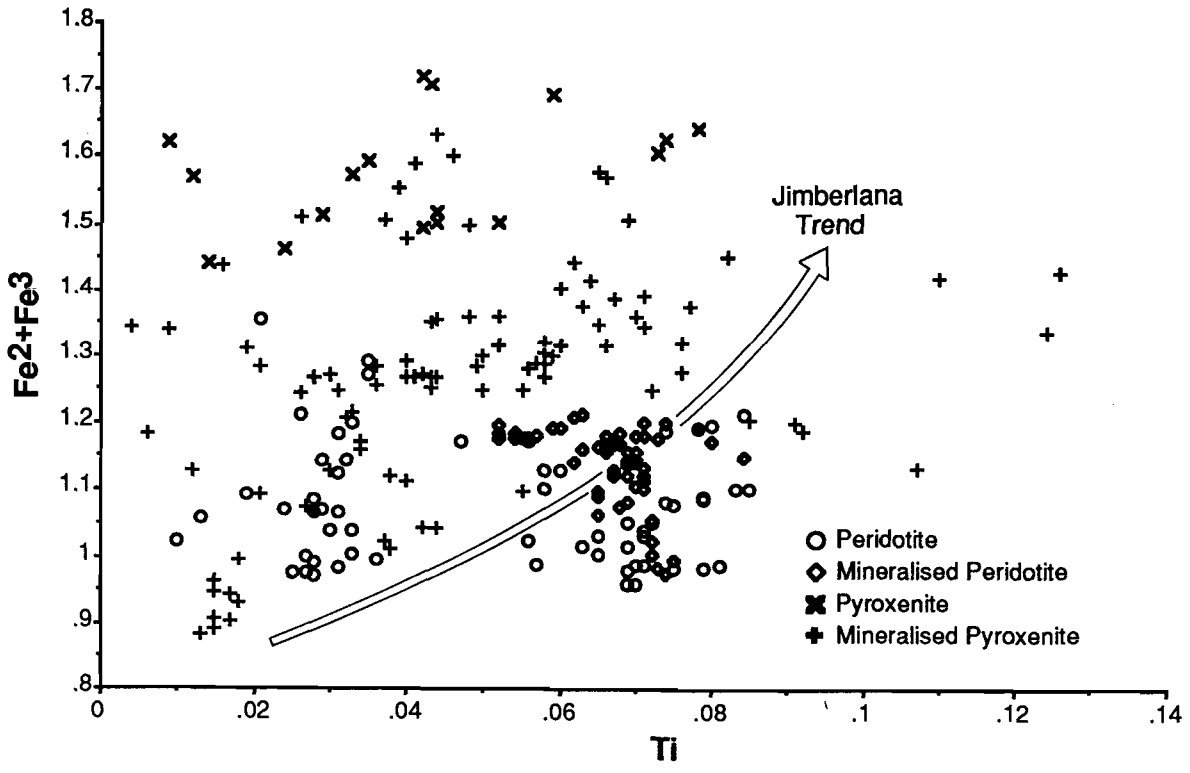

Figure 4B. Binary plot $Fe^{2+} + Fe^{3+}/Ti$ of fresh chromites from the two Ora Banda diamond drillholes.

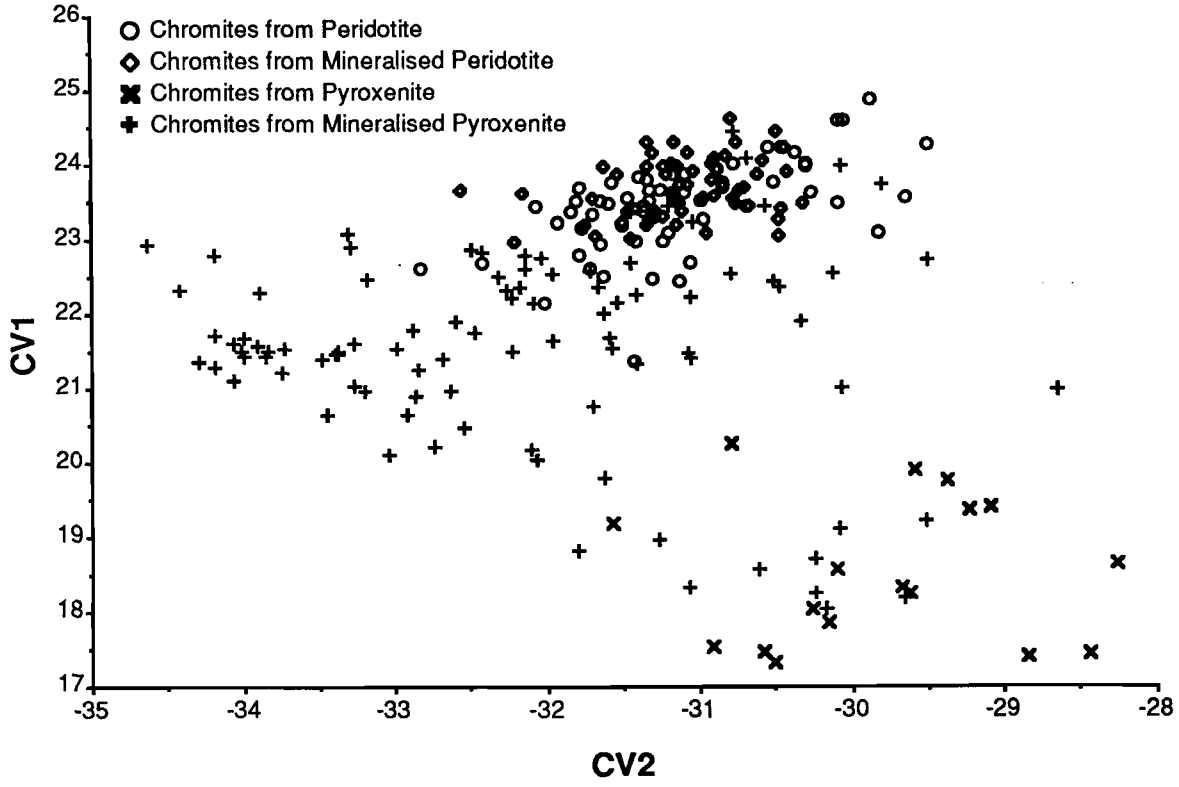

Figure 5. Canonical variate plot of discriminant analysis of fresh chromites from Ora Banda diamond drillholes.

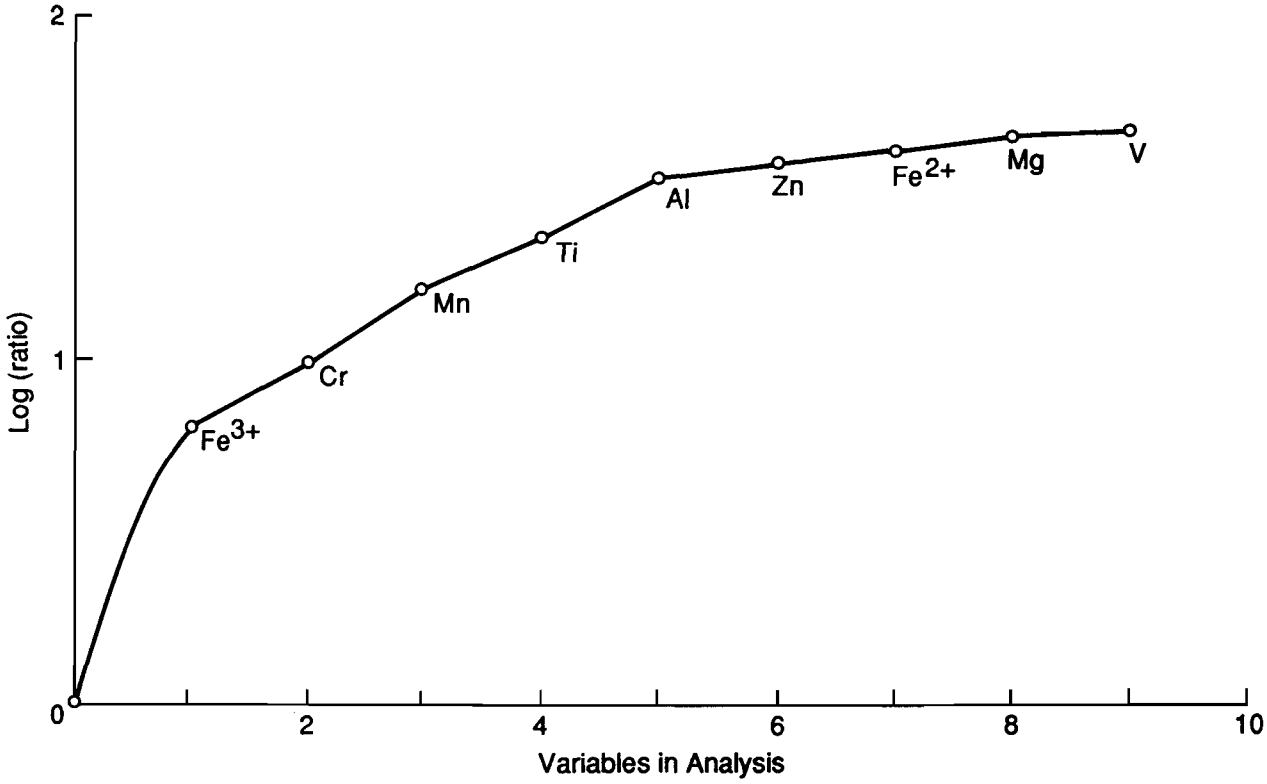

Figure 6. Results of investigation of contribution of each element to the fresh chromite discrimination.

TABLE 1
Fresh Chromite Allocations

A Priori Groups	% Allocations - *a posteriori*				
	Peridotite	**Min Peridotite**	**Pyroxenite**	**Min Pyroxenite**	**Unclassified**
Unmineralised Peridotite	64	28	0	8	0
Mineralised Peridotite	16	84	0	0	0
Unmineralised Pyroxenite	0	0	65	12	24
Mineralised Pyroxenite	17	11	10	51	11

The effectiveness of each variable and combinations of variables in making this classification is shown in Figure 6. The greatest part of the distinction is achieved using Fe^{3+}, Cr, Mn, Ti and Al. The contributions of Zn, Fe^{2+}, Mg and V are minimal.

4.3 Discussion

Many factors influence the compositions of chromite grains in cumulate rocks: the temperature, composition and oxygen fugacity of the parent magma (Murck and Campbell, 1986; Roeder and Reynolds, 1991); the extent of reaction of chromite grains with trapped interstitial melt in the intercumulus pore space (Roeder and Campbell, 1985); and the extent of subsolidus re-equilibration between chromite and solid silicate phases (Irvine, 1967). Subsequent metamorphism and alteration may also have influence but, for the fresh, unmetamorphosed rocks of the Ora Banda Sill, only the igneous processes need be considered.

Data on co-existing pyroxenes in the Ora Banda rocks suggest that most of the observed compositional scatter is due to variation in the abundance of trapped liquid, with a smaller component of scatter due to fractional crystallization of the parent magma. Crystallization of variable proportions of trapped liquid results in a shift in silicate mineral compositions. In the case of cumulus pyroxenes, this causes a wide spread in the Mg/Fe ratio, with a correspondingly smaller spread in Cr content (Barnes, 1986) as seen in the Ora Banda data (Figure 7). The peridotites are generally adcumulates to mesocumulates, and the pyroxenites are orthocumulates. The pyroxene data suggest an increase in the abundance of trapped liquid higher in the section. Most of the observed scatter in chromite composition is likely to be due to the same effect.

In a comprehensive study of chromite compositions in cumulates from the Jimberlana Dyke, Roeder and Campbell (1985) demonstrated that reaction with trapped liquid produces systematic trends in chromite composition from adcumulates to orthocumulates. Chromites that have reacted extensively with trapped liquid become enriched in total iron, in Fe^{3+} relative to Cr and Al, and in Ti, and depleted in Al due to selective partitioning of Al into intercumulus plagioclase. This produces the trends shown in Figure 8. Broadly speaking, the Ora Banda chromites show similar trends, but with some important differences (Figures 3A and B, 4A and B).

The most obvious feature of the Ora Banda data is the marked difference between chromite in peridotite and that in pyroxenite. There are two reasons for this. Firstly, the peridotites contained much less trapped liquid. Secondly, chromite is much more abundant and coarser grained in the peridotites, and therefore less susceptible to reaction. Peridotitic compositions, therefore, reflect the primary liquidus chromite.

A significant feature of the Ora Banda chromites is the difference between mineralized and unmineralised pyroxenite. Chromite in mineralized pyroxenite shows a trend of Al-depletion and Cr enrichment at approximately constant Fe^{3+}. This trend is consistent with the Al-depletion observed by Roeder and Campbell, but there is no sign of Fe^{3+} enrichment (Figure 3A). The lack of Fe^{3+} enrichment in the mineralized pyroxenite samples is also evident in Figure 4. In contrast, the unmineralised pyroxenite shows the Jimberlana trend of Fe^{3+} enrichment combined with Al depletion. These chromites also show strongly depleted Mg, indicating extensive reaction with differentiated trapped liquid.

The difference between the mineralized and unmineralised pyroxenite samples cannot be explained entirely in terms of differing proportions of trapped liquid, so it appears that the presence of sulphide may have played a role. A possible interpretation is that the presence of sulphide may have impeded the build-up of Fe^{3+} in the residual trapped liquid (normally responsible for the Jimberlana trend). A possible reaction is:-

$$\underset{\text{Melt}}{2Fe_2O_3} + \underset{\text{Solid or liquid sulphide}}{2FeS} = \underset{\text{Melt}}{6FeO} + \underset{\text{Fluid phase}}{S_2}$$

i.e., reduction of melt Fe^{3+} by reaction with sulphide. In this way, S is lost from the sulphide fraction, which consequently becomes enriched in Cu, Ni and PGE's, as proposed by Naldrett *et al.*, (1990) for the UG2 chromite of the Bushveld Complex.

It is unlikely that the chromite data contain any information about the primary magmatic processes which led to sulphide liquid formation. However, the data apparently record the influence of sulphides in the cumulates and have some bearing on the origin of this unusual, PGE-rich, S-poor occurrence.

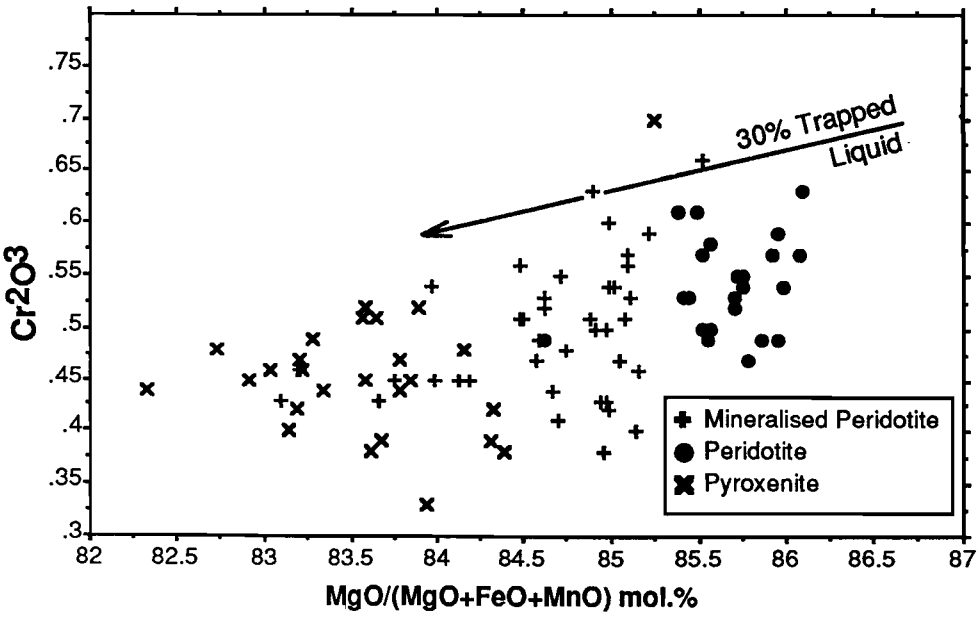

Figure 7. A wide spread in Fe/Mg ratio of fresh pyroxenes with a correspondingly small spread of Cr contents at Ora Banda (after Barnes, 1986).

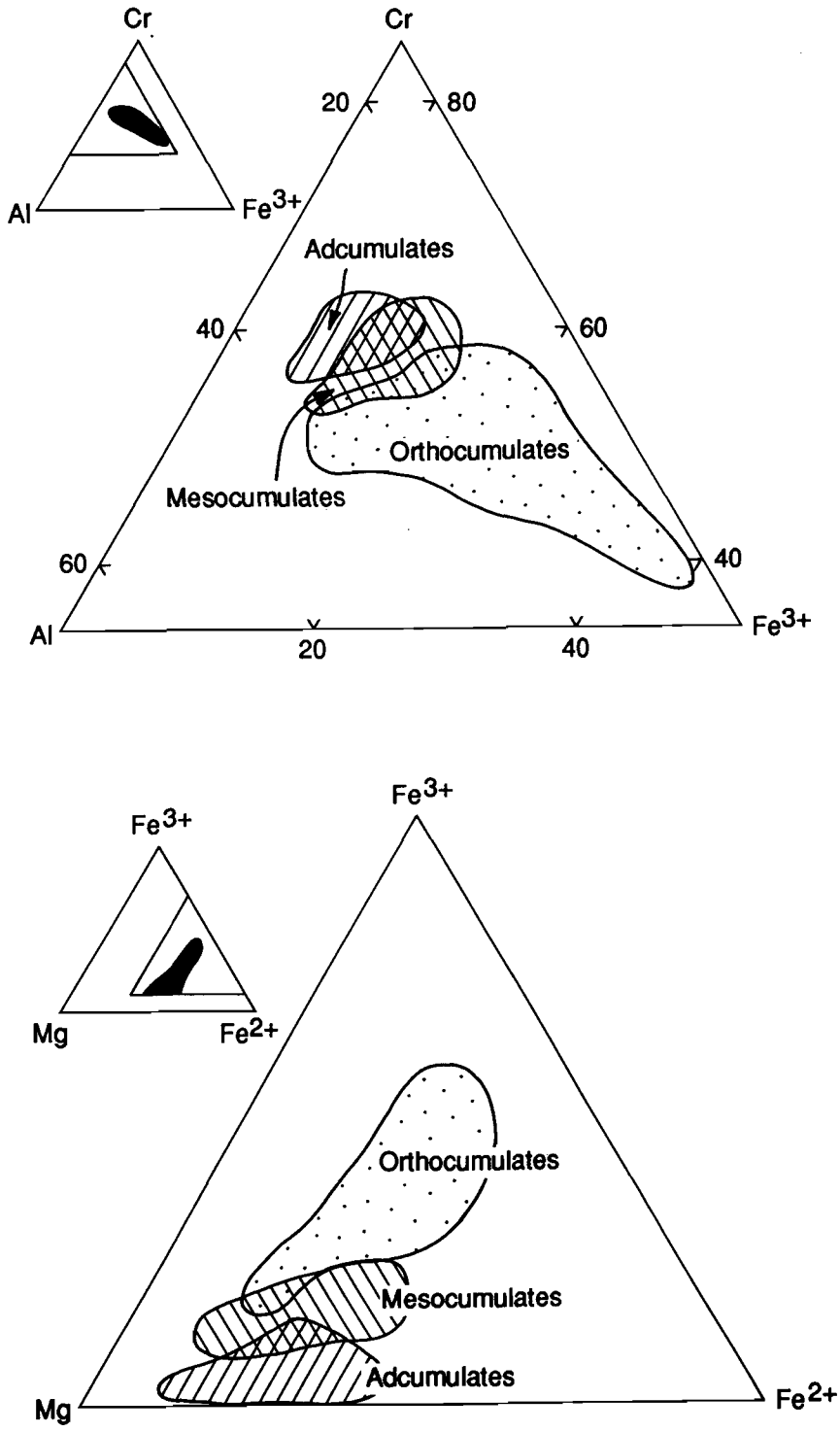

Figure 8. Systematic variations in chromite compositions from the Jimberlana Dyke (Roeder and Campbell, 1985) related to cumulate types and their contained trapped liquids.

5.0 LAG AND DURICRUST

5.1 Objectives

Lag types overlying peridotites and pyroxenites seem to be relatively easy to identify, on the basis of their morphology (types A and C lags respectively). Chromites found in these lags are petrographically relatively distinct, in that chromite from peridotitic lag is generally abundant, large and drop-like; chromite of pyroxenitic lag is far less abundant, small and lens-like. Many of these chromites show weathering phenomena (Volume IIA, Chapter 5; Figures 17H and 19C) so weathered and unweathered chromites require geochemical comparison to understand the changes they may have undergone during weathering. Where chromites have been separated from their containing weathered rocks, as in stream sediments, then a means of geochemical distinction of their source rock type and its mineralisation potential would be particularly valuable.

The objective was to distinguish chromites of lag overlying weathered pyroxenite (largely apparently mineralised) from those formed on peridotite and the mineralised upper part of the peridotite. The data comprised training sets from these three main groups. In addition, groups of chromites from the Fe-rich duricrust and its lag were included in the analysis as unknowns, to see if they were related to the peridotite or to the pyroxenite.

5.2 Chromite Compositions in the Lag and Duricrust

Much of pyroxenites that were lag sampled fall within the broad mineralised zone. A statistically significant group of unmineralised pyroxenitic lags could not be found, as lag did not occur south of the scarp (Unit 4), except as a mechanically dispersed pediment (Unit 3). Thus it was not possible to compare lag from mineralized and unmineralised pyroxenite areas.

A total of 199 acceptable analyses of weathered chromites from lag and duricrust were obtained. The weathered chromites were grouped according to the lag type in which they occur. Initially a five-fold classification was used. This included lag overlying largely mineralised pyroxenite (Samples 08-1499; 08-1522), unmineralised peridotite (Sample 08-1511) and lag from the mineralised top of the peridotite (Sample 08-1498). Additional chromites were from the Fe-rich duricrust outcrop (Sample 08-1556) and lag largely derived from both the Fe-rich duricrust and the peridotite (Sample 08-1516). The last two groups were included as unknowns to confirm that their chromites are similar to those of the peridotite, as implied by the petrography.

The effect of weathering of peridotitic chromites is apparent on the Cr-Al-Fe^{3+} ternary plot. The propotion of Fe^{3+} has decreased (Figure 9A), there appears to be a slight increase in Cr relative to the other trivalent ions but the range of Mg, relative to the divalent ions is similar (Figure 9B) and the means are not dissimilar. Weathering of the chromites of the pyroxenite has caused a similar decrease in Fe^{3+} (Figure 10A), but there is no significant increase in chromium (Figure 10B).

The chromites of the fresh pyroxenite shows a wide range in trivalent ions relative to the peridotites. On weathering they show a similar but lesser loss of Cr (Figure 11A) than those of the weathered peridotites. The chromites of both fresh and weathered pyroxenites show similar ranges in Mg relative to the divalent ions but the range in Cr relative to the trivalent ions is less (Figure 11B). Thus, chromite is not as impervious to weathering as is generally thought.

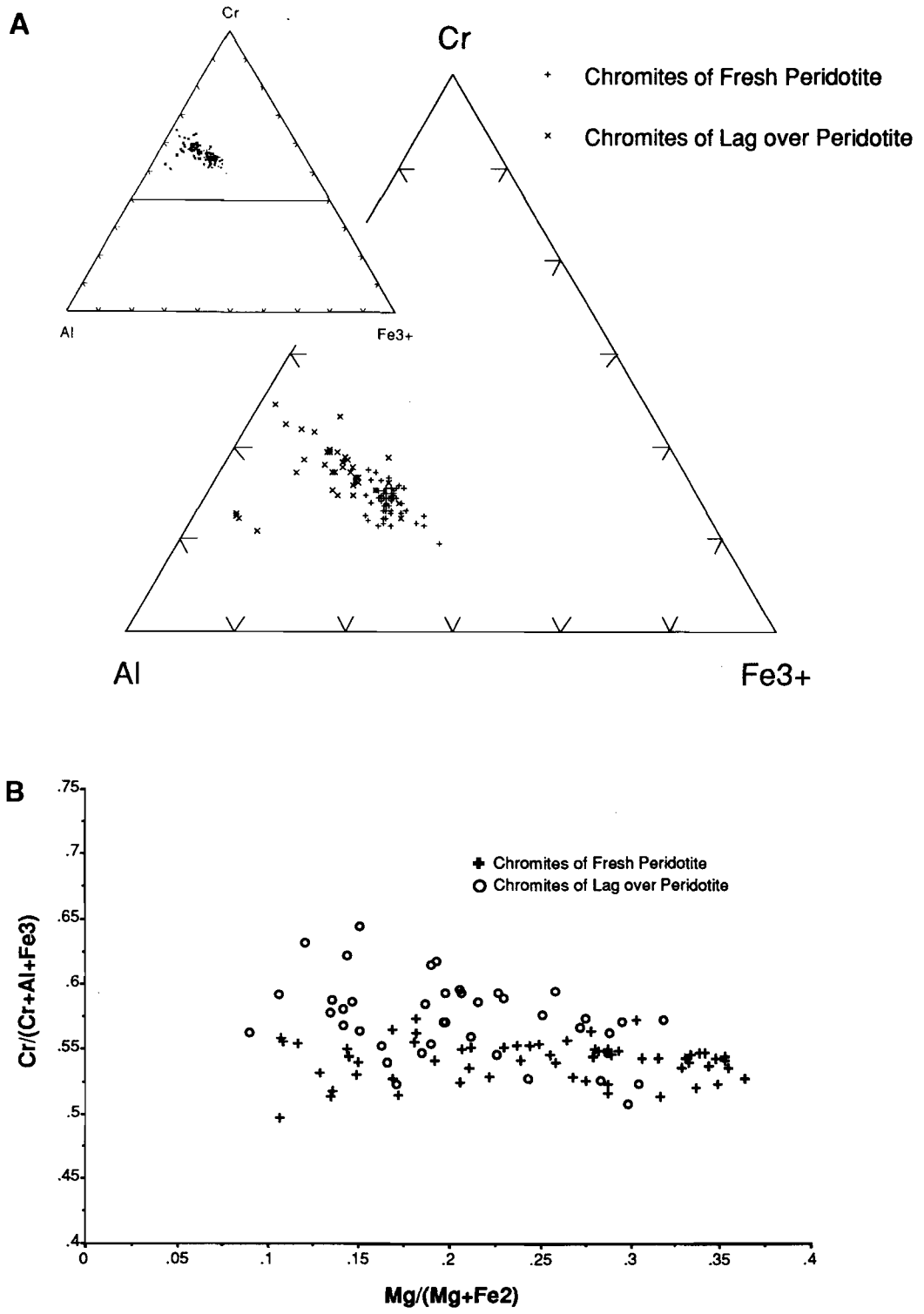

Figure 9. Comparison of chromites from fresh peridotites and the lag derived from them by weathering.

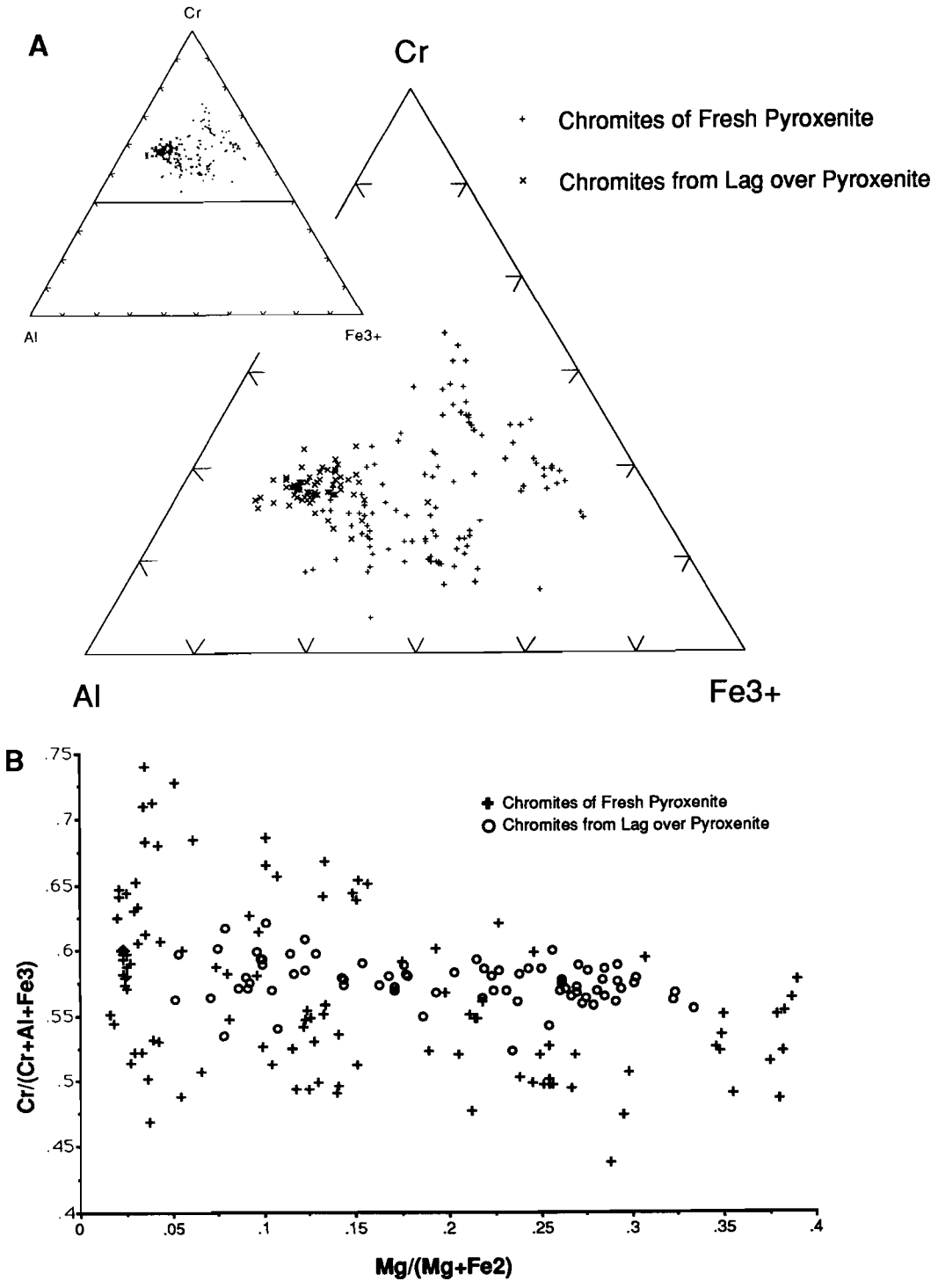

Figure 10. Comparison of chromites from fresh pyroxenites and the lag derived from them by weathering.

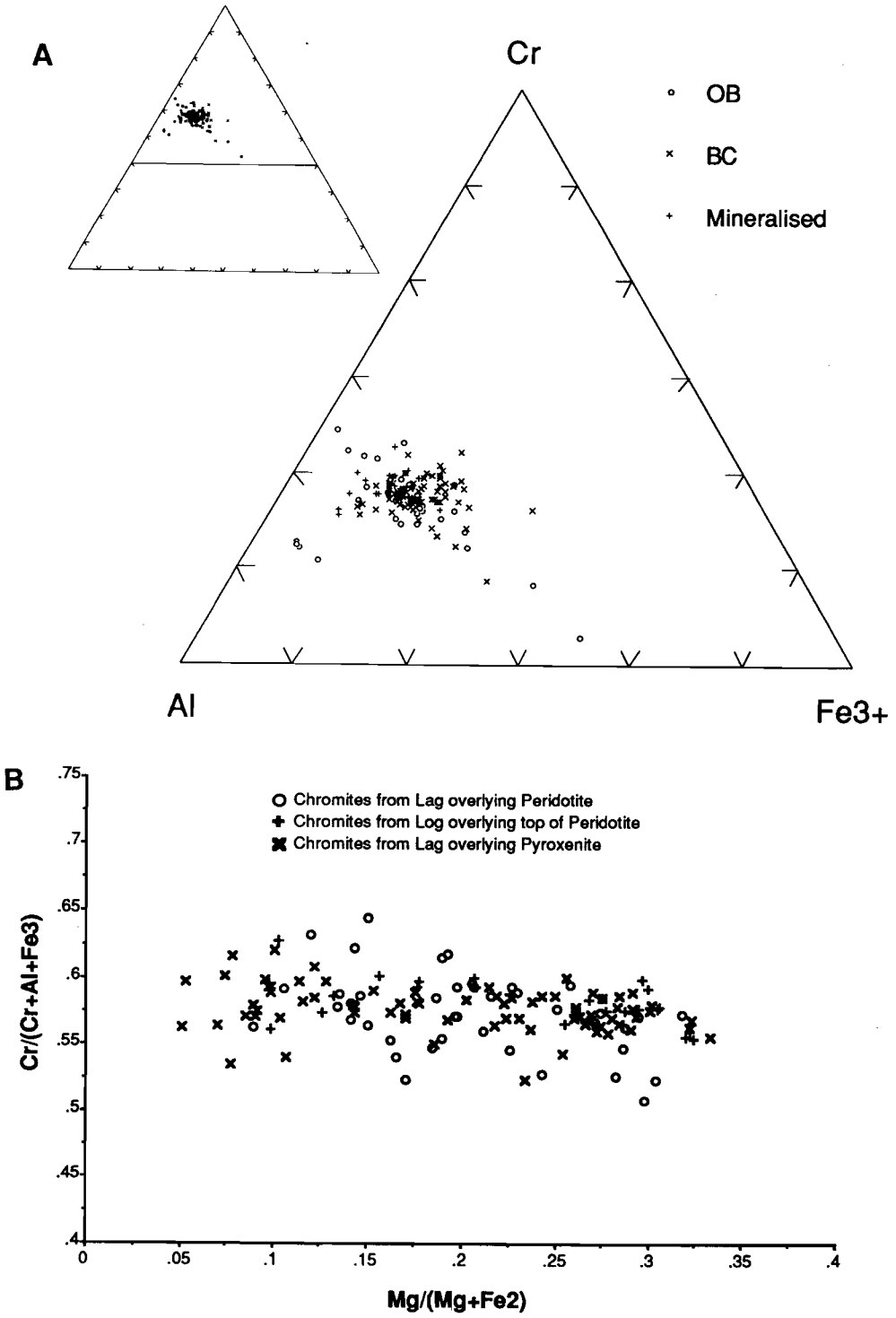

Figure 11. Comparison of chromites from lags derived from peridotites and pyroxenites.

5.3 Multivariate Analysis of Weathered Chromite Data

Quantile-quantile plots showed that, of the three training sets studied, each contained a major and a minor sub-population, designated 1 and 2 respectively. The minor sub-population of the peridotite group was relatively rich in Al but poor in Fe^{3+}, Ti and V; that of the upper part of the peridotite, rich in Fe^{3+} and poor in Cr; and that of the pyroxenite type, rich in Fe^{2+}, Mn and Zn but poor in Mg and Al.

Among the weathered chromites, no transformations were necessary for Cr and Mg. Log transformations were necessary for Fe^{2+}, Fe^{3+} and Mn; all other variables required Box-Cox power transformations. These were determined separately on each variable of each sub-population. One element (Zn) had been censored by its detection limit. A separate, compromise value for λ was selected to transform each element of the pooled groups during all subsequent phases of data analysis. First, robust estimations of means, standard deviations and correlations were made, then robust canonical variate analysis was used to provide an ordination of the reference groups. The results of this canonical variate analysis of six reference groups are five canonical variates (CV1 - CV5 in Appendix 2) of which the first two contain most of the useful information (Figure 12). There is a significant overlap of the fields of the chromites of the pyroxenitic and peridotitic lags but an even closer relationship between the chromites of the peridotitic lag and its uppermost part is also apparent. Lack of a satisfactory background population for the chromites of the pyroxenitic lag makes definition of a mineralised group in the type C lag extremely difficult, though the slightly more Mg-rich major population may represent this (Figure 13).

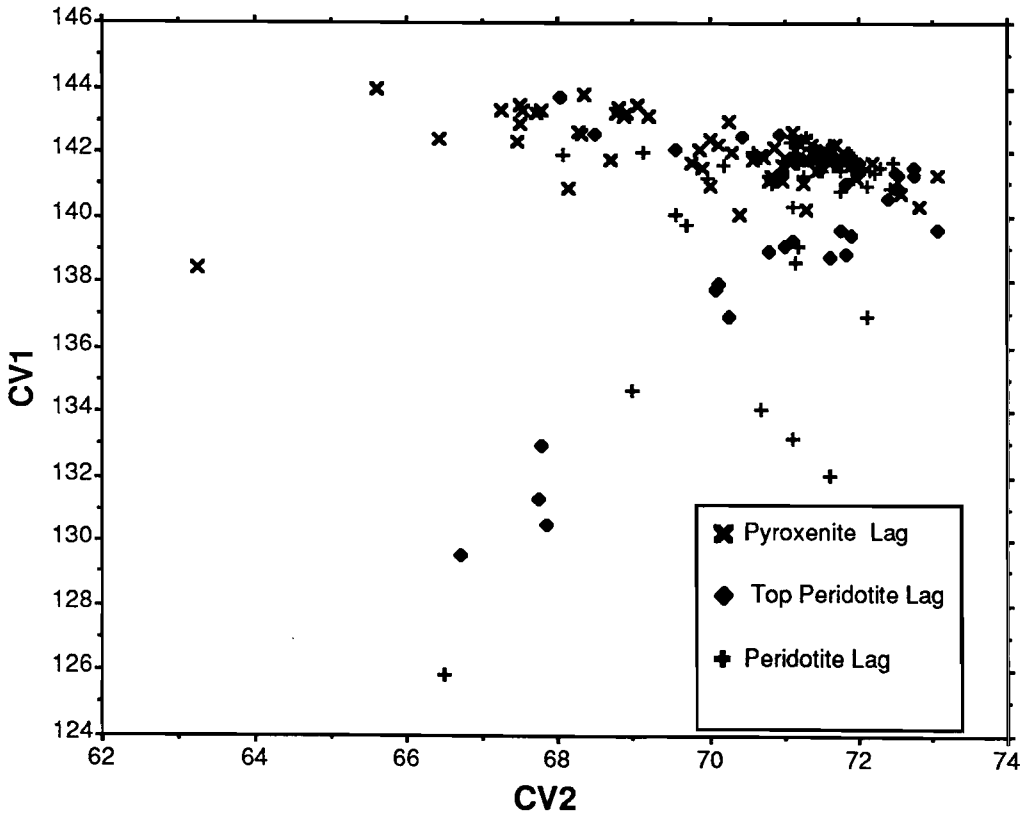

Figure 12. Canonical variate plot of discriminant analysis of weathered chromites from lag on peridotites and pyroxenites.

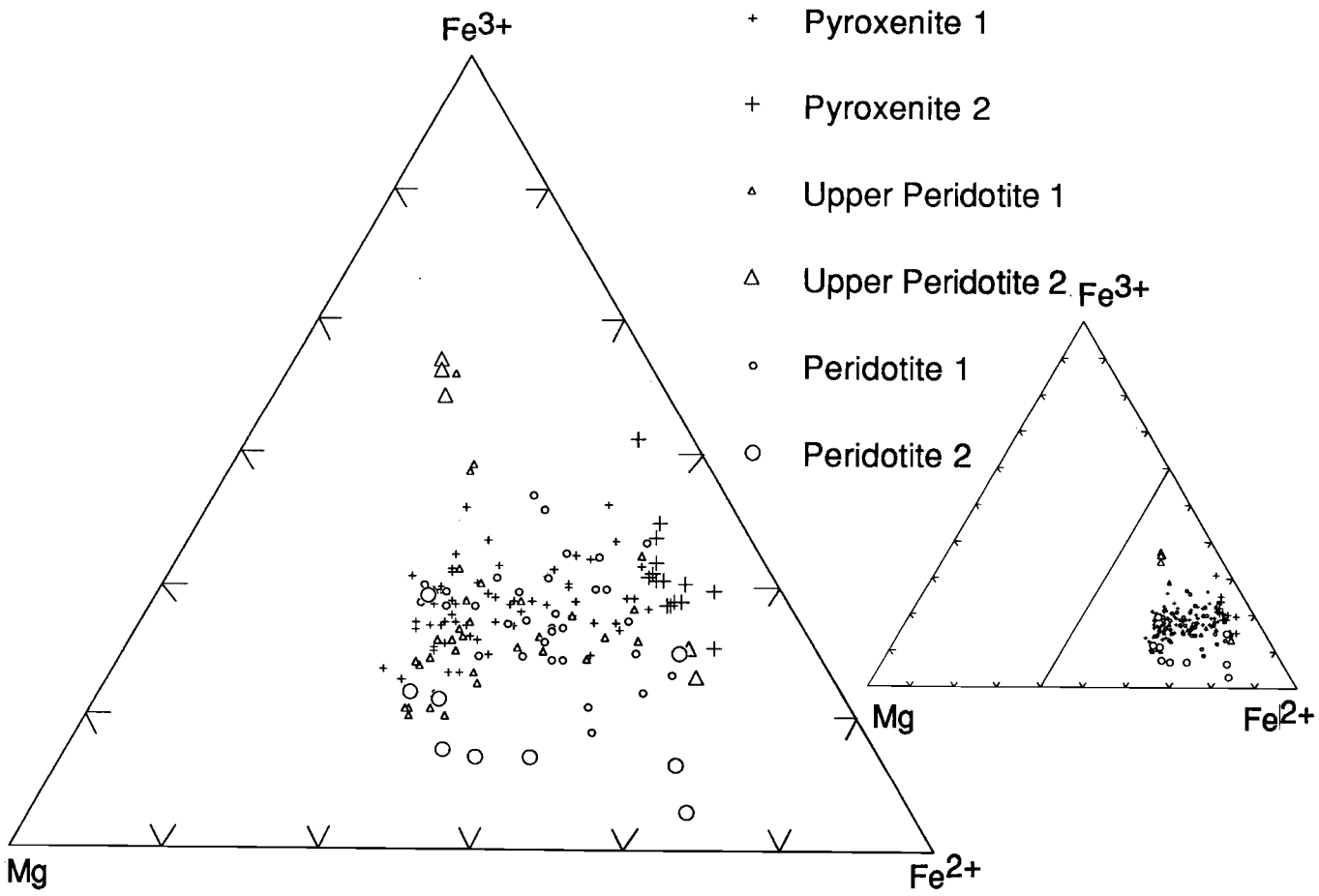

Figure 13. Expanded ternary plot of weathered chromites from lag overlying peridotites, upper portions of he peridotite and pyroxenite, each with a major and a minor sub-population.

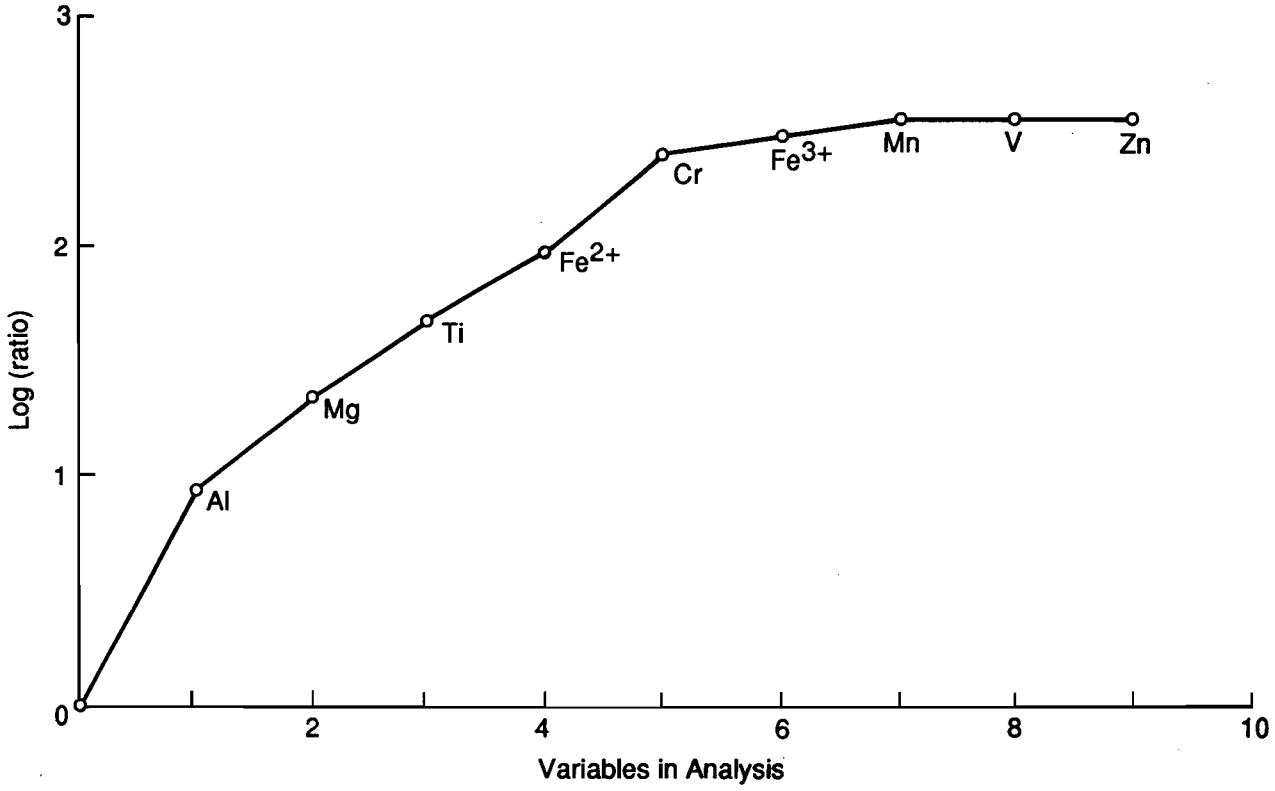

Figure 14. Results of investigation of contribution of each element to the weathered chromite discrimination.

A posteriori group membership probabilities and typicality indices for individual chromites were calculated using 95% confidence limits for the typicality. Assessment of the results (Appendix 2; final column) showed (Table 5) that chromites in lags on pyroxenites could be distinguished, on a grain-by-grain basis, with 72% certainty and those on peridotite also with an average of 72% certainty. Those of the lower peridotites and the upper part of the peridotite could be distinguished with only 39 and 63% certainty respectively. Chromites from the Fe-rich duricrust and its lag are very clearly peridotite- rather than pyroxenite-related, which supports the petrographic indications (Volume IIA, Chapter 5, Section 8). These results demonstrate that a statistically significant number of chromite analyses are necessary to make a valid distinction where the range of data is then apparent.

TABLE 2
Weathered Chromite Allocations

	% Allocations - *a posteriori*			
***A priori* groups**	**Peridotite**	**Top Peridotite**	**Min Pyroxenite**	**Unclassified**
Unmineralised Peridotite Lag	39	22	22	17
Lag from Top of Peridotite	20	63	15	2
Mineralised Pyroxenite	10	17	72	1
Fe-rich Duricrust	36	50	5	9
Lag from Fe-rich Duricrust	0	93	7	0

The effectiveness of each variable and combinations of variables in distinguishing the groups are shown in Figure 14. The greatest part of the distinction is achieved using Al, Mg, Ti, Fe^{2+} and Cr. The contributions of Fe^{3+}, Mn, V and Zn are minimal. This is a little different from the fresh chromites, where Fe^{3+}, Cr, Mn, Ti and Al are important.

6.0 CONCLUSIONS

6.1 Fresh Chromite

Chromite is most abundant and the grains large (100 μm) in the fresh peridotites and less abundant and the grains smaller (40 μm) in the pyroxenites. There is a marked difference between the compositions of chromites from the pyroxenites and the peridotites in that those from the pyroxenites are enriched in Fe^{3+} and because of their smaller grains, appear to have reacted more readily with a more abundant trapped liquid. Peridotitic chromites more closely represent the primary liquidus chromite.

Of greater significance is the difference between the chromite compositions of the mineralised and unmineralised pyroxenites, where the chromites of the mineralised pyroxenites show a trend of Al depletion and Cr enrichment at approximately constant Fe^{3+}. Here the presence of sulphide may have impeded an increase in Fe^{3+} in the trapped liquid. The data apparently record the influence of sulphides on the cumulates and may have some bearing on the origin of this PGE-rich, S-poor occurrence. Clearly further work is required on fresh rocks.

Discriminant analysis gave a slight improvement in the classification of the fresh chromites over and above that provided by the ternary Cr-Al-Fe^{3+} plot as only Mn and Ti added effective information to the multivariate discrimination. Other elements (Mg, Fe^{2+}, V and Zn) contributed little.

6.2 Weathered Chromite

Chromite is generally regarded as a resistant mineral but this work has clearly shown, both by microscopy and by geochemical analysis, that it is altered by extreme weathering. The most common phenomenon is a reticulate pattern of fine, wedge-shaped cracks which develop around the margins of the chromite grain (Volume IIA, Chapter 5, Figure 17C), becoming narrower towards the centre. Other chromite grains have bright margins of hematite or are internally pitted. These weathering phenomena may not, in fact, be due to the weathering of chromite but of fine-scale exsolved foreign material. Twinning in chromites is common (Deer *et al.*, 1967) on [111] (spinel law). Chromites can also be zoned and mantled by chromian-titanomagnetite and contain oxidation lamellae of related spinels (Haggerty, 1976); these could be more prone to weathering than their chromite host. More work, involving TEM and ATEM examination would be necessary to resolve this.

As for the fresh chromites, probably the best way to distinguish chromites of weathered peridotites from those of weathered pyroxenites is by their size and abundance. Lag from weathered peridotites have more abundant, rounder and larger chromite grains. Microprobe analysis indicates that there is a reduction in the content of Fe^{3+} in the chromite composition, on weathering of both peridotite- and pyroxenite-derived chromites. This may be due to migration of Fe^{3+} into the reticulate cracks on weathering. The chromites of the weathered pyroxenite show a lesser range in Cr compositions than their unweathered counterparts. An alternate and preferred interpretation is that the very fine-grained chromites of the weathered pyroxenites tend not to survive weathering. Thus, the population tends to be biased towards larger chromites, which are more resistant both to re-equilibration with the melt and to weathering.

Chromites from the Fe-rich duricrust are morphologically and geochemically more closely related to those of the weathered peridotites than to those of the pyroxenites.

7.0 ACKNOWLEDGEMENTS

Polished sections were prepared by A.G. Bowyer and R.J. Bilz. Assistance on the SEM and Cameca microprobe was ably given by B.W. Robinson and G. Burkhalter. N.A. Campbell and M. Palmer (CSIRO Division of Mathematics and Statistics) provided access to multivariate statistics programs and instructed the senior author in their use. Drafting and artwork was by C.R. Steel and A.D. Vartesi. J. Porter assisted with checking and formatting the final document and C.R.M. Butt supplied critical commentary on the manuscript. All this is acknowledged with appreciation.

8.0 REFERENCES

Barnes, S.J., 1986. The effect of trapped liquid crystallization on cumulus mineral compositions in layered intrusions. Contributions to Mineralogy and Petrology, 93:524-531.

Campbell, N.A. 1980. Robust procedures in multivariate analysis. I. Robust covariance estimation. Applied Statistics. 29. 231-237.

Campbell, N.A. 1982. Robust procedures in multivariate analysis. II. Robust canonical variate analysis. Applied Statistics. 31. 1-8.

Campbell, N.A. 1986. Censored, grouped and truncated geochemical data. CSIRO Division of Mathematics and Statistics Technical Files.

Deer, W.A., Howie, R.A., and Zussman, J. 1967. An introduction to the rock forming minerals. Longmans, Green and Co. Ltd. London. 528 pp.

Haggerty, S.E. 1981. Oxidation of opaque mineral oxides in basalts. In D. Rumble (ed). Oxide minerals. Miner. Soc Amer. Reviews in mineralogy. 3. Hg1-100.

Irvine, T.N., 1967. Chromian spinel as a petrogenetic indicator. Part 2. Petrologic implications. Canadian Journal of Earth Science, 4:71-103.

Murck, B.W. and Campbell, I.H., 1986. The effects of temperature, oxygen fugacity and melt composition on the behavior of chromium in basic and ultrabasic melts. Geochimica et Cosmochimica Acta, 50:1871-1887.

Naldrett, A.J., Lehmann, J. and Auge, T., 1989. Spinel non-stoichiometry and reactions between chromite and closely associated sulphides, with examples from ophiolite complexes. In: In Prendergast MD, Jones M.J. (eds), Magmatic Sulphides - the Zimbabwe Volume. Inst. Mining Metall., London, 221-229.

Peck, D.C. and Keays, R.R. 1990. Geology, Geochemistry, and Origin of Platinum-Group Element-Chromitite occurrence in the Heazlewood River Complex, Tasmania. Economic Geology 85, 763-793.

Roeder, P.L. and Campbell, I.H., 1985. The effect of postcumulus reactions on compositions of chrome-spinels from the Jimberlana Intrusion. Journal of Petrology 26:763-786.

Roeder, P.L. and Reynolds, I., 1991. Crystallization of chromite and chromium solubility in basaltic melts. Journal of Petrology 32:909-934.

Thayer, T.P. 1970. Chromite Segregations as Petrogenetic Indicators. The Geological Society of South Africa. Special Publication 1, 380 - 389.

Ware, N.G. 1981. Computer programs and calibration with the PIBS technique for quantitative electron probe analysis using a lithium-drifted silicon detector. Computers and Geosciences. 7, 167-184.

Witt, W.K., and Barnes, S.J. 1991. The Ora Banda Sill. In S.J. Barnes and R.E.T Hill (eds), Mafic-ultramafic complexes in Western Australia, Geol. Soc. Austr. WA Division Excursion Guidebook 3.

APPENDIX I

GEOCHEMISTRY AND STATISTICS OF FRESH CHROMITES - ORA BANDA PROSPECT

A priori types

OB	Peridotite
OBS	Mineralised Peridotite
BC	Pyroxenite
BCS	Mineralised Pyroxenite
OUT	Outlier

A posteriori types

1	Peridotite
2	Mineralised Peridotite
3	Pyroxenite
4	Mineralised Pyroxenite
0	Unclassified

This data also available on Data Disc (Volume 3B)

Thin Section	Analy No	Size (μm)	Loc	Strat Depth	Rock Type	Structural Formula										Mg	Cr	Fe3	Canonical Variates			Post Type
						Cr	Ti	V	Al	Fe3+	Fe2+	Mn	Mg	Ni	Zn	Fe2+Mg	Cr+Al+Fe3	Cr+Al+Fe3	CV1	CV2	CV3	
OBD2-193	44821	130	Core	193	BCS	1.017	0.032	0.010	0.473	0.464	0.743	0.008	0.247	0.004	0.005	0.2495	0.5205	0.2375	21.222	-33.740	11.439	4
OBD2-193	44822	130	Rim	193	BCS	1.017	0.034	0.010	0.486	0.449	0.725	0.008	0.267	0.000	0.005	0.2692	0.5210	0.2300	21.394	-33.483	11.325	4
OBD2-193	44823	20	Core	193	BCS	0.977	0.124	0.011	0.408	0.474	0.863	0.013	0.112	0.005	0.016	0.1149	0.5256	0.2550	22.373	-31.656	14.582	2
OBD2-193	44824	250	Core	193	BCS	0.914	0.067	0.013	0.399	0.603	0.783	0.007	0.211	0.005	0.000	0.2123	0.4770	0.3147	20.955	-32.627	11.872	0
OBD2-193	44825	250	Rim	193	BCS	1.039	0.064	0.011	0.328	0.552	0.862	0.013	0.119	0.004	0.012	0.1213	0.5414	0.2876	20.643	-33.445	13.337	4
OBD2-193	44826	100	Core	193	BCS	0.969	0.040	0.010	0.450	0.529	0.740	0.005	0.256	0.003	0.000	0.2570	0.4974	0.2716	21.112	-34.070	11.663	0
OBD2-193	44827	150	Core	193	BCS	0.965	0.043	0.012	0.461	0.516	0.738	0.009	0.252	0.003	0.005	0.2545	0.4969	0.2657	20.876	-32.855	11.184	4
OBD2-193	44828	150	Rim	193	BCS	0.964	0.044	0.012	0.453	0.522	0.745	0.008	0.250	0.003	0.000	0.2513	0.4972	0.2692	21.266	-32.836	11.445	4
OBD2-193	44829	150	Core	193	BCS	0.968	0.042	0.010	0.451	0.524	0.750	0.008	0.244	0.000	0.004	0.2455	0.4982	0.2697	21.033	-33.275	11.573	4
OBD2-193	44830	150	Core	193	BCS	0.977	0.043	0.010	0.455	0.512	0.756	0.007	0.236	0.006	0.000	0.2379	0.5026	0.2634	21.472	-33.376	11.948	4
OBD2-193	44831	150	Core	193	BCS	1.014	0.041	0.010	0.448	0.483	0.787	0.010	0.203	0.003	0.004	0.2051	0.5213	0.2483	21.485	-33.380	12.175	4
OBD2-193	44832	150	Rim	193	BCS	1.021	0.036	0.009	0.446	0.482	0.801	0.012	0.187	0.004	0.005	0.1893	0.5239	0.2473	21.518	-32.991	12.273	4
OBD1-119.1	44833	200	Rim	289	OB	1.024	0.055	0.009	0.572	0.335	0.842	0.012	0.147	0.000	0.008	0.1486	0.5303	0.1735	23.504	-31.319	12.510	2
OBD1-119.1	44834	200	Core	289	OB	0.995	0.056	0.008	0.577	0.357	0.817	0.016	0.169	0.000	0.010	0.1714	0.5158	0.1851	23.463	-30.092	12.352	2
OBD1-119.1	44835	100	Rim	289	OB	1.031	0.074	0.009	0.527	0.351	0.839	0.015	0.148	0.000	0.009	0.1499	0.5401	0.1839	23.691	-30.852	13.241	2
OBD1-119.1	44836	100	Core	289	OB	1.009	0.079	0.011	0.529	0.367	0.724	0.010	0.264	0.005	0.004	0.2672	0.5297	0.1927	23.273	-31.290	12.209	1
OBD1-119.1	44838	50	Rim	289	OB	1.062	0.080	0.011	0.515	0.324	0.874	0.018	0.105	0.002	0.014	0.1073	0.5587	0.1704	23.613	-30.258	13.397	2
OBD1-119.1	44839	50	Core	289	OB	1.056	0.084	0.009	0.509	0.335	0.878	0.015	0.106	0.003	0.009	0.1077	0.5558	0.1763	23.914	-30.879	14.028	2
OBD1-102	44840	300	Rim	272	BCS	1.114	0.063	0.015	0.332	0.469	0.905	0.016	0.078	0.003	0.010	0.0793	0.5817	0.2449	20.976	-33.202	13.631	4
OBD1-102	44841	300	Core	272	BCS	0.946	0.077	0.012	0.433	0.527	0.849	0.012	0.139	0.003	0.006	0.1407	0.4963	0.2765	21.648	-31.957	13.019	4
OBD1-102	44842	300	Rim	272	BCS	0.981	0.110	0.017	0.351	0.533	0.886	0.017	0.097	0.004	0.009	0.0987	0.5260	0.2858	21.455	-31.079	13.703	4
OBD1-102	44843	300	Core	272	BCS	0.907	0.126	0.017	0.366	0.578	0.848	0.012	0.137	0.004	0.008	0.1391	0.4900	0.3123	21.402	-31.064	13.122	0
OBD1-102	44844	75	Rim	272	BCS	1.156	0.052	0.013	0.344	0.427	0.933	0.018	0.055	0.000	0.007	0.0557	0.5999	0.2216	21.405	-32.691	14.078	4
OBD1-102	44845	75	Core	272	BCS	1.184	0.044	0.015	0.338	0.410	0.945	0.019	0.035	0.000	0.016	0.0357	0.6128	0.2122	20.452	-32.544	13.669	0
OBD1-102	44846	25	Core	272	BCS	1.216	0.058	0.013	0.376	0.327	0.943	0.019	0.030	0.000	0.022	0.0308	0.6337	0.1704	21.521	-31.577	14.077	0
OBD1-303.0	44847	200	Rim	473	OB	1.004	0.069	0.008	0.574	0.341	0.708	0.008	0.285	0.000	0.004	0.2870	0.5232	0.1777	23.649	-31.261	12.009	1
OBD1-303.0	44848	70	Core	473	OB	1.022	0.013	0.007	0.603	0.351	0.707	0.010	0.285	0.002	0.004	0.2873	0.5172	0.1776	22.479	-31.310	10.228	1
OBD1-303.0	44849	50	Core	473	OB	1.015	0.078	0.006	0.555	0.337	0.855	0.018	0.126	0.002	0.012	0.1284	0.5322	0.1767	24.250	-29.497	13.767	2
OBD1-303.0	44850	120	Core	473	OB	1.018	0.010	0.006	0.617	0.345	0.678	0.009	0.313	0.003	0.004	0.3158	0.5141	0.1742	22.436	-31.122	9.952	1
OBD1-303.0	44851	150	Core	473	OB	1.008	0.083	0.008	0.569	0.326	0.774	0.012	0.221	0.002	0.000	0.2221	0.5297	0.1713	24.875	-29.868	12.993	2
OBD1-303.0	44852	150	Core	473	OB	1.004	0.069	0.009	0.579	0.334	0.645	0.011	0.345	0.003	0.004	0.3485	0.5237	0.1742	23.519	-29.649	11.297	1
OBD1-303.0	44853	200	Rim	473	OB	1.035	0.019	0.008	0.623	0.311	0.782	0.009	0.203	0.003	0.010	0.2061	0.5256	0.1579	22.801	-31.774	10.534	1
OBD1-303.0	44854	200	Core	473	OB	1.023	0.025	0.007	0.623	0.317	0.656	0.011	0.332	0.005	0.004	0.3360	0.5211	0.1615	23.072	-29.824	10.101	1
OBD1-303.0	44855	150	Core	473	OB	1.016	0.058	0.008	0.506	0.409	0.720	0.009	0.273	0.000	0.004	0.2749	0.5262	0.2118	22.679	-32.424	12.339	4
OBD1-190.3	45941	150	Core	360	OB	1.036	0.065	0.010	0.585	0.298	0.732	0.011	0.255	0.004	0.006	0.2584	0.5399	0.1553	23.952	-30.301	11.485	1
OBD1-190.3	45943	150	Rim	360	OB	1.059	0.072	0.010	0.543	0.309	0.742	0.013	0.247	0.003	0.004	0.2497	0.5542	0.1617	24.128	-30.364	12.136	2
OBD1-190.3	45945	150	Core	360	OB	1.049	0.070	0.010	0.536	0.331	0.654	0.008	0.335	0.004	0.005	0.3387	0.5475	0.1728	23.185	-31.501	11.582	1
OBD1-190.3	45946	150	Rim	360	OB	1.045	0.071	0.009	0.545	0.326	0.660	0.008	0.330	0.003	0.005	0.3333	0.5454	0.1701	23.422	-31.359	11.737	1
OBD1-190.3	45947	200	Core	360	OB	1.045	0.070	0.009	0.556	0.316	0.644	0.009	0.351	0.003	0.000	0.3528	0.5451	0.1648	23.999	-30.305	11.684	1
OBD1-190.3	45948	200	Rim	360	OB	1.042	0.069	0.008	0.560	0.316	0.643	0.009	0.343	0.004	0.008	0.3479	0.5433	0.1648	23.445	-30.695	11.516	1
OBD1-190.3	45950	200	Rim	360	OB	1.035	0.074	0.009	0.546	0.330	0.750	0.012	0.236	0.003	0.008	0.2394	0.5416	0.1727	23.767	-30.854	12.370	2
OBD1-190.3	45951	200	Core	360	OB	1.039	0.075	0.010	0.552	0.321	0.663	0.008	0.329	0.002	0.003	0.3317	0.5434	0.1679	23.618	-31.095	11.685	1
OBD1-98.0	45952	80	Core	368	BCS	1.059	0.055	0.010	0.549	0.322	0.774	0.012	0.212	0.002	0.009	0.2150	0.5487	0.1668	23.370	-31.451	11.890	1
OBD1-98.0	45953	90	Core	368	BCS	1.034	0.107	0.009	0.492	0.351	0.782	0.013	0.209	0.002	0.004	0.2109	0.5509	0.1870	24.412	-30.780	13.813	2
OBD1-98.0	45954	80	Core	368	BCS	1.055	0.072	0.010	0.459	0.397	0.852	0.015	0.130	0.004	0.011	0.1324	0.5521	0.2077	22.748	-32.024	13.613	2
OBD1-98.0	45955	70	Core	368	BCS	1.055	0.092	0.009	0.501	0.335	0.854	0.016	0.131	0.000	0.011	0.1330	0.5579	0.1772	24.070	-30.690	13.926	2
OBD1-98.0	45956	100	Rim	368	BCS	1.034	0.091	0.010	0.514	0.342	0.857	0.019	0.119	0.004	0.015	0.1219	0.5471	0.1810	23.727	-29.802	13.624	2
OBD1-98.0	45957	50	Core	368	BCS	1.046	0.078	0.010	0.524	0.336	0.856	0.014	0.123	0.003	0.014	0.1256	0.5488	0.1763	23.442	-31.196	13.327	2

OBD1-236.5	45958	80	Core	406	OB	1.051	0.071	0.009	0.536	0.327	0.711	0.010	0.279	0.002	0.006	0.2818	0.5491	0.1708	23.638	-31.322	12.112	1
OBD1-236.5	45959	150	Rim	406	OB	1.045	0.071	0.010	0.543	0.326	0.703	0.008	0.286	0.003	0.007	0.2892	0.5460	0.1703	23.357	-31.841	11.828	1
OBD1-236.5	45960	50	Core	406	OB	1.069	0.060	0.009	0.537	0.317	0.814	0.016	0.180	0.002	0.000	0.1811	0.5559	0.1648	24.566	-30.094	12.826	2
OBD1-236.5	45961	70	Rim	406	OB	1.056	0.075	0.010	0.532	0.321	0.755	0.012	0.235	0.000	0.007	0.2374	0.5532	0.1682	23.849	-31.098	12.362	2
OBD1-236.5	45962	180	Core	406	OB	1.025	0.079	0.009	0.555	0.329	0.652	0.006	0.341	0.002	0.004	0.3434	0.5369	0.1723	23.486	-31.634	11.828	1
OBD1-236.5	45963	180	Rim	406	OB	1.051	0.079	0.009	0.547	0.308	0.777	0.013	0.209	0.002	0.008	0.2120	0.5514	0.1616	24.232	-30.538	12.642	2
OBD1-236.5	45965	150	Rim	406	OB	1.022	0.081	0.010	0.560	0.322	0.666	0.009	0.325	0.004	0.004	0.3280	0.5368	0.1691	23.737	-30.505	11.700	1
OBD1-236.5	45966	80	Core	406	OB	1.044	0.069	0.009	0.550	0.326	0.689	0.007	0.304	0.000	0.006	0.3061	0.5438	0.1698	23.413	-32.063	11.866	1
OBD1-236.5	45969	100	Core	406	OB	1.061	0.056	0.008	0.553	0.317	0.707	0.008	0.285	0.003	0.003	0.2873	0.5495	0.1642	23.664	-31.781	11.847	1
OBD1-236.5	45971	100	Core	406	OB	1.084	0.058	0.009	0.547	0.296	0.805	0.012	0.179	0.003	0.010	0.1819	0.5625	0.1536	23.828	-31.393	12.300	2
OBD1-98.0	45972	55	Core	368	BCS	1.017	0.085	0.008	0.521	0.361	0.844	0.017	0.138	0.005	0.008	0.1405	0.5355	0.1901	23.969	-30.076	13.803	2
OBD1-98.0	45973	50	Rim	368	BCS	0.988	0.058	0.007	0.513	0.426	0.878	0.017	0.102	0.002	0.014	0.1041	0.5127	0.2211	22.522	-30.785	13.533	2
OBD1-190.3	45974	50	Core	360	OB	1.087	0.057	0.010	0.568	0.273	0.714	0.010	0.275	0.002	0.006	0.2781	0.5638	0.1416	23.986	-30.783	11.168	1
OBD1-190.3	45975	150	Rim	360	OB	1.045	0.065	0.009	0.539	0.339	0.664	0.007	0.327	0.005	0.003	0.3300	0.5434	0.1763	23.226	-31.928	11.773	1
OBD1-190.3	45976	150	Core	360	OB	1.045	0.063	0.009	0.544	0.334	0.679	0.010	0.312	0.003	0.003	0.3148	0.5434	0.1737	23.484	-30.983	11.736	1
OBD1-190.3	45977	55	Core	360	OB	1.020	0.085	0.008	0.559	0.322	0.780	0.013	0.209	0.003	0.004	0.2113	0.5366	0.1694	24.571	-30.059	13.005	2
OBD1-098.0	46044	70	Core	268	OBS	1.075	0.072	0.010	0.523	0.316	0.736	0.010	0.261	0.000	0.000	0.2618	0.5617	0.1651	24.275	-31.340	12.482	2
OBD1-098.0	46045	50	Core	268	OBS	1.069	0.060	0.009	0.508	0.347	0.845	0.016	0.140	0.004	0.007	0.1421	0.5556	0.1804	23.519	-31.165	13.184	2
OBD1-098.0	46046	50	Core	268	OBS	1.045	0.084	0.009	0.492	0.366	0.783	0.009	0.208	0.003	0.004	0.2099	0.5491	0.1923	23.625	-32.555	13.432	2
OBD1-098.0	46047	70	Core	268	OBS	1.053	0.080	0.009	0.534	0.317	0.856	0.014	0.133	0.000	0.007	0.1345	0.5530	0.1665	24.272	-30.758	13.501	2
OBD1-098.0	46048	75	Core	268	OBS	1.079	0.065	0.009	0.531	0.310	0.778	0.012	0.210	0.003	0.006	0.2126	0.5620	0.1615	23.967	-31.333	12.496	2
OBD1-098.0	46049	40	Core	268	OBS	1.071	0.070	0.010	0.536	0.305	0.854	0.015	0.123	0.004	0.015	0.1259	0.5601	0.1595	23.654	-30.747	12.907	2
OBD1-098.0	46050	25	Core	268	OBS	1.056	0.063	0.008	0.514	0.348	0.863	0.019	0.115	0.000	0.017	0.1176	0.5506	0.1814	23.264	-30.482	13.327	2
OBD1-098.0	46051	25	Core	268	OBS	1.059	0.062	0.008	0.527	0.336	0.872	0.015	0.107	0.002	0.016	0.1093	0.5510	0.1748	23.269	-31.232	13.371	2
OBD1-098.0	46052	50	Rim	268	OBS	1.061	0.074	0.009	0.512	0.336	0.864	0.016	0.116	0.004	0.013	0.1184	0.5558	0.1760	23.565	-30.907	13.552	2
OBD1-098.0	46053	50	Rim	268	OBS	1.076	0.071	0.010	0.515	0.321	0.859	0.016	0.127	0.000	0.010	0.1288	0.5628	0.1679	23.796	-30.916	13.247	2
OBD1-098.0	46054	50	Core	268	OBS	1.069	0.070	0.009	0.520	0.324	0.856	0.015	0.131	0.000	0.009	0.1327	0.5588	0.1694	23.881	-31.034	13.337	2
OBD1-098.0	46055	50	Core	268	OBS	1.064	0.067	0.009	0.526	0.325	0.849	0.016	0.134	0.005	0.008	0.1363	0.5556	0.1697	23.871	-30.610	13.181	2
OBD1-098.0	46056	70	Rim	268	OBS	1.063	0.073	0.009	0.500	0.348	0.829	0.015	0.152	0.002	0.013	0.1549	0.5563	0.1821	23.404	-31.414	13.292	2
OBD1-098.0	46057	70	Rim	268	OBS	1.065	0.069	0.009	0.512	0.339	0.802	0.014	0.186	0.003	0.005	0.1883	0.5558	0.1769	23.853	-31.214	13.029	2
OBD1-098.0	46058	70	Core	268	OBS	1.033	0.067	0.008	0.504	0.381	0.787	0.014	0.199	0.004	0.006	0.2018	0.5386	0.1986	23.369	-31.295	13.052	2
OBD1-098.0	46059	70	Core	268	OBS	1.067	0.071	0.009	0.525	0.322	0.780	0.014	0.211	0.000	0.005	0.2129	0.5575	0.1682	24.114	-30.837	12.744	2
OBD1-098.0	46060	70	Core	268	OBS	1.079	0.070	0.009	0.525	0.310	0.795	0.013	0.191	0.002	0.009	0.1937	0.5637	0.1620	23.959	-31.232	12.719	2
OBD1-098.0	46061	45	Rim	268	OUT	1.082	0.031	0.006	0.640	0.235	0.779	0.016	0.204	0.004	0.009	0.2075	0.5529	0.1201	24.803	-28.376	10.671	0
OBD1-098.0	46062	45	Rim	268	OUT	1.081	0.031	0.008	0.636	0.238	0.746	0.012	0.244	0.000	0.008	0.2465	0.5529	0.1217	24.354	-29.390	10.077	1
OBD1-098.0	46063	45	Core	268	OUT	1.082	0.036	0.008	0.635	0.235	0.707	0.012	0.284	0.002	0.004	0.2866	0.5543	0.1204	24.629	-28.824	10.056	1
OBD1-098.0	46064	45	Core	268	OUT	1.073	0.032	0.008	0.634	0.250	0.677	0.008	0.314	0.004	0.003	0.3169	0.5483	0.1277	24.042	-30.060	9.925	1
OBD1-098.0	46065	45	Core	268	OUT	1.080	0.032	0.008	0.638	0.238	0.668	0.011	0.321	0.004	0.006	0.3246	0.5521	0.1217	24.166	-28.939	9.597	1
OBD1-098.0	46066	45	Core	268	OUT	1.083	0.031	0.008	0.635	0.236	0.649	0.012	0.340	0.004	0.004	0.3438	0.5542	0.1208	24.249	-28.327	9.429	1
OBD1-098.0	46069	150	Rim	268	OBS	1.051	0.069	0.010	0.492	0.371	0.788	0.015	0.197	0.004	0.008	0.2000	0.5491	0.1938	23.195	-31.345	12.805	2
OBD1-098.0	46070	150	Core	268	OBS	1.055	0.070	0.009	0.496	0.363	0.783	0.016	0.204	0.003	0.007	0.2067	0.5512	0.1897	23.520	-30.965	12.943	2
OBD1-098.0	46071	150	Core	268	OBS	1.068	0.071	0.009	0.537	0.310	0.804	0.011	0.183	0.003	0.008	0.1854	0.5577	0.1619	23.977	-31.618	12.798	2
OBD1-098.0	46072	150	Core	268	OBS	1.032	0.071	0.009	0.486	0.396	0.804	0.012	0.182	0.003	0.008	0.1846	0.5392	0.2069	22.970	-32.208	13.197	2
OBD1-098.0	46073	130	Rim	268	OBS	1.059	0.071	0.009	0.525	0.330	0.791	0.013	0.198	0.003	0.005	0.2002	0.5533	0.1724	23.974	-31.147	12.869	2
OBD1-098.0	46074	130	Rim	268	OBS	1.045	0.071	0.009	0.516	0.353	0.780	0.014	0.205	0.003	0.009	0.2081	0.5460	0.1844	23.485	-31.172	12.780	2
OBD1-098.0	46075	130	Core	268	OBS	1.034	0.070	0.011	0.520	0.359	0.781	0.014	0.203	0.003	0.009	0.2063	0.5405	0.1877	23.190	-31.140	12.403	1
OBD1-098.0	46077	130	Core	268	OBS	1.075	0.069	0.009	0.531	0.310	0.812	0.012	0.172	0.002	0.010	0.1748	0.5611	0.1618	23.853	-31.534	12.813	2
OBD1-098.0	46079	60	Rim	268	OBS	1.065	0.065	0.008	0.529	0.325	0.839	0.015	0.145	0.000	0.013	0.1474	0.5550	0.1694	23.709	-31.084	13.095	2
OBD1-098.0	46081	60	Rim	268	OBS	1.064	0.066	0.009	0.532	0.322	0.834	0.015	0.154	0.000	0.008	0.1559	0.5547	0.1679	23.929	-30.886	12.968	2
OBD1-098.0	46082	60	Core	268	OBS	1.062	0.063	0.010	0.530	0.327	0.836	0.017	0.152	0.002	0.006	0.1538	0.5534	0.1704	23.881	-30.424	12.795	2

OBD1-098.0	46083	60	Core	268	OBS	1.059	0.066	0.009	0.534	0.324	0.845	0.016	0.132	0.004	0.016	0.1351	0.5524	0.1690	23.469	-30.749	12.939	2
OBD1-098.0	46084	150	Rim	268	OBS	1.106	0.065	0.009	0.529	0.282	0.816	0.016	0.167	0.002	0.012	0.1699	0.5769	0.1471	24.202	-30.431	12.522	2
OBD1-098.0	46085	150	Rim	268	OBS	1.090	0.065	0.010	0.533	0.294	0.767	0.014	0.218	0.005	0.007	0.2213	0.5686	0.1534	24.052	-30.576	12.094	1
OBD1-098.0	46086	150	Core	268	OBS	1.088	0.072	0.009	0.534	0.292	0.731	0.010	0.258	0.002	0.006	0.2609	0.5684	0.1526	24.134	-31.311	12.207	1
OBD1-098.0	46087	150	Core	268	OBS	1.088	0.072	0.010	0.531	0.293	0.708	0.011	0.283	0.000	0.006	0.2856	0.5690	0.1532	24.000	-30.913	11.855	1
OBD1-098.0	46088	150	Core	268	OBS	1.080	0.075	0.010	0.529	0.302	0.692	0.007	0.297	0.002	0.007	0.3003	0.5651	0.1580	23.594	-32.156	11.896	1
OBD1-098.0	46089	150	Core	268	OBS	1.078	0.073	0.008	0.535	0.301	0.680	0.009	0.312	0.002	0.003	0.3145	0.5632	0.1573	24.130	-31.073	12.142	1
OBD1-098.0	46090	150	Core	268	OBS	1.088	0.074	0.011	0.534	0.289	0.686	0.008	0.310	0.002	0.000	0.3112	0.5693	0.1512	24.278	-31.159	11.808	1
OBD1-098.0	46091	85	Rim	268	OBS	1.036	0.068	0.009	0.534	0.346	0.839	0.013	0.144	0.003	0.012	0.1465	0.5407	0.1806	23.370	-31.459	13.029	2
OBD1-098.0	46092	85	Core	268	OBS	1.046	0.069	0.008	0.529	0.342	0.805	0.014	0.185	0.002	0.004	0.1869	0.5456	0.1784	24.054	-30.900	13.132	2
OBD1-098.0	46093	85	Core	268	OBS	1.046	0.067	0.010	0.530	0.341	0.780	0.013	0.209	0.002	0.006	0.2113	0.5456	0.1779	23.599	-31.188	12.458	2
OBD1-098.0	46094	85	Core	268	OBS	1.066	0.069	0.008	0.532	0.319	0.761	0.012	0.236	0.000	0.000	0.2367	0.5561	0.1664	24.590	-30.790	12.858	2
OBD1-098.0	46095	85	Core	268	OBS	1.059	0.068	0.010	0.531	0.326	0.748	0.012	0.241	0.004	0.005	0.2437	0.5527	0.1701	23.729	-31.127	12.220	1
OBD1-098.0	46096	70	Rim	268	OBS	1.052	0.059	0.010	0.517	0.354	0.839	0.014	0.145	0.002	0.011	0.1474	0.5471	0.1841	23.051	-31.669	12.767	2
OBD1-098.0	46097	70	Core	268	OBS	1.043	0.057	0.010	0.521	0.363	0.819	0.013	0.169	0.003	0.006	0.1711	0.5413	0.1884	23.166	-31.740	12.636	2
OBD1-098.0	46098	70	Core	268	OBS	1.048	0.062	0.009	0.516	0.360	0.782	0.012	0.209	0.004	0.003	0.2109	0.5447	0.1871	23.522	-31.697	12.745	2
OBD1-098.0	46099	65	Rim	268	OBS	1.055	0.052	0.010	0.525	0.350	0.847	0.017	0.135	0.003	0.011	0.1375	0.5466	0.1813	23.059	-30.949	12.605	2
OBD1-098.0	46100	65	Rim	268	OBS	1.047	0.054	0.008	0.532	0.350	0.831	0.018	0.150	0.004	0.011	0.1529	0.5428	0.1814	23.382	-30.459	12.783	2
OBD1-098.0	46101	65	Core	268	OBS	1.051	0.054	0.010	0.526	0.352	0.832	0.015	0.152	0.000	0.012	0.1545	0.5448	0.1825	22.992	-31.443	12.496	2
OBD1-098.0	46102	65	Core	268	OBS	1.049	0.054	0.010	0.531	0.349	0.829	0.015	0.158	0.003	0.006	0.1601	0.5438	0.1809	23.353	-31.117	12.552	2
OBD1-098.0	46103	65	Core	268	OBS	1.036	0.052	0.010	0.531	0.362	0.821	0.018	0.160	0.004	0.010	0.1631	0.5371	0.1877	23.032	-30.481	12.314	1
OBD1-098.0	46104	65	Core	268	OBS	1.047	0.052	0.008	0.529	0.357	0.820	0.014	0.165	0.002	0.009	0.1675	0.5416	0.1847	23.225	-31.505	12.725	2
OBD1-098.0	46105	65	Core	268	OBS	1.046	0.056	0.008	0.535	0.346	0.831	0.017	0.153	0.000	0.012	0.1555	0.5428	0.1796	23.426	-30.676	12.772	2
OBD1-098.0	46109	110	Core	268	OBS	1.035	0.068	0.010	0.531	0.349	0.822	0.015	0.164	0.005	0.005	0.1663	0.5405	0.1822	23.691	-30.704	12.867	2
OBD1-098.0	46110	110	Core	268	OBS	1.043	0.069	0.008	0.529	0.343	0.796	0.014	0.198	0.002	0.000	0.1992	0.5446	0.1791	24.443	-30.485	13.183	2
OBD1-098.0	46111	110	Core	268	OBS	1.044	0.067	0.009	0.540	0.334	0.796	0.012	0.195	0.004	0.003	0.1968	0.5443	0.1741	23.983	-31.184	12.764	2
OBD1-098.0	46112	110	Core	268	OBS	1.027	0.066	0.010	0.532	0.357	0.808	0.017	0.176	0.003	0.008	0.1789	0.5360	0.1863	23.465	-30.310	12.590	2
OBD1-098.0	46113	110	Core	268	OBS	1.037	0.066	0.010	0.539	0.340	0.841	0.015	0.143	0.003	0.009	0.1453	0.5412	0.1775	23.531	-30.783	12.820	2
OBD1-63	47649	50	Core	233	BCS	1.229	0.058	0.017	0.244	0.441	0.878	0.021	0.134	0.006	0.007	0.1324	0.6421	0.2304	21.451	-33.387	12.738	4
OBD1-63	47650	50	Core	233	BCS	1.287	0.049	0.016	0.230	0.408	0.878	0.019	0.135	0.000	0.007	0.1333	0.6686	0.2119	21.504	-34.016	12.560	4
OBD1-63	47652	50	Core	233	BCS	1.254	0.056	0.017	0.239	0.424	0.857	0.018	0.153	0.004	0.010	0.1515	0.6541	0.2212	21.271	-34.181	12.429	4
OBD1-63	47653	50	Core	233	BCS	1.234	0.059	0.018	0.245	0.434	0.865	0.019	0.151	0.003	0.006	0.1486	0.6451	0.2269	21.494	-33.826	12.541	4
OBD1-63	47654	50	Rim	233	BCS	1.262	0.052	0.018	0.248	0.411	0.905	0.019	0.109	0.000	0.007	0.1075	0.6569	0.2140	21.420	-33.985	12.755	4
OBD1-63	47656	50	Core	233	BCS	1.253	0.058	0.018	0.234	0.428	0.860	0.017	0.154	0.004	0.006	0.1519	0.6543	0.2235	21.375	-34.294	12.463	4
OBD1-63	47657	50	Core	233	BCS	1.249	0.057	0.018	0.239	0.428	0.860	0.018	0.160	0.000	0.004	0.1569	0.6519	0.2234	21.599	-34.066	12.472	4
OBD1-63	47658	50	Core	233	BCS	1.221	0.060	0.018	0.244	0.448	0.866	0.018	0.153	0.004	0.003	0.1501	0.6383	0.2342	21.564	-33.911	12.656	4
OBD1-63	47659	50	Rim	233	BCS	1.278	0.050	0.017	0.252	0.392	0.909	0.020	0.102	0.000	0.009	0.1009	0.6649	0.2040	21.534	-33.721	12.794	4
OBD1-63	47660	50	Rim	233	BCS	1.327	0.040	0.016	0.240	0.366	0.904	0.022	0.102	0.000	0.009	0.1014	0.6865	0.1893	21.609	-33.275	12.464	4
OBD1-63	47661	20	Core	233	BCS	1.334	0.026	0.015	0.306	0.308	0.937	0.021	0.062	0.000	0.009	0.0621	0.6848	0.1581	21.903	-32.589	12.444	4
OBD1-63	47662	20	Core	233	BCS	1.317	0.043	0.018	0.217	0.392	0.959	0.025	0.035	0.005	0.017	0.0352	0.6838	0.2035	20.180	-32.099	12.961	4
OBD1-63	47663	20	Core	233	BCS	1.294	0.066	0.018	0.257	0.352	0.962	0.026	0.043	0.008	0.014	0.0428	0.6800	0.1850	21.678	-31.581	13.651	4
OBD1-63	47667	10	Core	233	BCS	1.420	0.021	0.012	0.186	0.347	0.937	0.027	0.051	0.000	0.015	0.0516	0.7271	0.1777	20.752	-31.698	12.277	0
OBD1-63	47674	50	Core	233	BCS	1.347	0.076	0.018	0.205	0.340	0.980	0.027	0.040	0.004	0.007	0.0392	0.7119	0.1797	22.225	-31.052	13.862	2
OBD1-63	47675	50	Core	233	BCS	1.347	0.071	0.018	0.186	0.365	0.977	0.026	0.035	0.005	0.012	0.0346	0.7097	0.1923	21.319	-31.420	13.664	4
OBD1-63	47676	50	Core	233	BCS	1.399	0.076	0.019	0.194	0.298	0.980	0.027	0.036	0.006	0.009	0.0354	0.7398	0.1576	22.365	-30.480	13.372	0
OBD1-63	47677	40	Core	233	BCS	1.055	0.070	0.017	0.388	0.461	0.897	0.019	0.126	0.004	0.003	0.1232	0.5541	0.2421	22.320	-32.265	13.095	4
OBD1-63	47679	14	Core	233	BCS	1.007	0.082	0.012	0.412	0.475	0.976	0.023	0.040	0.006	0.014	0.0394	0.5317	0.2508	21.885	-30.325	14.614	2
OBD1-86.8	47680	30	Core	257	BCS	0.947	0.062	0.011	0.417	0.556	0.888	0.014	0.126	0.007	0.007	0.1243	0.4932	0.2896	21.494	-32.216	12.887	4
OBD1-86.8	47681	20	Core	257	BCS	0.979	0.048	0.012	0.391	0.562	0.935	0.014	0.066	0.005	0.015	0.0659	0.5067	0.2909	20.204	-32.746	12.981	4
OBD1-86.8	47682	15	Core	257	BCS	1.145	0.050	0.009	0.376	0.414	0.833	0.013	0.176	0.004	0.009	0.1744	0.5917	0.2140	22.317	-34.417	13.323	4

OBD1-86.8	47683	15	Core	257	BCS	1.139	0.048	0.008	0.365	0.433	0.927	0.015	0.074	0.004	0.015	0.0739	0.5880	0.2235	21.686	-34.000	14.348	0
OBD1-86.8	47684	25	Core	257	BCS	0.984	0.060	0.010	0.397	0.541	0.862	0.015	0.153	0.006	0.006	0.1507	0.5120	0.2815	21.746	-32.466	13.013	4
OBD1-86.8	47685	40	Core	257	BCS	0.959	0.018	0.006	0.702	0.312	0.619	0.007	0.379	0.003	0.007	0.3798	0.4861	0.1581	22.713	-29.509	8.891	1
OBD1-86.8	47686	40	Rim	257	BCS	0.969	0.015	0.007	0.686	0.320	0.643	0.007	0.353	0.004	0.006	0.3544	0.4906	0.1620	22.523	-30.127	8.954	1
OBD1-86.8	47687	80	Core	257	BCS	0.926	0.030	0.011	0.464	0.566	0.707	0.007	0.296	0.003	0.006	0.2951	0.4734	0.2894	20.122	-33.043	10.203	4
OBD1-86.8	47688	80	Rim	257	BCS	0.969	0.028	0.010	0.455	0.534	0.734	0.010	0.267	0.003	0.006	0.2667	0.4949	0.2727	20.639	-32.909	10.843	4
OBD1-86.8	47689	20	Core	257	BCS	1.207	0.055	0.011	0.387	0.333	0.915	0.013	0.093	0.005	0.012	0.0923	0.6264	0.1728	22.798	-34.184	13.746	4
OBD1-86.8	47690	20	Core	257	BCS	1.044	0.071	0.014	0.403	0.461	0.931	0.016	0.082	0.007	0.012	0.0809	0.5472	0.2416	21.785	-32.887	13.730	4
OBD1-86.8	47691	20	Core	257	BCS	0.955	0.065	0.014	0.497	0.462	0.884	0.016	0.131	0.003	0.011	0.1291	0.4990	0.2414	22.127	-31.531	12.379	4
OBD1-86.8	47692	175	Core	257	BCS	1.028	0.038	0.008	0.552	0.370	0.751	0.010	0.256	0.003	0.007	0.2542	0.5272	0.1897	22.811	-32.417	11.569	4
OBD1-86.8	47693	175	Core	257	BCS	1.021	0.038	0.007	0.545	0.385	0.626	0.007	0.386	0.003	0.003	0.3814	0.5233	0.1973	22.364	-32.178	10.998	1
OBD1-86.8	47694	175	Rim	257	BCS	1.006	0.037	0.008	0.551	0.394	0.630	0.009	0.378	0.006	0.003	0.3750	0.5156	0.2019	22.255	-31.414	10.736	1
OBD1-86.8	47695	175	Core	257	BCS	0.988	0.040	0.006	0.553	0.408	0.707	0.011	0.300	0.003	0.006	0.2979	0.5069	0.2093	22.694	-31.451	11.596	1
OBD1-86.8	47696	175	Rim	257	BCS	0.959	0.040	0.009	0.570	0.415	0.878	0.013	0.116	0.005	0.017	0.1167	0.4933	0.2135	22.015	-31.621	12.076	4
OBD1-265.0	47741	70	Core	435	OB	1.084	0.028	0.008	0.570	0.305	0.760	0.011	0.246	0.000	0.005	0.2445	0.5533	0.1557	23.509	-31.797	11.116	1
OBD1-265.0	47742	70	Rim	435	OB	1.085	0.026	0.007	0.538	0.335	0.878	0.018	0.115	0.004	0.012	0.1158	0.5541	0.1711	23.060	-31.200	12.434	2
OBD1-265.0	47743	100	Core	435	OB	1.066	0.030	0.008	0.577	0.313	0.724	0.011	0.280	0.004	0.005	0.2789	0.5450	0.1600	23.351	-31.360	10.868	1
OBD1-265.0	47745	60	Core	435	OB	1.074	0.027	0.008	0.599	0.287	0.711	0.010	0.294	0.000	0.006	0.2925	0.5480	0.1464	23.498	-31.141	10.370	1
OBD1-265.0	47746	40	Core	435	OB	1.118	0.031	0.009	0.555	0.282	0.699	0.010	0.304	0.004	0.005	0.3031	0.5719	0.1442	23.457	-31.591	10.578	1
OBD1-265.0	47748	70	Core	435	OB	1.052	0.027	0.008	0.580	0.329	0.647	0.008	0.356	0.003	0.005	0.3549	0.5365	0.1678	22.618	-31.715	10.271	1
OBD1-265.0	47750	150	Core	435	OB	1.035	0.028	0.007	0.574	0.351	0.640	0.010	0.365	0.003	0.004	0.3632	0.5281	0.1791	22.661	-31.055	10.515	1
OBD1-265.0	47751	80	Core	435	OB	1.067	0.031	0.008	0.572	0.315	0.749	0.013	0.257	0.000	0.006	0.2555	0.5461	0.1612	23.478	-31.135	11.078	1
OBD1-265.0	47752	60	Core	435	OB	1.063	0.028	0.008	0.579	0.319	0.651	0.008	0.354	0.004	0.003	0.3522	0.5421	0.1627	22.914	-31.644	10.395	1
OBD1-265.0	47753	30	Core	435	OB	1.095	0.024	0.008	0.533	0.336	0.734	0.010	0.264	0.003	0.008	0.2645	0.5575	0.1711	22.612	-32.823	11.110	4
OBD1-265.0	47754	50	Core	435	OB	1.080	0.029	0.007	0.579	0.298	0.770	0.014	0.230	0.004	0.008	0.2300	0.5519	0.1523	23.720	-30.846	11.221	1
OBD1-265.0	47755	60	Core	435	OB	1.122	0.028	0.007	0.568	0.267	0.817	0.016	0.181	0.003	0.008	0.1814	0.5733	0.1364	24.223	-30.449	11.462	1
OBD1-147.0	47757	200	Core	317	OB	1.029	0.033	0.009	0.554	0.368	0.833	0.016	0.169	0.004	0.007	0.1687	0.5274	0.1886	22.981	-31.231	11.854	1
OBD1-147.0	47758	200	Core	317	OB	1.000	0.035	0.010	0.525	0.423	0.869	0.015	0.135	0.000	0.010	0.1345	0.5133	0.2171	22.145	-32.004	12.122	4
OBD1-147.0	47759	30	Core	317	OB	1.009	0.035	0.009	0.536	0.403	0.868	0.016	0.136	0.000	0.010	0.1355	0.5180	0.2069	22.508	-31.628	12.234	4
OBD1-147.0	47761	50	Core	317	OB	0.975	0.021	0.007	0.518	0.470	0.886	0.017	0.105	0.000	0.015	0.1060	0.4967	0.2394	21.361	-31.426	12.147	4
OBD1-147.0	47763	60	Core	317	OB	1.067	0.047	0.008	0.558	0.313	0.861	0.015	0.144	0.002	0.012	0.1433	0.5506	0.1615	23.800	-31.339	12.495	2
OBD1-147.0	47764	150	Core	317	OB	1.068	0.036	0.007	0.554	0.329	0.665	0.009	0.345	0.002	0.004	0.3416	0.5474	0.1686	23.152	-31.765	11.059	1
OBD1-147.0	47765	30	Core	317	OB	1.106	0.029	0.007	0.541	0.310	0.834	0.015	0.169	0.002	0.006	0.1685	0.5652	0.1584	23.759	-31.570	12.137	2
OBD1-147.0	47766	40	Core	317	OB	1.075	0.031	0.008	0.551	0.328	0.797	0.014	0.208	0.003	0.004	0.2070	0.5502	0.1679	23.547	-31.473	11.725	1
OBD1-147.0	47767	50	Core	317	OB	1.062	0.031	0.009	0.561	0.330	0.854	0.017	0.144	0.003	0.009	0.1443	0.5438	0.1690	23.256	-30.974	11.882	1
OBD1-147.0	47768	80	Core	317	OB	1.076	0.033	0.008	0.566	0.313	0.725	0.011	0.282	0.000	0.007	0.2800	0.5504	0.1601	23.324	-31.700	11.034	1
OBD1-147.0	47769	150	Core	317	OB	1.054	0.033	0.009	0.569	0.330	0.674	0.010	0.336	0.000	0.004	0.3327	0.5397	0.1690	22.956	-31.417	10.555	1
OBD1-147.0	47770	70	Core	317	OB	1.057	0.032	0.008	0.560	0.336	0.808	0.015	0.192	0.004	0.009	0.1920	0.5412	0.1720	23.248	-31.321	11.686	1
OBD2-213	47771	30	Core	213	BCS	1.114	0.015	0.007	0.578	0.283	0.610	0.007	0.385	0.004	0.007	0.3869	0.5641	0.1433	22.575	-31.705	9.563	1
OBD2-213	47772	30	Core	213	BCS	1.171	0.028	0.009	0.476	0.310	0.754	0.011	0.247	0.002	0.008	0.2468	0.5984	0.1584	22.902	-33.281	11.428	4
OBD2-213	47773	25	Core	213	BCS	1.175	0.030	0.009	0.460	0.320	0.810	0.013	0.194	0.000	0.007	0.1932	0.6010	0.1637	23.082	-33.307	12.090	4
OBD2-213	47774	20	Core	213	BCS	1.215	0.027	0.009	0.447	0.297	0.777	0.008	0.228	0.000	0.007	0.2269	0.6202	0.1516	22.936	-34.620	11.661	4
OBD2-213	47775	25	Core	213	BCS	1.207	0.019	0.008	0.345	0.413	0.898	0.018	0.096	0.000	0.011	0.0966	0.6142	0.2102	21.417	-33.854	13.168	4
OBD2-213	47776	20	Core	213	BCS	1.129	0.036	0.010	0.461	0.354	0.901	0.018	0.096	0.003	0.013	0.0963	0.5808	0.1821	22.511	-32.314	12.939	4
OBD2-213	47777	25	Core	213	BCS	0.982	0.021	0.011	0.630	0.349	0.744	0.012	0.254	0.003	0.007	0.2545	0.5008	0.1780	22.432	-30.511	9.690	1
OBD2-213	47778	18	Core	213	BCS	1.094	0.015	0.007	0.591	0.290	0.616	0.006	0.382	0.003	0.006	0.3828	0.5539	0.1468	22.544	-31.957	9.569	1
OBD2-213	47779	35	Core	213	BCS	1.088	0.017	0.007	0.604	0.281	0.624	0.008	0.380	0.003	0.000	0.3785	0.5514	0.1424	23.439	-30.561	9.773	1
OBD2-213	47780	25	Core	213	BCS	1.088	0.017	0.006	0.591	0.294	0.650	0.009	0.350	0.004	0.003	0.3500	0.5514	0.1490	23.216	-31.045	10.167	1
OBD2-213	47781	35	Core	213	BCS	0.866	0.006	0.006	0.638	0.478	0.706	0.009	0.285	0.004	0.007	0.2876	0.4369	0.2412	20.991	-30.061	8.984	0
OBD2-213	47782	35	Core	213	BCS	1.034	0.031	0.010	0.538	0.379	0.868	0.014	0.127	0.004	0.013	0.1276	0.5300	0.1943	22.212	-32.216	11.969	4

OBD2-213	47783	30	Core	213	BCS	1.094	0.034	0.010	0.478	0.379	0.784	0.010	0.219	0.004	0.007	0.2183	0.5607	0.1943	22.279	-33.888	11.892	4
OBD2-213	47784	40	Core	213	BCS	1.070	0.033	0.009	0.454	0.428	0.787	0.010	0.214	0.004	0.009	0.2138	0.5482	0.2193	21.725	-34.184	12.069	4
OBD2-213	47785	60	Core	213	BCS	1.143	0.013	0.006	0.562	0.273	0.609	0.006	0.389	0.002	0.005	0.3898	0.5779	0.1380	22.798	-32.131	9.757	1
OBD2-213	47786	40	Core	213	BCS	1.173	0.015	0.006	0.544	0.256	0.692	0.011	0.307	0.003	0.004	0.3073	0.5945	0.1298	23.775	-31.155	10.356	1
OBD2-169	47789	20	Core	169	BCS	1.056	0.018	0.008	0.568	0.345	0.650	0.008	0.348	0.004	0.005	0.3487	0.5363	0.1752	22.148	-32.090	10.073	1
OBD2-169	47790	100	Core	169	BCS	1.024	0.044	0.006	0.543	0.380	0.664	0.007	0.350	0.004	0.003	0.3452	0.5259	0.1952	22.869	-32.495	11.678	1
OBD2-169	47791	100	Core	169	BCS	1.019	0.042	0.007	0.544	0.384	0.659	0.008	0.351	0.005	0.004	0.3475	0.5234	0.1972	22.601	-32.136	11.324	1
OBD2-169	47798	15	Core	169	BCS	1.122	0.012	0.008	0.520	0.333	0.796	0.011	0.197	0.003	0.007	0.1984	0.5681	0.1686	22.468	-33.183	11.217	4
OBD2-169	47799	30	Core	169	BCS	1.010	0.069	0.016	0.352	0.544	0.962	0.018	0.043	0.003	0.021	0.0428	0.5299	0.2854	20.032	-32.070	13.492	4
OBD2-141	47803	60	Core	136	BCS	1.149	0.046	0.017	0.147	0.627	0.976	0.026	0.025	0.004	0.011	0.0250	0.5975	0.3261	18.240	-30.238	12.396	3
OBD2-141	47804	60	Core	136	BCS	1.151	0.041	0.018	0.159	0.616	0.974	0.030	0.023	0.005	0.012	0.0231	0.5976	0.3198	18.180	-29.655	12.276	3
OBD2-141	47805	60	Core	136	BCS	1.119	0.044	0.018	0.152	0.655	0.978	0.025	0.025	0.004	0.009	0.0249	0.5810	0.3401	18.052	-30.170	12.146	3
OBD2-141	47806	40	Core	136	BCS	1.282	0.009	0.013	0.291	0.392	0.949	0.027	0.030	0.000	0.018	0.0306	0.6524	0.1995	19.778	-31.616	12.531	0
OBD2-141	47807	40	Core	136	BCS	1.232	0.016	0.017	0.240	0.482	0.955	0.026	0.029	0.002	0.014	0.0295	0.6305	0.2467	18.805	-31.807	12.314	3
OBD2-141	47808	15	Core	136	BCS	1.241	0.037	0.014	0.159	0.534	0.973	0.031	0.021	0.000	0.017	0.0211	0.6417	0.2761	18.725	-30.242	13.018	3
OBD2-141	47810	8	Core	136	BCS	1.216	0.026	0.015	0.189	0.541	0.970	0.027	0.020	0.000	0.016	0.0202	0.6249	0.2780	18.327	-31.068	12.769	3
OBD2-141	47811	50	Core	136	BCS	1.084	0.065	0.021	0.225	0.591	0.985	0.028	0.025	0.002	0.013	0.0248	0.5705	0.3111	19.094	-30.091	13.051	3
OBD2-141	47812	50	Core	136	BCS	1.098	0.066	0.020	0.214	0.586	0.984	0.031	0.024	0.003	0.013	0.0238	0.5785	0.3087	19.213	-29.525	13.179	3
OBD2-141	47813	15	Core	136	BCS	0.963	0.004	0.007	0.593	0.421	0.924	0.024	0.053	0.000	0.020	0.0542	0.4871	0.2129	20.958	-28.655	11.332	0
OBD2-141	47814	60	Core	136	BCS	1.244	0.040	0.015	0.176	0.512	0.968	0.027	0.025	0.003	0.017	0.0252	0.6439	0.2650	18.953	-31.267	13.135	3
OBD2-141	47815	70	Core	136	BCS	1.170	0.039	0.018	0.171	0.589	0.966	0.028	0.031	0.004	0.011	0.0311	0.6062	0.3052	18.561	-30.619	12.352	3
OBD2-119	47816	15	Core	119	BC	1.251	0.029	0.023	0.136	0.547	0.967	0.028	0.021	0.003	0.016	0.0213	0.6468	0.2828	17.453	-30.582	11.324	3
OBD2-119	47819	120	Core	119	BC	1.121	0.074	0.022	0.134	0.635	0.990	0.027	0.024	0.003	0.014	0.0237	0.5931	0.3360	18.337	-29.682	12.337	3
OBD2-119	47820	120	Core	119	BC	1.097	0.078	0.023	0.137	0.652	0.991	0.026	0.024	0.004	0.014	0.0236	0.5817	0.3457	18.238	-29.634	12.242	3
OBD2-119	47821	120	Core	119	BC	1.134	0.073	0.022	0.141	0.617	0.989	0.026	0.025	0.004	0.012	0.0247	0.5994	0.3261	18.559	-30.112	12.549	3
OBD2-119	47822	20	Core	119	OUT	1.151	0.020	0.010	0.329	0.479	0.918	0.021	0.078	0.000	0.008	0.0783	0.5875	0.2445	20.773	-32.920	13.015	4
OBD2-119	47823	60	Core	119	BC	0.893	0.059	0.024	0.290	0.723	0.971	0.024	0.038	0.008	0.006	0.0377	0.4685	0.3793	18.646	-28.265	11.091	0
OBD2-119	47824	10	Core	119	BC	1.127	0.009	0.014	0.180	0.657	0.963	0.025	0.024	0.000	0.011	0.0243	0.5738	0.3345	17.310	-30.518	11.449	3
OBD2-119	47825	30	Core	119	BC	1.049	0.042	0.014	0.144	0.736	0.983	0.027	0.018	0.000	0.014	0.0180	0.5438	0.3815	17.424	-28.438	11.857	0
OBD2-119	47826	30	Core	119	BC	1.064	0.043	0.014	0.141	0.725	0.984	0.025	0.016	0.002	0.013	0.0160	0.5513	0.3756	17.382	-28.844	12.083	0
OBD2-136	47828	10	Core	136	BC	1.179	0.012	0.014	0.175	0.606	0.963	0.026	0.023	0.000	0.015	0.0233	0.6015	0.3092	17.535	-30.912	11.822	3
OBD2-136	47829	10	Core	136	BC	1.162	0.052	0.017	0.218	0.536	0.965	0.029	0.044	0.005	0.005	0.0436	0.6065	0.2797	20.247	-30.801	13.304	4
OBD2-136	47830	20	Core	136	BC	1.135	0.035	0.019	0.172	0.625	0.968	0.028	0.025	0.003	0.014	0.0252	0.5875	0.3235	17.845	-30.157	11.914	3
OBD2-136	47831	20	Core	136	BC	1.162	0.033	0.018	0.171	0.602	0.973	0.028	0.022	0.003	0.012	0.0221	0.6005	0.3111	18.041	-30.268	12.232	3
OBD2-136	47832	15	Core	136	BC	1.152	0.024	0.014	0.295	0.503	0.959	0.025	0.027	0.003	0.017	0.0274	0.5908	0.2579	19.176	-31.564	13.075	4
OBD2-97.1	47834	10	Core	97	BC	0.985	0.014	0.010	0.465	0.512	0.932	0.027	0.035	0.005	0.028	0.0362	0.5020	0.2610	19.372	-29.229	12.028	0
OBD2-97.1	47835	20	Core	97	BC	1.009	0.044	0.012	0.376	0.545	0.957	0.029	0.029	0.005	0.024	0.0294	0.5228	0.2824	19.736	-29.373	13.332	3
OBD2-97.1	47836	20	Core	97	BC	1.008	0.042	0.013	0.385	0.538	0.956	0.028	0.033	0.005	0.020	0.0334	0.5220	0.2786	19.898	-29.587	13.124	3
OBD2-97.1	47837	20	Core	97	BC	0.990	0.044	0.015	0.379	0.557	0.961	0.029	0.027	0.004	0.023	0.0273	0.5140	0.2892	19.392	-29.097	12.825	3
OBD2-97.1	47838	100	Core	97	OUT	1.014	0.017	0.007	0.606	0.353	0.629	0.007	0.374	0.000	0.004	0.3729	0.5139	0.1789	22.166	-31.578	9.802	1
OBD2-97.1	47839	100	Core	97	OUT	1.015	0.017	0.006	0.605	0.352	0.645	0.010	0.355	0.004	0.002	0.3550	0.5147	0.1785	22.669	-30.537	10.154	1
OBD2-97.1	47840	40	Core	97	OUT	1.003	0.022	0.009	0.557	0.398	0.896	0.023	0.092	0.005	0.013	0.0931	0.5123	0.2033	22.104	-29.709	11.902	1
OBD2-97.1	47841	30	Core	97	OUT	0.952	0.102	0.014	0.342	0.573	0.995	0.033	0.024	0.002	0.022	0.0236	0.5099	0.3069	20.835	-27.691	14.457	0

APPENDIX II

GEOCHEMISTRY AND STATISTICS OF WEATHERED CHROMITES - ORA BANDA PROSPECT

A priori groups and *a posteriori* types

Pyx1 Pyx2	Pyroxenite Lag
PdT1 PdT2	Top of Peridotite Lag
Prd1 Prd2	Peridotite Lag
FeDc	Fe-rich Duricrust
DcLag	Lag from Fe-rich Duricrust
UNCL	Unclassified

This data also available on Data Disc (Volume 3B)

Thin Section	Analy No	Size µm	Loc	Lag Type	Structural Formula Cr	Ti	V	Al	Fe3+	Fe2+	Mn	Mg	Ni	Zn	Cr Cr+Al+Fe3+	Mg Mg+Fe2+	Fe3+ Cr+Al+Fe3+	Canonical Variates CV1	CV2	CV3	CV4	CV5	Group	Post Type
08-1499A	46254	150	Rim	C	1.096	0.086	0.011	0.596	0.204	0.843	0.014	0.141	0.005	0.007	0.5781	0.1434	0.1077	142.976	70.275	18.566	-22.830	17.711	Pyx1	Pyx2
08-1499A	46255	150	Core	C	1.118	0.085	0.011	0.608	0.171	0.815	0.015	0.173	0.002	0.007	0.5894	0.1753	0.0899	142.031	71.562	18.172	-22.314	17.844	Pyx1	Pyx1
08-1499A	46257	170	Rim	C	1.035	0.083	0.008	0.585	0.287	0.737	0.005	0.252	0.004	0.006	0.5427	0.2549	0.1504	141.009	71.253	16.075	-22.278	18.812	Pyx1	Pyx1
08-1499A	46259	170	Core	C	0.995	0.085	0.010	0.560	0.347	0.757	0.007	0.232	0.004	0.005	0.5233	0.2347	0.1824	140.020	70.400	15.678	-22.326	17.640	Pyx1	Pyx1
08-1499B	46267	110	Rim	C	1.096	0.061	0.009	0.580	0.248	0.816	0.013	0.168	0.003	0.010	0.5696	0.1702	0.1289	141.966	70.676	17.284	-23.040	18.116	Pyx1	Prd1
08-1499B	46279	175	Rim	C	1.037	0.067	0.010	0.529	0.351	0.878	0.012	0.106	0.003	0.010	0.5408	0.1074	0.1831	140.870	68.120	17.411	-24.130	17.544	Pyx1	Pyx2
08-1499C	46283	120	Core	C	1.076	0.069	0.010	0.665	0.179	0.701	0.005	0.288	0.004	0.005	0.5605	0.2914	0.0932	141.897	71.602	18.153	-22.056	17.006	Pyx1	PdT1
08-1499C	46284	120	Core	C	1.109	0.068	0.009	0.629	0.182	0.712	0.004	0.282	0.005	0.000	0.5775	0.2837	0.0948	141.745	71.736	17.432	-23.472	17.767	Pyx1	PdT1
08-1499C	46288	135	Rim	C	1.133	0.065	0.009	0.615	0.175	0.703	0.007	0.289	0.002	0.004	0.5893	0.2917	0.0908	141.767	71.709	17.041	-22.210	16.999	Pyx1	Pyx1
08-1499C	46289	135	Core	C	1.089	0.064	0.009	0.611	0.225	0.712	0.005	0.284	0.003	0.000	0.5657	0.2850	0.1171	141.542	72.008	16.443	-23.518	17.897	Pyx1	PdT1
08-1499C	46290	125	Rim	C	1.089	0.075	0.010	0.620	0.203	0.712	0.007	0.278	0.003	0.005	0.5697	0.2808	0.1061	142.219	71.685	17.075	-22.034	16.928	Pyx1	Pyx1
08-1499C	46291	125	Core	C	1.106	0.077	0.010	0.607	0.196	0.692	0.006	0.299	0.004	0.003	0.5795	0.3017	0.1027	142.681	71.104	17.029	-22.136	15.879	Pyx1	Pyx1
08-1499C	46299	300	Core	C	1.088	0.086	0.009	0.604	0.204	0.825	0.018	0.161	0.003	0.006	0.5740	0.1629	0.1077	142.202	70.879	17.773	-21.675	18.672	Pyx1	Pyx1
08-1499C	46301	125	Rim	C	1.122	0.067	0.009	0.645	0.154	0.719	0.008	0.274	0.000	0.005	0.5842	0.2760	0.0802	140.737	72.558	17.430	-21.750	18.018	Pyx1	PdT1
08-1499C	46302	125	Core	C	1.125	0.067	0.009	0.642	0.152	0.711	0.008	0.284	0.003	0.000	0.5863	0.2850	0.0793	141.161	71.964	17.594	-22.591	17.084	Pyx1	PdT1
08-1499C	46304	165	Rim	C	1.103	0.077	0.008	0.607	0.196	0.841	0.018	0.140	0.003	0.011	0.5786	0.1425	0.1029	142.451	70.025	18.464	-21.520	18.843	Pyx1	Pyx1
08-1499C	46305	165	Core	C	1.102	0.077	0.009	0.609	0.200	0.703	0.006	0.290	0.003	0.003	0.5764	0.2920	0.1047	142.025	71.778	16.689	-22.143	17.372	Pyx1	Pyx1
08-1499C	46306	165	Core	C	1.097	0.080	0.009	0.607	0.204	0.693	0.007	0.298	0.003	0.005	0.5748	0.3007	0.1071	142.287	71.224	16.605	-21.274	17.102	Pyx1	Pyx1
08-1522A	46314	85	Core	B	1.109	0.080	0.008	0.585	0.213	0.815	0.011	0.175	0.004	0.004	0.5816	0.1765	0.1117	141.756	71.402	17.025	-22.529	19.712	Pyx1	Prd1
08-1522A	46315	80	Rim	B	1.114	0.080	0.008	0.594	0.200	0.765	0.010	0.224	0.003	0.005	0.5841	0.2269	0.1046	141.743	71.792	16.750	-21.915	18.874	Pyx1	Pyx1
08-1522A	46316	80	Core	B	1.084	0.050	0.008	0.608	0.245	0.720	0.008	0.270	0.004	0.005	0.5597	0.2726	0.1265	141.459	71.448	16.467	-22.770	17.089	Pyx1	PdT1
08-1522A	46317	80	Core	B	1.093	0.050	0.009	0.602	0.243	0.717	0.008	0.271	0.005	0.004	0.5641	0.2747	0.1254	141.834	71.026	16.630	-23.039	16.395	Pyx1	PdT1
08-1522A	46318	125	Rim	B	1.097	0.042	0.007	0.619	0.228	0.776	0.011	0.217	0.000	0.005	0.5642	0.2185	0.1174	140.272	72.822	16.558	-23.528	19.283	Pyx1	Prd1
08-1522A	46319	125	Core	B	1.089	0.109	0.010	0.562	0.225	0.773	0.010	0.222	0.002	0.000	0.5804	0.2228	0.1201	141.601	71.907	15.767	-21.994	18.876	Pyx1	Pyx1
08-1522A	46320	125	Core	B	1.073	0.109	0.010	0.544	0.263	0.730	0.006	0.261	0.004	0.004	0.5710	0.2633	0.1397	141.851	70.727	15.467	-21.467	17.708	Pyx1	Pyx1
08-1522A	46322	50	Core	B	1.071	0.106	0.010	0.543	0.266	0.734	0.006	0.258	0.004	0.003	0.5696	0.2602	0.1415	141.777	71.068	15.461	-21.995	17.460	Pyx1	Pyx1
08-1522A	46324	150	Core	B	1.073	0.058	0.010	0.702	0.155	0.662	0.005	0.331	0.003	0.003	0.5558	0.3336	0.0804	141.578	70.978	18.861	-21.895	15.424	Pyx1	PdT1
08-1522A	46326	150	Core	B	1.088	0.056	0.009	0.700	0.145	0.672	0.004	0.319	0.004	0.004	0.5628	0.3220	0.0752	141.076	70.990	19.110	-22.264	16.280	Pyx1	PdT1
08-1522A	46328	100	Rim	B	1.096	0.058	0.008	0.688	0.147	0.671	0.006	0.320	0.003	0.004	0.5676	0.3227	0.0759	141.262	70.818	18.618	-21.278	16.083	Pyx1	PdT1
08-1522A	46329	100	Core	B	1.115	0.069	0.010	0.593	0.208	0.760	0.010	0.238	0.000	0.000	0.5820	0.2382	0.1086	141.302	73.070	16.188	-23.659	18.255	Pyx1	PdT1
08-1522A	46330	100	Core	B	1.132	0.065	0.009	0.574	0.215	0.721	0.009	0.267	0.003	0.006	0.5893	0.2704	0.1118	142.362	71.170	16.366	-22.352	16.415	Pyx1	Pyx1
08-1522A	46331	30	Core	B	1.152	0.067	0.009	0.582	0.187	0.737	0.004	0.254	0.002	0.005	0.5996	0.2566	0.0975	141.716	72.169	16.859	-23.796	18.001	Pyx1	Prd1
08-1522A	46335	45	Core	B	1.127	0.096	0.009	0.529	0.232	0.861	0.014	0.127	0.000	0.009	0.5970	0.1287	0.1228	142.256	70.120	16.864	-22.378	19.405	Pyx1	Prd1
08-1522A	46342	105	Rim	B	1.084	0.093	0.011	0.526	0.278	0.847	0.014	0.141	0.003	0.005	0.5740	0.1429	0.1472	142.109	69.864	16.658	-23.171	17.672	Pyx1	Pyx1
08-1522A	46346	120	Core	B	1.102	0.087	0.009	0.568	0.230	0.822	0.009	0.166	0.003	0.006	0.5800	0.1681	0.1212	142.080	71.137	17.084	-23.065	19.243	Pyx1	Prd1
08-1522A	46347	120	Core	B	1.067	0.089	0.008	0.596	0.236	0.752	0.009	0.234	0.004	0.008	0.5617	0.2370	0.1245	141.806	71.171	16.512	-20.872	18.984	Pyx1	Pyx1
08-1522A	46348	120	Core	B	1.079	0.086	0.010	0.615	0.207	0.721	0.007	0.267	0.005	0.006	0.5676	0.2701	0.1087	142.419	71.277	17.163	-21.456	17.198	Pyx1	Pyx1

08-1522A	46349	60	Core	B	1.062	0.085	0.008	0.636	0.205	0.714	0.007	0.276	0.003	0.005	0.5582	0.2789	0.1079	141.791	71.714	17.010	-20.880	18.437	Pyx1	Pyx1
08-1522A	46350	110	Rim	B	1.117	0.072	0.009	0.568	0.230	0.787	0.008	0.201	0.003	0.007	0.5834	0.2035	0.1199	141.909	71.537	16.690	-23.292	18.467	Pyx1	Prd1
08-1522A	46351	110	Core	B	1.062	0.114	0.010	0.584	0.226	0.798	0.009	0.191	0.003	0.005	0.5675	0.1934	0.1206	141.826	71.582	16.874	-21.621	19.332	Pyx1	PdT1
08-1522A	46352	110	Core	B	1.074	0.117	0.011	0.592	0.202	0.730	0.008	0.259	0.003	0.005	0.5751	0.2620	0.1081	142.216	71.367	16.675	-20.536	17.667	Pyx1	Pyx1
08-1522A	46353	110	Core	B	1.058	0.113	0.010	0.590	0.226	0.726	0.006	0.264	0.004	0.004	0.5646	0.2669	0.1205	141.987	71.360	16.338	-20.904	18.252	Pyx1	Pyx1
08-1522B	46354	105	Rim	B	1.070	0.109	0.010	0.574	0.233	0.761	0.009	0.229	0.004	0.004	0.5700	0.2314	0.1243	141.830	71.469	16.154	-21.202	18.668	Pyx1	Pyx1
08-1522B	46356	105	Core	B	1.126	0.099	0.010	0.535	0.222	0.871	0.016	0.112	0.005	0.007	0.5979	0.1140	0.1178	143.364	68.801	17.980	-22.791	17.802	Pyx1	Pyx2
08-1522B	46358	65	Core	B	1.102	0.090	0.010	0.490	0.302	0.874	0.013	0.115	0.004	0.004	0.5820	0.1166	0.1594	141.791	68.696	16.423	-24.017	17.884	Pyx1	Prd1
08-1522B	46359	65	Core	B	1.111	0.101	0.011	0.485	0.286	0.839	0.011	0.152	0.004	0.003	0.5903	0.1531	0.1520	141.650	69.767	15.703	-23.713	17.908	Pyx1	Pyx1
08-1522B	46361	65	Core	B	1.043	0.091	0.009	0.595	0.257	0.803	0.011	0.183	0.002	0.010	0.5505	0.1855	0.1357	141.665	71.066	16.953	-21.272	19.313	Pyx1	Pyx1
08-1522B	46365	100	Core	B	1.087	0.113	0.009	0.517	0.267	0.815	0.015	0.176	0.000	0.006	0.5811	0.1778	0.1428	141.128	70.780	15.218	-21.095	19.403	Pyx1	Pyx1
08-1522B	46366	100	Core	B	1.065	0.113	0.010	0.505	0.302	0.767	0.010	0.222	0.005	0.003	0.5689	0.2242	0.1612	140.976	70.024	14.774	-21.336	17.927	Pyx1	Pyx1
08-1522B	46367	100	Rim	B	1.104	0.123	0.010	0.538	0.221	0.781	0.009	0.214	0.002	0.000	0.5927	0.2154	0.1184	141.599	71.715	15.609	-22.174	18.895	Pyx1	Pyx1
08-1522B	46368	100	Core	B	1.122	0.025	0.008	0.595	0.245	0.819	0.010	0.169	0.003	0.007	0.5717	0.1708	0.1250	140.243	71.287	17.424	-25.577	18.292	Pyx1	PdT1
08-1522B	46374	150	Core	B	1.092	0.122	0.009	0.600	0.172	0.742	0.010	0.248	0.003	0.004	0.5860	0.2504	0.0922	141.595	71.467	16.861	-19.942	18.538	Pyx1	Pyx1
08-1522B	46376	50	Core	B	1.078	0.119	0.010	0.600	0.189	0.733	0.009	0.260	0.004	0.000	0.5775	0.2619	0.1011	141.797	71.572	16.510	-20.730	18.238	Pyx1	Pyx1
08-1522B	46378	215	Core	B	1.128	0.128	0.009	0.496	0.232	0.863	0.015	0.120	0.005	0.008	0.6080	0.1224	0.1248	142.678	68.258	16.798	-21.257	18.911	Pyx1	Pyx1
08-1522B	46379	215	Core	B	1.088	0.131	0.010	0.493	0.273	0.772	0.009	0.216	0.005	0.005	0.5866	0.2191	0.1473	141.484	69.889	14.945	-20.970	18.032	Pyx1	Pyx1
08-1522B	46380	215	Core	B	1.086	0.131	0.010	0.517	0.252	0.750	0.009	0.241	0.004	0.004	0.5857	0.2431	0.1357	141.788	70.566	15.138	-20.876	17.688	Pyx1	Pyx1
08-1522B	46382	105	Rim	B	1.069	0.106	0.009	0.538	0.271	0.882	0.014	0.102	0.005	0.008	0.5692	0.1036	0.1443	142.576	68.319	17.659	-22.114	19.158	Pyx1	Pyx2
08-1522B	46386	140	Rim	B	1.092	0.078	0.009	0.589	0.229	0.725	0.007	0.267	0.002	0.004	0.5718	0.2695	0.1198	141.875	71.853	16.196	-22.270	17.730	Pyx1	Pyx1
08-1522B	46387	140	Core	B	1.108	0.088	0.009	0.555	0.232	0.860	0.017	0.120	0.004	0.013	0.5848	0.1221	0.1224	143.225	68.768	18.100	-21.978	18.033	Pyx1	Pyx2
08-1522B	46388	140	Core	B	1.081	0.094	0.008	0.553	0.260	0.699	0.008	0.291	0.003	0.005	0.5708	0.2938	0.1374	142.029	70.298	15.242	-20.399	17.196	Pyx1	Pyx1
08-1499A	46256	80	Core	C	1.068	0.135	0.011	0.523	0.254	0.893	0.018	0.088	0.004	0.010	0.5787	0.0897	0.1377	143.315	67.245	18.165	-21.192	17.819	Pyx2	Pyx2
08-1499B	46263	120	Core	C	1.074	0.099	0.011	0.580	0.229	0.896	0.012	0.089	0.003	0.009	0.5704	0.0907	0.1216	143.461	69.062	19.232	-23.270	18.418	Pyx2	Pyx2
08-1499B	46268	110	Core	C	1.100	0.059	0.009	0.600	0.226	0.897	0.012	0.085	0.004	0.012	0.5709	0.0863	0.1174	143.164	68.867	19.739	-24.296	18.532	Pyx2	Pyx2
08-1499B	46272	110	Core	C	1.094	0.151	0.011	0.497	0.240	0.926	0.014	0.053	0.003	0.015	0.5973	0.0537	0.1312	143.976	65.600	18.954	-21.264	18.061	Pyx2	Pyx2
08-1499B	46276	100	Rim	C	1.061	0.101	0.011	0.494	0.325	0.913	0.015	0.070	0.003	0.011	0.5641	0.0711	0.1730	142.416	66.409	17.823	-23.109	17.226	Pyx2	Pyx2
08-1499B	46278	100	Core	C	1.084	0.100	0.010	0.526	0.274	0.891	0.012	0.090	0.005	0.011	0.5755	0.0916	0.1453	143.199	67.714	18.191	-22.996	18.056	Pyx2	Pyx2
08-1499C	46298	300	Rim	C	1.022	0.069	0.009	0.583	0.307	0.903	0.021	0.077	0.002	0.013	0.5348	0.0781	0.1604	142.333	67.457	18.957	-22.559	17.870	Pyx2	Pyx2
08-1522A	46323	150	Rim	B	1.101	0.114	0.010	0.508	0.259	0.882	0.015	0.097	0.004	0.014	0.5891	0.0992	0.1388	143.304	67.522	17.784	-21.838	17.907	Pyx2	Pyx2
08-1522A	46332	80	Rim	B	1.183	0.065	0.011	0.558	0.175	0.904	0.014	0.077	0.002	0.013	0.6172	0.0787	0.0914	143.787	68.348	19.992	-24.675	16.806	Pyx2	Pyx2
08-1522A	46333	80	Core	B	1.131	0.093	0.011	0.533	0.225	0.892	0.016	0.095	0.000	0.009	0.5989	0.0959	0.1189	143.173	69.205	18.027	-23.262	18.106	Pyx2	Pyx2
08-1522A	46334	80	Core	B	1.072	0.076	0.010	0.393	0.441	0.931	0.016	0.051	0.000	0.014	0.5622	0.0520	0.2315	138.461	63.249	16.169	-24.134	15.476	Pyx2	UNCL
08-1522A	46336	35	Core	B	1.127	0.082	0.009	0.552	0.224	0.886	0.014	0.098	0.003	0.009	0.5924	0.0991	0.1176	143.219	68.904	18.430	-23.327	18.598	Pyx2	Pyx2
08-1522A	46337	85	Rim	B	1.144	0.080	0.009	0.512	0.248	0.908	0.016	0.074	0.000	0.014	0.6011	0.0752	0.1300	143.307	67.762	18.133	-23.316	18.352	Pyx2	Pyx2
08-1522B	46355	105	Core	B	1.119	0.095	0.009	0.520	0.249	0.881	0.016	0.096	0.004	0.016	0.5926	0.0980	0.1320	143.514	67.494	18.088	-22.040	18.035	Pyx2	Pyx2
08-1522B	46357	65	Rim	B	1.168	0.103	0.010	0.453	0.259	0.884	0.014	0.099	0.004	0.009	0.6212	0.1011	0.1378	142.924	67.482	16.651	-23.343	17.556	Pyx2	Pyx2
08-1498A	46391	65	Core	C	1.126	0.086	0.010	0.559	0.214	0.815	0.010	0.175	0.002	0.005	0.5929	0.1771	0.1128	141.977	71.549	16.746	-23.020	19.022	PdT1	Prd1

08-1498A	46392	65	Core	C	1.075	0.054	0.007	0.741	0.118	0.676	0.007	0.318	0.004	0.000	0.5558	0.3201	0.0611	139.063	71.026	19.260	-20.895	17.090	PdT1	UNCL
08-1498A	46393	65	Core	C	1.085	0.051	0.009	0.740	0.113	0.674	0.004	0.321	0.000	0.004	0.5598	0.3224	0.0583	138.732	71.630	19.754	-21.873	16.680	PdT1	Prd2
08-1498A	46394	50	Core	C	1.075	0.050	0.009	0.745	0.119	0.673	0.005	0.323	0.000	0.003	0.5544	0.3245	0.0612	138.836	71.814	19.440	-21.548	16.885	PdT1	PdT1
08-1498A	46395	20	Core	C	1.078	0.063	0.011	0.557	0.284	0.892	0.014	0.098	0.002	0.004	0.5616	0.0990	0.1482	142.105	69.549	18.003	-25.216	17.881	PdT1	Pyx2
08-1498A	46396	20	Core	C	1.170	0.034	0.008	0.673	0.112	0.696	0.007	0.294	0.003	0.005	0.5986	0.2971	0.0571	138.924	70.810	19.040	-22.722	15.809	PdT1	PdT1
08-1498A	46397	65	Rim	C	1.157	0.031	0.009	0.667	0.133	0.697	0.007	0.299	0.002	0.000	0.5911	0.3002	0.0681	139.422	71.913	18.228	-24.210	16.192	PdT1	PdT1
08-1498A	46399	65	Core	C	1.145	0.067	0.010	0.606	0.166	0.813	0.013	0.176	0.003	0.005	0.5975	0.1778	0.0866	141.678	71.545	18.089	-23.199	18.161	PdT1	Prd1
08-1498B	46400	55	Core	C	1.139	0.064	0.010	0.608	0.174	0.784	0.010	0.206	0.004	0.003	0.5928	0.2085	0.0906	141.675	72.022	17.712	-23.691	17.805	PdT1	PdT1
08-1498B	46404	60	Rim	C	1.122	0.068	0.011	0.622	0.175	0.722	0.004	0.275	0.002	0.000	0.5849	0.2761	0.0909	141.538	72.757	17.493	-24.716	17.200	PdT1	PdT1
08-1498B	46407	75	Rim	C	1.099	0.071	0.009	0.596	0.219	0.863	0.012	0.124	0.003	0.007	0.5742	0.1258	0.1146	142.476	70.453	18.432	-23.681	18.975	PdT1	Prd1
08-1498B	46408	75	Core	C	1.142	0.085	0.011	0.565	0.190	0.833	0.012	0.154	0.003	0.007	0.6017	0.1562	0.1003	142.604	70.948	17.818	-23.373	17.928	PdT1	Prd1
08-1498B	46411	60	Core	C	1.110	0.038	0.007	0.698	0.142	0.727	0.009	0.262	0.004	0.005	0.5692	0.2648	0.0730	139.560	71.739	18.720	-22.213	18.030	PdT1	PdT1
08-1498B	46412	25	Core	C	1.127	0.040	0.009	0.704	0.118	0.688	0.006	0.303	0.004	0.003	0.5783	0.3061	0.0604	139.204	71.116	19.287	-22.462	16.103	PdT1	PdT1
08-1498B	46413	40	Core	C	1.137	0.090	0.010	0.571	0.189	0.785	0.007	0.205	0.003	0.006	0.5994	0.2076	0.0996	141.869	71.846	16.919	-22.754	18.916	PdT1	Prd1
08-1498B	46418	165	Core	C	1.119	0.065	0.010	0.605	0.196	0.724	0.009	0.266	0.004	0.004	0.5829	0.2689	0.1019	142.251	71.644	17.059	-22.743	16.416	PdT1	Pyx1
08-1498B	46419	165	Core	C	1.106	0.063	0.009	0.630	0.189	0.709	0.005	0.286	0.000	0.003	0.5747	0.2877	0.0980	141.244	72.747	16.868	-22.855	17.952	PdT1	PdT1
08-1498B	46420	165	Core	C	1.087	0.066	0.009	0.604	0.231	0.737	0.005	0.252	0.005	0.005	0.5656	0.2552	0.1202	141.867	71.691	16.925	-23.284	17.849	PdT1	PdT1
08-1498B	46421	165	Core	C	1.106	0.062	0.009	0.633	0.186	0.719	0.006	0.277	0.003	0.000	0.5746	0.2777	0.0965	141.323	72.501	17.098	-23.492	17.917	PdT1	PdT1
08-1498B	46422	165	Rim	C	1.129	0.066	0.009	0.612	0.180	0.769	0.009	0.225	0.003	0.000	0.5880	0.2267	0.0936	141.291	72.548	17.128	-23.793	18.431	PdT1	Prd1
08-1498B	46432	50	Core	C	1.131	0.054	0.009	0.613	0.186	0.857	0.014	0.131	0.000	0.008	0.5863	0.1325	0.0962	141.768	71.241	18.666	-23.929	18.753	PdT1	Prd1
08-1498B	46436	90	Core	C	1.114	0.058	0.008	0.648	0.169	0.698	0.007	0.292	0.004	0.004	0.5771	0.2951	0.0874	141.456	71.484	17.575	-21.848	17.134	PdT1	Pyx1
08-1498B	46437	90	Core	C	1.112	0.060	0.009	0.654	0.162	0.694	0.007	0.305	0.000	0.000	0.5769	0.3051	0.0841	140.881	72.539	17.221	-22.594	17.337	PdT1	PdT1
08-1516	46438	125	Rim	A	1.118	0.060	0.008	0.647	0.164	0.692	0.006	0.307	0.000	0.000	0.5799	0.3075	0.0848	140.835	72.490	17.088	-22.726	17.736	PdT1	PdT1
08-1516	46449	150	Rim	A	1.103	0.035	0.010	0.697	0.152	0.728	0.008	0.266	0.000	0.005	0.5649	0.2676	0.0779	139.587	73.068	18.554	-23.706	17.129	PdT1	PdT1
08-1516	46456	65	Core	A	0.968	0.048	0.008	0.565	0.408	0.777	0.008	0.213	0.002	0.006	0.4988	0.2151	0.2103	136.974	70.248	15.262	-23.268	18.399	PdT1	PdT2
08-1516	46460	80	Core	A	1.121	0.076	0.009	0.600	0.190	0.723	0.007	0.265	0.003	0.007	0.5864	0.2685	0.0996	142.056	71.466	16.869	-21.556	17.728	PdT1	Pyx1
08-1516	46464	65	Core	A	1.093	0.051	0.009	0.640	0.204	0.732	0.006	0.254	0.005	0.007	0.5643	0.2577	0.1053	141.775	71.595	17.857	-23.273	17.245	PdT1	PdT1
08-1516	46465	65	Core	A	1.074	0.050	0.010	0.612	0.252	0.752	0.006	0.238	0.004	0.004	0.5543	0.2407	0.1298	141.356	71.983	17.088	-24.485	17.277	PdT1	PdT1
08-1516	46466	60	Core	A	1.038	0.050	0.010	0.657	0.240	0.713	0.008	0.278	0.003	0.004	0.5364	0.2803	0.1241	141.390	72.007	17.310	-22.853	16.541	PdT1	PdT1
08-1516	46467	80	Rim	A	1.094	0.034	0.009	0.629	0.231	0.780	0.007	0.209	0.002	0.007	0.5601	0.2114	0.1180	140.532	72.411	17.580	-25.034	18.209	PdT1	PdT1
08-1516	46468	80	Core	A	0.856	0.052	0.008	0.523	0.557	0.790	0.007	0.201	0.000	0.008	0.4423	0.2028	0.2877	131.344	67.724	14.398	-22.495	17.870	PdT1	PdT2
08-1516	46471	75	Core	A	1.055	0.058	0.009	0.606	0.269	0.740	0.007	0.251	0.003	0.004	0.5465	0.2534	0.1394	141.065	71.827	16.432	-23.267	17.831	PdT1	PdT1
08-1516	46474	80	Core	A	1.012	0.054	0.010	0.523	0.397	0.772	0.008	0.220	0.003	0.003	0.5236	0.2217	0.2055	137.915	70.108	14.787	-24.061	16.959	PdT1	PdT2
08-1516	46475	80	Core	A	0.991	0.053	0.009	0.545	0.399	0.773	0.004	0.218	0.004	0.005	0.5122	0.2199	0.2060	137.803	70.075	15.517	-24.600	17.835	PdT1	PdT2
08-1498A	46398	65	Core	C	1.141	0.065	0.010	0.602	0.175	0.877	0.015	0.096	0.004	0.019	0.5951	0.0983	0.0910	143.744	68.014	20.500	-22.821	17.244	PdT2	Pyx2
08-1498B	46434	70	Core	C	1.210	0.051	0.010	0.573	0.146	0.879	0.020	0.101	0.003	0.013	0.6272	0.1027	0.0757	142.560	68.475	19.931	-24.075	16.385	PdT2	Pyx2
08-1516	46451	150	Core	A	0.871	0.053	0.007	0.478	0.588	0.784	0.007	0.211	0.003	0.000	0.4495	0.2124	0.3037	129.566	66.687	13.170	-23.130	18.110	PdT2	PdT2
08-1516	46452	150	Core	A	0.875	0.051	0.008	0.498	0.566	0.780	0.005	0.215	0.000	0.004	0.4513	0.2164	0.2919	130.539	67.829	13.645	-23.245	18.055	PdT2	PdT2
08-1516	46453	60	Rim	A	0.918	0.052	0.007	0.500	0.519	0.771	0.006	0.220	0.003	0.005	0.4740	0.2220	0.2677	132.953	67.779	13.920	-22.814	17.891	PdT2	PdT2

08-1511A	46118	90	Core	A	1.092	0.076	0.009	0.590	0.230	0.698	0.008	0.292	0.003	0.005	0.5711	0.2950	0.1201	142.348	71.080	16.208	-21.523	16.574	Prd1	Pyx1
08-1511A	46119	90	Core	A	1.074	0.076	0.010	0.584	0.252	0.707	0.006	0.286	0.003	0.003	0.5622	0.2878	0.1319	142.068	71.441	16.112	-22.656	16.517	Prd1	Pyx1
08-1511A	46128	40	Core	A	1.140	0.053	0.009	0.592	0.203	0.762	0.008	0.228	0.002	0.006	0.5890	0.2301	0.1051	141.447	72.140	16.841	-23.634	18.038	Prd1	PdT1
08-1511A	46129	40	Core	A	1.147	0.053	0.010	0.614	0.171	0.762	0.010	0.224	0.002	0.009	0.5937	0.2271	0.0887	141.677	71.666	17.887	-23.029	16.978	Prd1	PdT1
08-1511A	46132	200	Core	A	1.145	0.062	0.009	0.606	0.173	0.738	0.010	0.257	0.003	0.000	0.5949	0.2583	0.0900	141.368	72.236	16.823	-23.287	17.449	Prd1	PdT1
08-1511A	46134	200	Core	A	1.147	0.059	0.010	0.607	0.169	0.788	0.014	0.205	0.004	0.000	0.5963	0.2062	0.0880	141.469	71.975	17.555	-23.987	17.354	Prd1	PdT1
08-1511A	46136	200	Core	A	1.141	0.064	0.008	0.614	0.168	0.795	0.011	0.196	0.003	0.003	0.5933	0.1979	0.0871	140.971	72.113	17.521	-22.910	19.508	Prd1	Prd1
08-1511A	46137	200	Rim	A	1.041	0.057	0.009	0.542	0.346	0.821	0.010	0.164	0.004	0.009	0.5397	0.1660	0.1794	140.080	69.555	16.394	-23.877	17.667	Prd1	PdT1
08-1511A	46139	100	Rim	A	1.080	0.082	0.009	0.576	0.247	0.848	0.012	0.139	0.003	0.006	0.5674	0.1410	0.1298	141.981	70.565	17.380	-22.787	19.568	Prd1	Prd1
08-1511A	46140	100	Rim	A	1.000	0.075	0.010	0.546	0.365	0.819	0.008	0.168	0.004	0.008	0.5235	0.1706	0.1908	139.709	69.685	16.291	-23.368	18.007	Prd1	Pyx1
08-1511A	46142	100	Core	A	1.097	0.081	0.009	0.580	0.227	0.746	0.011	0.250	0.002	0.000	0.5761	0.2511	0.1194	141.548	72.273	15.727	-22.542	18.122	Prd1	Pyx1
08-1511A	46143	100	Core	A	1.091	0.081	0.011	0.586	0.227	0.718	0.008	0.272	0.004	0.004	0.5730	0.2746	0.1192	142.479	71.309	16.462	-22.109	16.433	Prd1	Pyx1
08-1511A	46144	100	Core	A	1.081	0.079	0.009	0.584	0.242	0.725	0.009	0.271	0.002	0.000	0.5667	0.2720	0.1270	141.555	72.031	15.590	-22.339	17.703	Prd1	Pyx1
08-1511A	46147	100	Rim	A	1.090	0.075	0.009	0.619	0.201	0.791	0.013	0.195	0.002	0.009	0.5707	0.1979	0.1051	141.844	71.628	17.596	-21.646	18.720	Prd1	Pyx1
08-1511A	46149	100	Core	A	1.059	0.072	0.009	0.565	0.289	0.825	0.010	0.160	0.004	0.009	0.5533	0.1624	0.1513	141.595	70.207	17.035	-23.092	18.375	Prd1	Pyx1
08-1511A	46150	50	Core	A	1.131	0.059	0.010	0.509	0.285	0.851	0.013	0.133	0.005	0.008	0.5875	0.1355	0.1481	141.974	69.120	16.789	-24.688	17.269	Prd1	Prd1
08-1511A	46156	150	Rim	A	1.070	0.054	0.009	0.646	0.215	0.799	0.013	0.187	0.004	0.006	0.5540	0.1898	0.1115	141.406	71.755	18.023	-22.915	18.658	Prd1	PdT1
08-1511A	46157	150	Core	A	1.055	0.053	0.010	0.616	0.260	0.770	0.010	0.225	0.003	0.000	0.5463	0.2259	0.1345	140.902	72.428	16.623	-24.305	17.733	Prd1	PdT1
08-1511A	46158	150	Core	A	1.056	0.057	0.008	0.617	0.258	0.806	0.010	0.183	0.002	0.006	0.5468	0.1851	0.1338	140.796	71.774	17.040	-23.022	19.728	Prd1	Prd1
08-1511B	46165	60	Core	A	1.089	0.079	0.010	0.621	0.196	0.794	0.008	0.195	0.000	0.009	0.5712	0.1972	0.1030	141.689	72.482	17.784	-22.767	19.010	Prd1	Prd1
08-1511B	46167	60	Rim	A	1.118	0.080	0.009	0.653	0.135	0.841	0.009	0.144	0.003	0.009	0.5863	0.1463	0.0710	140.991	70.814	19.985	-22.460	19.620	Prd1	Prd1
08-1511B	46168	60	Core	A	1.106	0.082	0.008	0.625	0.174	0.849	0.010	0.140	0.000	0.009	0.5805	0.1411	0.0912	141.452	71.519	18.603	-22.337	20.761	Prd1	Prd1
08-1511B	46169	60	Core	A	1.068	0.079	0.008	0.598	0.244	0.780	0.007	0.210	0.003	0.004	0.5593	0.2123	0.1278	141.208	71.943	16.512	-22.473	19.956	Prd1	Prd1
08-1511B	46175	40	Core	A	1.218	0.063	0.008	0.554	0.154	0.874	0.007	0.119	0.000	0.005	0.6324	0.1201	0.0797	141.375	70.976	18.367	-25.436	19.904	Prd1	UNCL
08-1511B	46181	50	Core	A	1.057	0.107	0.009	0.521	0.302	0.898	0.009	0.089	0.004	0.007	0.5621	0.0904	0.1606	141.907	68.064	17.510	-23.165	19.866	Prd1	Pyx2
08-1511B	46182	55	Rim	A	1.118	0.074	0.009	0.593	0.203	0.806	0.007	0.185	0.004	0.003	0.5840	0.1869	0.1061	141.682	71.972	17.330	-23.722	19.570	Prd1	Prd1
08-1511B	46183	55	Core	A	1.133	0.079	0.008	0.589	0.187	0.786	0.008	0.205	0.004	0.003	0.5936	0.2069	0.0978	141.601	71.915	17.019	-22.842	19.339	Prd1	Prd1
08-1511B	46184	55	Core	A	1.121	0.074	0.010	0.583	0.209	0.777	0.006	0.214	0.004	0.004	0.5861	0.2157	0.1094	141.955	71.883	17.031	-23.722	18.521	Prd1	Prd1
08-1511B	46185	200	Rim	A	1.159	0.112	0.011	0.618	0.098	0.802	0.004	0.192	0.004	0.000	0.6179	0.1934	0.0523	138.610	71.139	19.276	-22.985	19.388	Prd1	UNCL
08-1511B	46186	200	Rim	A	1.155	0.107	0.010	0.602	0.122	0.802	0.007	0.188	0.004	0.005	0.6146	0.1897	0.0651	140.321	71.107	18.545	-21.823	19.317	Prd1	Prd1
08-1511B	46187	200	Core	A	1.066	0.098	0.008	0.580	0.244	0.840	0.007	0.149	0.005	0.005	0.5640	0.1505	0.1291	141.867	70.693	17.460	-22.844	20.542	Prd1	Prd1
08-1511B	46188	200	Core	A	1.095	0.096	0.008	0.590	0.208	0.859	0.004	0.133	0.003	0.004	0.5783	0.1339	0.1100	141.691	71.178	18.131	-23.942	21.864	Prd1	UNCL
08-1511A	46127	170	Core	A	1.070	0.033	0.009	0.648	0.237	0.704	0.005	0.283	0.004	0.008	0.5471	0.2868	0.1213	141.281	71.266	17.784	-24.128	15.976	Prd2	PdT1
08-1511A	46130	200	Rim	A	1.124	0.024	0.008	0.707	0.135	0.677	0.006	0.316	0.003	0.003	0.5718	0.3180	0.0688	139.058	71.193	18.979	-23.445	15.921	Prd2	PdT1
08-1511A	46153	70	Core	A	1.219	0.030	0.007	0.669	0.070	0.843	0.012	0.141	0.003	0.010	0.6227	0.1431	0.0356	134.639	68.975	21.456	-23.044	18.456	Prd2	UNCL
08-1511B	46177	45	Core	A	1.262	0.031	0.007	0.665	0.031	0.839	0.009	0.148	0.000	0.011	0.6445	0.1502	0.0159	125.843	66.502	23.013	-21.920	17.401	Prd2	UNCL
08-1511B	46178	45	Core	A	1.158	0.034	0.007	0.624	0.172	0.880	0.010	0.105	0.003	0.010	0.5923	0.1063	0.0882	141.233	69.981	19.805	-25.125	19.554	Prd2	UNCL
08-1511B	46194	120	Rim	A	0.997	0.029	0.007	0.836	0.129	0.696	0.005	0.295	0.002	0.005	0.5082	0.2979	0.0658	136.987	72.118	20.598	-21.632	18.429	Prd2	Prd2
08-1511B	46195	120	Rim	A	1.026	0.033	0.007	0.850	0.082	0.690	0.004	0.301	0.003	0.006	0.5238	0.3038	0.0419	134.112	70.698	22.036	-21.058	17.649	Prd2	Prd2

08-1511B	46196	120	Core	A	1.032	0.033	0.005	0.851	0.076	0.750	0.006	0.242	0.002	0.005	0.5271	0.2436	0.0386	132.091	71.599	21.730	-20.602	20.886	Prd2	UNCL
08-1511B	46197	120	Core	A	1.031	0.030	0.008	0.852	0.077	0.711	0.004	0.281	0.003	0.005	0.5260	0.2832	0.0391	133.209	71.119	22.252	-21.673	17.724	Prd2	Prd2
08-1556	46202	275	Rim	FeD	1.032	0.073	0.008	0.556	0.329	0.836	0.003	0.153	0.003	0.008	0.5386	0.1548	0.1714	140.127	70.290	16.980	-24.832	20.360	FeDc	UNCL
08-1556	46203	275	Core	FeD	1.135	0.075	0.009	0.622	0.154	0.770	0.008	0.220	0.002	0.007	0.5940	0.2220	0.0807	141.147	72.145	17.937	-22.428	18.595	FeDc	Prd1
08-1556	46204	275	Core	FeD	1.128	0.078	0.010	0.615	0.168	0.746	0.006	0.243	0.004	0.005	0.5903	0.2455	0.0878	141.797	71.748	17.785	-22.730	17.948	FeDc	Prd1
08-1556	46205	275	Core	FeD	1.139	0.076	0.010	0.622	0.150	0.728	0.005	0.262	0.005	0.004	0.5960	0.2648	0.0785	141.618	71.531	18.077	-22.787	17.074	FeDc	PdT1
08-1556	46209	275	Core	FeD	1.121	0.055	0.009	0.655	0.157	0.760	0.007	0.229	0.002	0.007	0.5800	0.2316	0.0811	140.704	72.402	18.344	-22.965	18.458	FeDc	PdT1
08-1556	46210	110	Rim	FeD	1.111	0.059	0.008	0.676	0.141	0.717	0.010	0.271	0.004	0.006	0.5762	0.2745	0.0732	140.677	71.436	18.504	-21.225	17.216	FeDc	Pyx1
08-1556	46211	110	Core	FeD	1.112	0.060	0.011	0.667	0.147	0.718	0.007	0.271	0.003	0.007	0.5775	0.2739	0.0762	141.241	71.838	18.772	-22.647	16.208	FeDc	PdT1
08-1556	46212	110	Core	FeD	1.114	0.066	0.010	0.665	0.141	0.730	0.008	0.261	0.002	0.006	0.5801	0.2633	0.0734	140.676	72.194	18.422	-21.992	17.318	FeDc	PdT1
08-1556	46215	115	Core	FeD	1.077	0.064	0.009	0.596	0.250	0.788	0.007	0.204	0.002	0.005	0.5602	0.2057	0.1301	141.175	72.315	16.763	-23.978	19.056	FeDc	Prd1
08-1556	46216	115	Core	FeD	1.050	0.058	0.008	0.571	0.311	0.782	0.005	0.210	0.002	0.005	0.5434	0.2115	0.1608	139.916	71.619	16.066	-24.511	19.330	FeDc	Prd1
08-1556	46220	110	Rim	FeD	1.130	0.086	0.009	0.609	0.162	0.806	0.007	0.183	0.004	0.006	0.5945	0.1849	0.0854	141.497	71.591	18.167	-22.768	19.625	FeDc	Prd1
08-1556	46221	110	Rim	FeD	1.030	0.085	0.008	0.548	0.327	0.835	0.005	0.151	0.000	0.013	0.5406	0.1535	0.1715	140.223	70.105	16.546	-22.818	20.547	FeDc	Prd1
08-1556	46222	110	Core	FeD	0.974	0.087	0.009	0.524	0.405	0.848	0.004	0.137	0.003	0.011	0.5119	0.1387	0.2127	138.564	68.222	16.662	-23.661	19.457	FeDc	UNCL
08-1556	46224	110	Core	FeD	1.206	0.051	0.011	0.588	0.140	0.806	0.009	0.181	0.003	0.008	0.6238	0.1833	0.0723	141.118	71.362	18.577	-24.704	17.175	FeDc	PdT1
08-1556	46225	110	Core	FeD	1.102	0.058	0.011	0.543	0.282	0.830	0.007	0.158	0.003	0.008	0.5720	0.1595	0.1464	141.658	70.670	17.065	-25.425	17.507	FeDc	PdT1
08-1556	46228	80	Core	FeD	1.102	0.077	0.011	0.605	0.203	0.766	0.006	0.224	0.005	0.003	0.5769	0.2260	0.1061	142.067	71.986	17.437	-23.566	18.064	FeDc	PdT1
08-1556	46232	110	Rim	FeD	1.016	0.066	0.009	0.576	0.331	0.827	0.006	0.160	0.004	0.008	0.5285	0.1618	0.1720	140.251	70.281	17.084	-24.038	19.348	FeDc	Prd1
08-1556	46234	110	Core	FeD	1.041	0.068	0.009	0.568	0.313	0.780	0.006	0.205	0.003	0.011	0.5416	0.2077	0.1629	140.679	70.518	16.474	-23.058	18.654	FeDc	Prd1
08-1556	46235	110	Core	FeD	1.017	0.066	0.009	0.555	0.350	0.827	0.006	0.156	0.002	0.013	0.5290	0.1582	0.1823	140.040	69.432	16.963	-23.593	18.881	FeDc	PdT2
08-1556	46236	150	Rim	FeD	1.099	0.036	0.010	0.656	0.196	0.745	0.006	0.247	0.003	0.004	0.5633	0.2491	0.1004	140.708	72.724	17.922	-24.777	17.310	FeDc	PdT1
08-1556	46237	150	Core	FeD	1.084	0.040	0.009	0.656	0.209	0.765	0.004	0.225	0.003	0.006	0.5563	0.2270	0.1073	140.697	72.555	18.214	-24.980	18.714	FeDc	PdT1
08-1556	46238	150	Core	FeD	1.069	0.036	0.010	0.651	0.232	0.755	0.006	0.232	0.002	0.009	0.5477	0.2352	0.1190	140.914	72.226	18.058	-24.678	17.267	FeDc	PdT1
08-1516	46438	125	Rim	A	1.118	0.060	0.008	0.647	0.164	0.692	0.006	0.307	0.000	0.000	0.5799	0.3075	0.0848	140.835	72.490	17.088	-22.726	17.736	DcLag	PdT1
08-1516	46449	150	Rim	A	1.103	0.035	0.010	0.697	0.152	0.728	0.008	0.266	0.000	0.005	0.5649	0.2676	0.0779	139.587	73.068	18.554	-23.706	17.129	DcLag	PdT1
08-1516	46451	150	Core	A	0.871	0.053	0.007	0.478	0.588	0.784	0.007	0.211	0.003	0.000	0.4495	0.2124	0.3037	129.566	66.687	13.170	-23.130	18.110	DcLag	PdT2
08-1516	46452	150	Core	A	0.875	0.051	0.008	0.498	0.566	0.780	0.005	0.215	0.000	0.004	0.4513	0.2164	0.2919	130.539	67.829	13.645	-23.245	18.055	DcLag	PdT2
08-1516	46453	60	Rim	A	0.918	0.052	0.007	0.500	0.519	0.771	0.006	0.220	0.003	0.005	0.4740	0.2220	0.2677	132.953	67.779	13.920	-22.814	17.891	DcLag	PdT2
08-1516	46456	65	Core	A	0.968	0.048	0.008	0.565	0.408	0.777	0.008	0.213	0.002	0.006	0.4988	0.2151	0.2103	136.974	70.248	15.262	-23.268	18.399	DcLag	PdT2
08-1516	46460	80	Core	A	1.121	0.076	0.009	0.600	0.190	0.723	0.007	0.265	0.003	0.007	0.5864	0.2685	0.0996	142.056	71.466	16.869	-21.556	17.728	DcLag	Pyx1
08-1516	46464	65	Core	A	1.093	0.051	0.009	0.640	0.204	0.732	0.006	0.254	0.005	0.007	0.5643	0.2577	0.1053	141.775	71.595	17.857	-23.273	17.245	DcLag	PdT1
08-1516	46465	65	Core	A	1.074	0.050	0.010	0.612	0.252	0.752	0.006	0.238	0.004	0.004	0.5543	0.2407	0.1298	141.356	71.983	17.088	-24.485	17.277	DcLag	PdT1
08-1516	46466	60	Core	A	1.038	0.050	0.010	0.657	0.240	0.713	0.008	0.278	0.003	0.004	0.5364	0.2803	0.1241	141.390	72.007	17.310	-22.853	16.541	DcLag	PdT1
08-1516	46467	80	Rim	A	1.094	0.034	0.009	0.629	0.231	0.780	0.007	0.209	0.002	0.007	0.5601	0.2114	0.1180	140.532	72.411	17.580	-25.034	18.209	DcLag	PdT1
08-1516	46468	80	Core	A	0.856	0.052	0.008	0.523	0.557	0.790	0.007	0.201	0.000	0.008	0.4423	0.2028	0.2877	131.344	67.724	14.398	-22.495	17.870	DcLag	PdT2
08-1516	46471	75	Core	A	1.055	0.058	0.009	0.606	0.269	0.740	0.007	0.251	0.003	0.004	0.5465	0.2534	0.1394	141.065	71.827	16.432	-23.267	17.831	DcLag	PdT1
08-1516	46474	80	Core	A	1.012	0.054	0.010	0.523	0.397	0.772	0.008	0.220	0.003	0.003	0.5236	0.2217	0.2055	137.915	70.108	14.787	-24.061	16.959	DcLag	PdT2
08-1516	46475	80	Core	A	0.991	0.053	0.009	0.545	0.399	0.773	0.004	0.218	0.004	0.005	0.5122	0.2199	0.2060	137.803	70.075	15.517	-24.600	17.835	DcLag	PdT2